LATS2 positively regulates repressive epigenetic integrity via Polycomb repressive complex 2

Kosuke Torigata

LATS2 positively regulates repressive epigenetic integrity via Polycomb repressive complex 2

Kosuke Torigata

A dissertation
submitted in partial fulfillment of the
requirements for degree of

Doctor of Engineering

Osaka University

2016

Reading Committee:
Hiroshi Nojima, Chair
Hiroshi Sasaki
Hiroaki Miki
Nobuyuki Takakura

Program Authorized to Offer Degree:
Graduate School of Frontier Biosciences

Abstract

LATS2 (large tumor suppressor 2), a pivotal Ser/Thr kinase of the Hippo signaling pathway, plays important roles in many biological processes. LATS2 and its homolog LATS1 function in many tumor-suppressive signals, including some that involve canonical Hippo signaling and others that are Hippo-independent. On the other hand, because *Lats2* knockout (KO) mice exhibit embryonic lethality due to a defect in neurogenesis, whereas *Lats1* KO mice do not, it is likely that LATS2 has essential functions that it does not share with LATS1. Furthermore, a recent study reported that Lats2 is indispensable for maintenance of stemness in murine embryonic stem cells. Therefore, elucidation of novel non-canonical signals of LATS2 would improve our understanding of the role of this protein in normal development and tumorigenesis. In this thesis, I demonstrate that *LATS2* KO causes dysregulation of Polycomb repressive complex 2 (PRC2), followed by reduction of tri-methylation of histone H3 at K27 (H3K27me3) levels in both mouse and human cells. Chromatin-modifying activities involved in the generation of appropriate epigenetic landscapes by PRC2 play an essential role in development and tumorigenesis. However, the spatiotemporal mechanisms by which PRC2 generates diverse epigenomes in specific tissue or cellular contexts remain poorly understood

To profile the effect of *LATS2* KO on the epigenome and transcriptome in human cells, I constructed a new *LATS2* KO HeLa-S3 cell line using TAL-effector nuclease (TALEN) technology. Omics analyses of this HeLa-S3 line and mouse embryonic fibroblasts revealed that *LATS2* depletion causes induction of genes involved in development, especially neurogenesis, in a manner that is partially independent of canonical Hippo signals. LATS2 binds to EZH2, a component of PRC2 on chromatin and can phosphorylate EZH2 *in vivo* and *in vitro*. LATS2 positively regulates histone methyltransferase activity of EZH2 in a kinase dependent fashion. Dysregulation of PRC2 also interferes with the normal pattern of the H3K4me3 modification, further reinforcing the failure of PRC2. This LATS2-dependent H3K27me3 module correlates with a dedifferentiated state in the nervous system. Indeed, in glioblastoma multiforme, LATS2-high tumors are associated with poor prognosis accompanied by silencing of PRC2 targets. Overall, these results suggest that LATS2, a known tumor suppressor, may coordinate oncogenic epigenetic signatures in specific tissues via PRC2. Therefore, these findings provide insights into the oncogenic role of LATS2 in specific contexts, as well as its importance in regulation of epigenome-associated signals in normal development and tumorigenesis.

研究要旨

LATS2 (Large tumor suppressor 2)は Hippo シグナル経路を構成する主要な Ser/Thr キナーゼであり、多くの細胞過程において重要な役割を果たしている。LATS2 はそのホモログである LATS1 と共に、Hippo シグナル経路や他のシグナル経路において、その名の通り腫瘍抑制的に機能する。一方で *Lats1* ノックアウト(KO)マウスが正常に発生するのに対して、*Lats2* の KO マウスは中枢神経の発生異常による胎生致死を示すことから、Lats2 には Lats1 と共有しない重要な働きがあることが示唆される。加えて最近では *Lats2* がマウス ES 細胞の未分化性の維持や、正常な分化開始に必須であることも報告されている。これらのことから、既知の Hippo シグナル経路以外 (non-canonical Hippo) の LATS2 の役割を明らかにすることは、LATS2 の正常発生や細胞のがん化における役割のさらなる理解に必須であると言える。本研究で申請者は *LATS2* の欠失がマウスとヒト両方において、エピジェネティック制御を司る Polycomb repressive complex 2 (PRC2) と PRC2 が触媒するヒストン H3 の 27 番目リジンのトリメチル化 (H3K27me3) の制御異常を引き起すことを報告する。PRC2 による H3K27me3 制御による適切なエピゲノムは発生や細胞のがん化の両方に深く関わるが、PRC2 が特定の細胞文脈で多様なエピゲノムを構築する時空間的な制御は殆ど明らかになっていなかった。

LATS2 の欠失がヒト細胞のエピゲノムやトランスクリプトームに与える影響を解析するために、申請者は人工制限酵素 TALEN を用いて新規に *LATS2* を欠く HeLa-S3 細胞株を樹立した。この細胞や *LATS2* の KO マウス由来胎生線維芽細胞のオミクス解析から、LATS2 の欠失は発生分化、特に神経発生に関わる遺伝子の脱抑制を引き起こすことが明らかになった。またこれらの相関は既知の Hippo シグナル経路のアウトプットのみでは説明できない、新規な LATS2 依存性のシグナルであることが示唆された。さらに詳細な解析から、LATS2 は PRC2 の構成因子のひとつ EZH2 とクロマチン上で結合し、リン酸化することが明らかになった。LATS2 はそのリン酸化活性依存的に EZH2 のヒストンメチル化活性を正に制御する。また LATS2 の欠失による PRC2 の制御異常は転写亢進性のエピジェネティック修飾である H3K4me3 の下方制御をも引き起こし、PRC2 の発現を転写レベルでも抑制し、エピゲノム全体の制御異常に繋がることが明らかになった。興味深いことに LATS2 依存的な H3K27me3 制御を受ける遺伝子群には神経発生に関わるものが多く含まれており、LATS2 は PRC2 を介して神経発生に関わる遺伝子の発現を抑制する姿が明らかとなった。実際、神経膠芽腫では LATS2 の発現が高い症例ほど PRC2 による抑制標的の発現が低く、より未分化なトランスクリプトームを示し、予後不良と相関した。LATS2 は長らく腫瘍抑制遺伝子として特徴づけられてきたが、特定の細胞文脈においては PRC2 を介してがん進展性の役割を果たすことが示唆された。これらの結果は PRC2 の上流キナーゼを明らかにした他に、エピゲノム制御の正常発生と細胞のがん化における重要性を改めて示すものである。

Achievements

Original paper (***** co-first authoring article equally contributed)

1. LATS2 kinase positively regulates Polycomb repressive complex 2.
   Manuscript submitted for publication
   Kosuke Torigata, Daisuke Okuzaki,Satomi Mukai, Akira Hatanaka, Fumiharu Ohka, Daisuke Motooka,Shota Nakamura, Yasuyuki Ohkawa,Norikazu Yabuta, Yutaka Kondo, Hiroshi Nojima

2. LATS2 knockout induces epigenomic alternations by dysregulation of KDM1A
   Manuscript in preparation for publication
   Kosuke Torigata, Daisuke Okuzaki, Norikazu Yabuta, Hiroshi Nojima.

3. Phosphorylation of CHO1 by Lats1/2 regulates the centrosomal activation of LIMK1 during cytokinesis.
   Cell Cycle, 2015 14:10, 1568-1582
   Ayumi Okamoto, Norikazu Yabuta, Satomi Mukai, **Kosuke Torigata**, Hiroshi Nojima
   Contributions: Construction and maintenance of the *LATS2* KO HeLa-S3 cell line.

4. Lats2 phosphorylates p21/CDKN1A after UV irradiation and regulates apoptosis.
   Journal of Cell Science, 2013, 126, 4358-68
   Hirokazu Suzuki, Norikazu Yabuta,Nobuhiro Okada, **Kosuke Torigata**,Yael Aylon, Moshe Oren, Hiroshi Nojima
   Contributions: Co-immunopecipitation analysis and pulldown assay for Lats2 and p21.

5. CAWS administration increases the expression of interferon γ and complement factors that lead to severe vasculitis in DBA/2 mice.
   BMC Immunology, 2013, 14:44
   Noriko Nagi-Miura, Daisuke Okuzaki, **Kosuke Torigata**, Minami A Sakurai,Akihiko Ito, Naohito Ohno, HiroshiNojima
   Contributions: Maintenance and analysis of CAWS-mediated vasculitis model mice.

6*****. A simple and efficient method for the preparation of live leukocytes from peripheral blood using the LeukoCatch™ system.
   Advances in Bioscience and Biotechnology, 2012, 3:630-42
   Ayumi Okamoto*, **Kosuke Torigata***, Minami A. Sakurai, Daisuke Okuzaki, Hodaka Fujii, Toshinari Ohmine, Daisaku Miura, Shoichi Kimura, Norikazu Yabuta, Hiroshi Nojima
   *These two authors are equally contributed.
   Contributions: performed experiments and wrote the relevant text.

7. Ficolin 1 Expression is Elevated in the Peripheral Blood Mononuclear Cells of Takayasu's Vasculitis Patients.
   Molecular Biomarkers & Diagnosis, 2012, 2:125
   Daisuke Okuzaki, Shigeto Kobayashi, Minami A. Sakurai, **Kosuke Torigata**, Ayumi Okamoto, Toshiharu Matsumoto, Hiroyuki Daida, Akihiko Ito, Hiroshi Nojima
   Contributions: RT-qPCR of Takayasu's vasculitis patients for validation of microarray data.

International conference

1. rChum, A Novel RNA Molecule to Aid PCR Amplification and Detection of Ultralow Amount of Nucleic Acids
   The Asia Pacific Meeting of Vasculitis and ANCA Workshop 2012 PD1-08, March 29, 2012 in Tokyo (poster)
   Kosuke Torigata, Daisuke Okuzaki, Ayumi Okamoto, Hiroshi Nojima

Domestic conference

1. LATS2 による PRC2 を介したエピジェネティック制御は膠芽腫の予後不良と相関する
   第 74 回日本癌学会学術総会 J-1190, 2015 年 10 月 9 日 名古屋国際会議場 (口頭発表)
   鳥形康輔、奥崎大介、向井智美、畑中彬良、大岡史治、藪田紀一、近藤豊、野島博

2. Lats2 は PRC2 複合体を介して抑制性エピゲノムを制御する
   第 37 回日本分子生物学会年会 1P-0201, 2014 年 11 月 25 日 パシフィコ横浜 (ポスター)
   鳥形康輔、奥崎大介、大川恭行、藪田紀一、野島博

3. エピゲノムの多様性・特異性を生み出す新規上流シグナルの探索
   第 8 回日本エピジェネティクス研究会年会 P-70, 2014 年 5 月 27 日 東京大学伊藤国際学術研究センター (ポスター)
   鳥形康輔、奥崎大介、大岡史治、畑中彬良、大川恭行、小根山千歳、近藤豊、藪田紀一、野島博

4. LATS2 はエピゲノム調節機構を介して HOX　cluster や DLK1－MEG3 locus の発現を制御する
   第 37 回日本分子生物学会年会 2P-0232, 2013 年 12 月 4 日 神戸国際会議場 (ポスター)
   鳥形康輔、奥崎大介、藪田紀一、野島博

5. Lats2 依存的な新規エピジェネティック制御機構の探索

第 7 回日本エピジェネティクス研究会年会 P-20, 2013 年 5 月 30 日 奈良新公会堂 (ポスター)
鳥形康輔、向井智美、鈴木宏和、奥崎大介、藪田紀一、野島博

6. Expression profiling of Lats2 knockout MEF cells using dye-swapped DNA microarray
第 45 回日本発生生物学会, 第 64 回日本細胞生物学会合同大会 P3-096,2012 年 5 月 31 日 神戸国際会議場 (ポスター)
鳥形康輔、奥崎大介、藪田紀一、野島博

7. Lats2 ノックアウトマウス胎性線維芽細胞のトランスクリプトーム解析
第 59 回日本生化学会近畿支部例会 D-14, 2012 年 5 月 19 日 京都大学宇治キャンパス (ポスターおよび口頭発表)
鳥形康輔、奥崎大介、藪田紀一、野島博

Research fellowship

1. Research Fellowships for Young Scientists (DC1)
Japan Society for the Promotion of Science, April 2013 – March 2016

Acknowledgements

I would like to begin thanking to my advisor Dr. Daisuke Okuzaki, Asis. Prof. of DNA-chip Development Center for Infectious Diseases, for all. He taught me how to handle genome-scale data and to interpret them to biological meanings. We've been pursuing our research together hand-in-hand since I've decided to adopt the omics-based approach to my thesis. I learned a lot of things from him about not only research techniques but also way of thinking as a scientist. I also thank to Dr. Hodaka Fujii and Dr. Toshitugu Fujita, Assoc. Prof. and Asis. Prof. of Chromatin Biochemistry Research Group, and Dr. Chitose Oneyama, Prof. of Department of Oncogene Research, respectively for many critical advices in many times of research discussion. They all pointed out reasonable approach for characterization of epigenetic state and instructed some concrete experimental procedures. I won't forget thanking to Dr. Akira Hatanaka, Dr. Fumiharu Ohka and Dr. Yutaka Kondo, research fellows and prof. of Department of epigenomics, Nagoya-city university, for giving me important insights of the association of our data with clinical outcomes of glioblastoma multiforme. In addition, I was also much helped by Dr. Shota Nakamura and Dr. Daisuke Motooka, Asis. Prof. and a research fellow of Department of Infection Metagenomics and Dr. Yasuyuki Ohkawa, Assoc. Prof. of Department of Advanced Medical Initiatives, Kyushu university, for generating very good quality high-throughput sequencing data using HiSeq 2000/2500 systems. I thank all the current and former members of Nojima Lab, for their help and experience shared with. Especially I am grateful to Prof. Hiroshi Nojima and Assoc. Prof. Norikazu Yabuta for their kind supports throughout my research life. Finally, I would like to thank my family and especially to my wife Miku for their never-ending support and care. It was obviously impossible for me to persevere my research without their warm encouragements.

Abbreviations

3'UTR	3'-untranslated region
5-aza-dC	5-aza-2'-deoxycytidine
5-hmC	5-hydroxymethylcytosine
A.U.	arbitrary unit
aa.	amino acid
ACTB	actin beta
AMOT	angiomotin
AR	androgen receptor
ATP	adenosine triphosphate
ATR	ataxia telangiectasia and Rad3-related protein
BCL9	B-cell CLL/lymphoma 9 protein
bp	base pair
BSA	bovine serum albumin
CCNA2	cyclin-A2
CDK1	cyclin-dependent kinase 1
ChIP	chromatin immunoprecipitation
ChIP-qPCR	ChIP followed by quantitative PCR
ChIP-seq	ChIP followed by high-throughput DNA sequencing
CHK1	checkpoint kinase 1
CHO1	kinesin-like protein 1 subfamily identified in CHO cell
CO2	carbon dioxide
CpG	C followed by G dinucleotide
C-terminal	carboxy terminnal of protein
CTGF	connective tissue growth factor
CTNNB1	catenin (cadherin-associated protein), beta 1
DEG	differentially expressed gene
DMEM	Dulbecco's modified Eagle's medium
DNA	deoxyribonucleic acid
DNMT	DNA methyltransferase
DTT	dithiothreitol
DZNep	3-deazaneplanocin A
E	embryonic day
EDTA	Ethylene diamine tetraacetic acid
EGTA	thylene glycol tetraacetic acid
EED	embryonic ectoderm development
EMT	epithelial to mesenchymal transition

ENCODE	The Encyclopedia of DNA Elements
ES	enrichment score
EV	empty vector
EZH2	enhancer of zeste 2
F2R	coagulation factor II (thrombin) receptor
FBS	fetal bovine serum
FBXO32	F-box protein 32
FDR	false discovery rate
FPKM	fragments per kilobase of transcript per Million fragments sequenced
GAPDH	glyceraldehyde-3-phosphate dehydrogenase
GO	gene ontology
GSEA	gene set enrichment analysis
H2AK119ub	ubiquitinylated Histone H2A at lysine 119
H3K27ac	acetylated Histone H3 at lysine 27
H3K27me3	tri-methylated Histone H3 at lysine 27
H3K27me3	di-methylated Histone H3 at lysine 27
H3K36me3	tri-methylated Histone H3 at lysine 6
H3K4me3	tri-methylated Histone H3 at lysine 4
H3K9ac	acetylated Histone H3 at lysine 9
HAT	histone acetyltransferases
HCP	promoter with high CpG content
HDAC	histone deacetylase
HDM	histone demethylase
hES	human embryonic
HIPK	homeodomain-interacting protein kinase
HMT	histone methyltransferase
HMTase	histone methytransferase activity
HOXA11	Homeobox A11
HRK	Activator of apoptosis harakiri
ICP	promoter with intermediate CpG content
IGFBP3	Insulin-like growth factor-binding protein 3
IgG	immunoglobulin G
IP	immunoprecipitation
KCl	potassium chloride
KCNH3	Potassium voltage-gated channel subfamily H member 3
kDa	kilo dalton
KDM1A	lysine-specific histone demethylase 1A

KO	knockout
KRT17	cytoskeletal 17
LATS1/Lats1	large tumor suppressor homolog 1
LATS2 KD	kinase inactive LATS2
LATS2 WT	kinase active LATS2
LATS2/Lats2	large tumor suppressor homolog 2
LCD1/2	Lats conserved domain 1/2
LCP	promoter with low CpG content
LHX2	LIM Homeobox 2
LiCl	lithium chloride
LIF	leukemia inhibitory factor
LIMK1	LIM kinase-1
MASK	multiple ankyrin repeats single KH domain
MDM2	mouse double minute 2
MEF	mouse embryonic fibroblast
mES	murine/mouse embryonic stem
mg	milligram
MgCl2	magnesium chloride
MgSO4	magnesium sulfate
miRNA	micro RNA
mRNA	messenger RNA
MSigDB	The Molecular Signatures Database
MST1/2	mammalian sterile 20-like kinase 1/2
NaCl	sodium chloride
NaOH	sodium hydroxide
ncRNA	non-coding RNA
NES	normalized enrichment score
NHEJ	non-homologous end joining
N-terminal	amino terminnal of protein
ORF	open reading frame
PAGE	polyacrylamide gel electrophoresis
PBD	protein binding domain
P-body	processing body
PBS	phosphate buffered saline
PcG	Polycomb group
PCR	polymerase chain reaction
POLR2	DNA-directed RNA polymerase II subunit RPB1

PP2A	protein phosphatase 2A
pRb	retinoblastoma protein
PRC2	Polycomb repressive complex 2
PTPN14	tyrosine-protein phosphatase non-receptor type 14
RNA	ribonucleic acid
RNA-seq	mRNA profiling using high-throughput DNA sequencing
RT-qPCR	reverse transcription followed by quantitative PCR
SAM	S-adenosylmethionine
SD	standard deviation
SDS	sodium dodecyl sulfate
SDS-PAGE	SDS-polyacrylamide gel electrophoresis
Ser	serine
siRNA	small interfering RNA
SUZ12	suppressor of zeste 12 homolog
TALEN	TAL-effector nuclease
TBS	Tris buffered saline
TBS-T	Tris buffered saline with Tween-20
TCGA	The Cancer Genome Atlas
thr	threonine
TMEM59L	transmembrane protein 59 like
TP53	tumor protein p53
TPPP3	Tubulin Polymerization-Promoting Protein Family Member 3
TSA	trichostatin A
TSS	transcription start site
UBA	ubiquitin associated domain
UV	ultraviolet
WBP2	WW domain-binding protein 2
WCE	whole cell extract
WNT10B	protein Wnt-10b
WWTR1/TAZ	WW domain-containing transcription regulator protein 1
YAP1	Yes-associated protein 1
ZBTB16	zinc finger and BTB domain containing 16
λPPase	lambda protein phosphatase
µg	microgram
µl	microliter
µm	micrometer

Table of Contents

1. General Introduction

In this Ph.D. thesis, I mainly focused on the functional association of *LATS2* gene with Polycomb repressive complex 2 (PRC2). In this chapter, I reviewed general background and previous studies. I described the recent trend of developing anticancer drugs that target epigenetic mechanisms including PRC2, and clarified the problems surrounding them in actual clinical applications. At the end of this chapter, I described the goal of this thesis based on these circumstances.

1.1 Large tumor suppressor kinase 2

1.1.1 General features of LATS2 and Hippo pathway

Large tumor suppressor kinase 2 (LATS2) is a serine/threonine kinase that belongs to NDR family of kinases. *Lats2* and its homolog *Lats1* have been identified as mammalian homologs of the *Drosophila melanogaster* gene *Wts*, which controls cell shape and proliferation (Justice et al., 1995). LATS2 has kinase domain at its C-terminal region and shows high-homology with its paralog, LATS1 (Fig. GI-1). *Lats1* was first identified as a mammalian homolog of *Drosophila Wts* gene (St John et al., 1999), then *Lats2* was identified as a paralog of *Lats1* in mouse and human (Yabuta et al., 2000). Both LATS1 and LATS2 have been well characterized in the Hippo signaling pathway (Yu et al., 2015). The Hippo signaling pathway is a central kinase signaling cascade for initiation and regulation of contact inhibition processes, which define the size of tissues or organs at whole-body level and proliferation properties at cellular level (Figure GI-2). In mammalian Hippo pathway, both LATS1 and LATS2 phosphorylate YAP1 and TAZ (also known as WWTR1) that are transcription co-activators of the genes for cell survival and proliferation, and promote their cytoplasmic retention and proteasomal degradation processes (Figure GI-2).

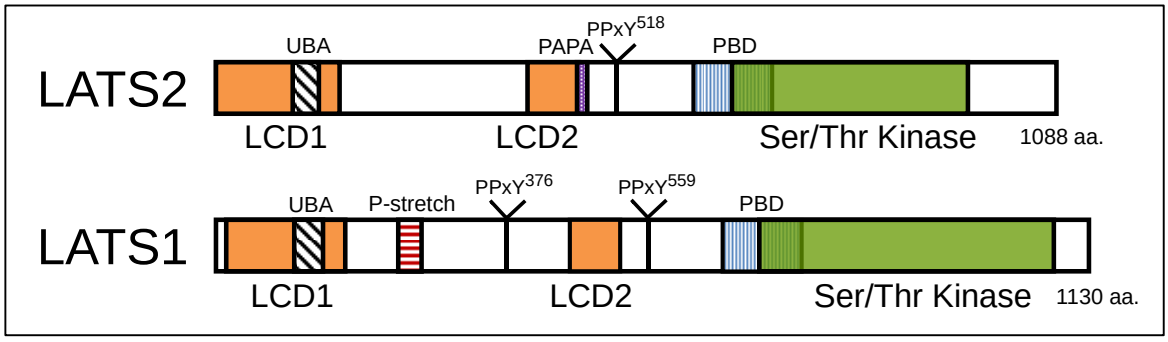

Figure GI-1. Structure of LATS2 and its homolog LATS1.

LATS2 shares several conserved domains with LATS1 including the C-terminal Ser/Thr kinase domain (LATS2: aa.668–973; LATS1: aa.705–1084), a Protein Binding Domain (PBD) (LATS2: aa.618–720; LATS1: aa.656–758), two LATS Conserved Domains (LCD1 and LCD2) (LATS2: aa.1–160, aa.403–463; LATS1: aa.13–167, aa.458–523, respectively) and an ubiquitin binding domain (UBA) (LATS2: aa.99–133; LATS1:

aa.101–138). In addition, both LATS1 and LATS2 have at least one PPxY motif (LATS1: Y376, Y559; LATS2: Y518). LATS2 and LATS1 are distinct proteins; LATS2 possesses a PAPA repeat (aa.467–480), whereas LATS1 possesses a P-stretch (aa.236–266). Adopted from Visser and Yang, 2010.

As down-regulation of Hippo pathway, including LATS1/2 and other upstream regulators, causes YAP1/TAZ activation, followed by unregulated over cell growth, LATS1/2 function as tumor suppressors in the Hippo pathway. Indeed, over-expression of YAP1/TAZ and/or their accumulation in cell nuclei is often observed in many types of human cancer cells (Chan et al., 2008; Moroishi et al., 2015; Steinhardt et al., 2008). The Hippo pathway is also crucial for normal development or organ/tissue regeneration. The Hippo signaling is finely tuned by many upstream coordinators through complicated cross-talks: in brief, the LATS1/2 and YAP1/TAZ activities, the main event of Hippo regulation, can be fluctuated by not only cell-cell contact but also cellular geometry, metabolic status, cytoskeleton dynamics and mechanical stimuli (Yu et al., 2015). In summary, albeit overall upstream signals are complex, the final destination of Hippo signal cascades is the phosphorylation of YAP1/TAZ by LATS1/2 kinase (I referred this to the function of LATS1/2 in 'canonical Hippo' pathway).

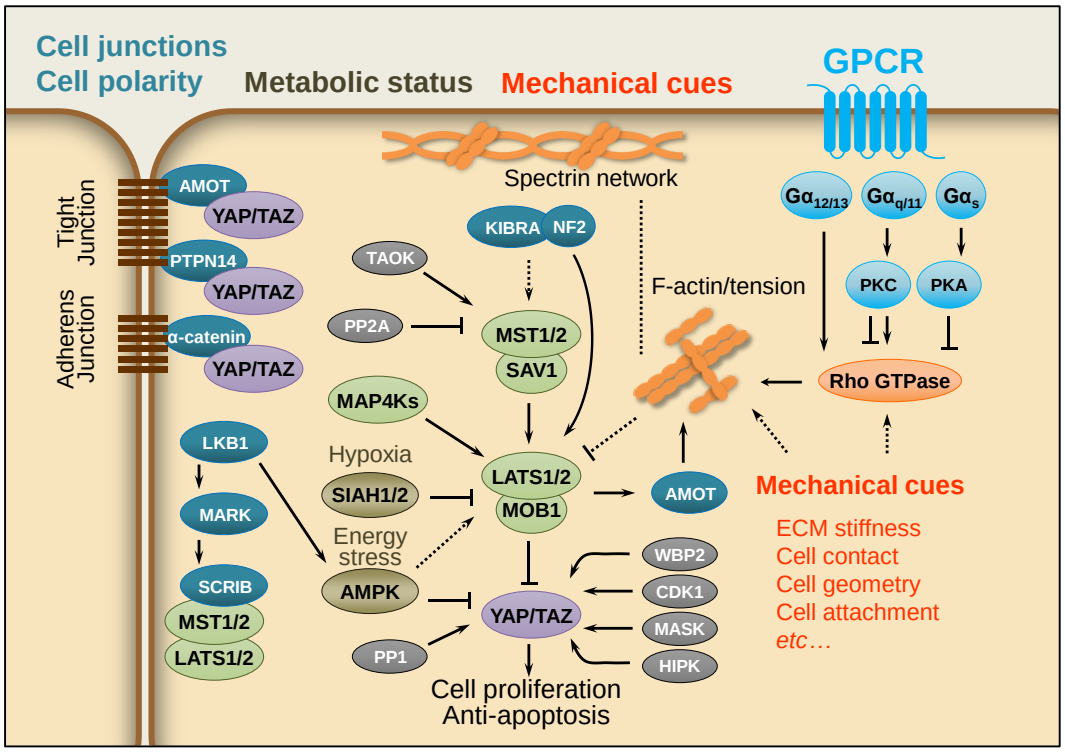

Figure GI-2. Overview of the canonical Hippo pathway.

The Hippo pathway is regulated by various signals: (1) determinants of cell-cell junctions and cell polarity, such as SCRIB, which interacts with MST1/2 and LATS1/2, AMOT, PTPN14, and α-catenin, which sequesters YAP/TAZ to cell junctions; (2) mechanical cues, such as cell contact, stiffness and cell geometry that regulate the Hippo pathway by modulating activity of Rho GTPases, remodeling the actin cytoskeleton, or altering cellular tension; both apical and basolateral spectrin networks function as sensors for mechanical cues in Hippo pathway regulation; (3) soluble extracellular factors, such as ligands for GPCRs, regulate LATS1/2 likely through Rho GTPases and actin dynamics; (4) metabolic state, such as cellular energy and oxygen stress (hypoxia), also regulate Hippo signaling; many other proteins such as protein phosphatase 2A (PP2A), protein phosphatase 1 (PP1), WBP2, CDK1, MASK, and HIPK can also regulate activities of different Hippo pathway components. Arrows, blunt ends, and dashed lines indicate activation, inhibition, and indirect regulation, respectively. Adopted from Yu et al., 2015.

1.1.2 LATS2 in non-canonical Hippo pathway.

As can be inferred from their high homology and similarity in action, LATS2 often shares with LATS1 the substrates of phosphorylation in many cellular context including Hippo signaling, thereby sharing complementary functions each other (Visser and Yang, 2010). On the other hand, the homology of N-terminal region between LATS2 and LATS1 is relatively low; this observation suggests some functional differences between these kinases. Indeed, the insights of the different functions of LATS2 from LATS1 can be seen in previous studies that observed knockout mice for each gene. Although *Lats1* knockout (KO) mice exhibit decrease of body size (Mukai et al., 2015; St John et al., 1999), they are born healthy. In contrast, *Lats2* KO mice exhibit developmental delay and consequent embryonic lethality at E13.5 stage (McPherson et al., 2004; Yabuta et al., 2007). Intriguingly, *Lats2* KO mice show developmental defects in the central nervous system (Yabuta et al., 2007). These findings suggest that Lats2 plays critical roles, which are not shared with Lats1, in other than Hippo pathway. Indeed, as will be described below, some recent works often focused on and reported the differences in many 'non-canonical Hippo' contexts. I summarized some cellular signals that associates with LATS1/2 other than Hippo pathway as follows.

Regulation of cell cycle checkpoints: LATS2 drives G1/S checkpoints to maintain chromosomal stability through TP53 induction by both direct and indirect fashions (Aylon et al., 2006; Aylon et al., 2010; Li et al., 2003). Under various tumorigenic cellular stresses, such as dysfunction of mitotic apparatuses or Ras-mediated oncogenic stress, LATS2 is translocated from centrosome to nucleus to enhance TP53-dependent tumor suppressive signals (Aylon et al., 2006). LATS2 can directory induce

transcription of TP53 gene in concert with TP53 (i.e., LATS2 forms positive feedback loop). Indirectly, nuclear LATS2 inhibits MDM2, which destabilizes TP53 protein through proteasomal degradation processes (Aylon et al., 2010). Intriguingly LATS2 is one of the direct transcription targets of TP53. Thus, LATS2 exerts tumor suppressive ability with TP53 and avoid aneuploidy *via* unknown pathway other than canonical Hippo pathway.

Regulation of mitosis (AuroraA – LATS1/2 – AuroraB pathway): In the initial study, it was revealed that Lats1 associates with the mitotic apparatus by tow-hybrid screening (Hirota et al., 2000). Moreover, observation of *Lats2* KO MEFs revealed that loss of *Lats2* caused mitotic defects (Yabuta et al., 2007). These studies strongly suggest important roles of Lats1/2 in mitotic regulation. Indeed, precise characterization revealed a detailed regulatory cascade. Aurora-A, a central kinase to proceed into mitosis, phosphorylates Lats2 at S83 and S380 at centrosome (Toji et al., 2004). Then phosphorylated Lats2 translocates to central spindle and interacts with Lats1 and Aurora-B. Interestingly, the associating Lats1 can phosphorylate Aurora-B at central spindle to form Aurra-A – Lats2/1 – Aurora-B axis (Yabuta et al., 2011). This axis is indispensable for accurate chromosome segregation, followed by cytokinesis. **(LATS1/2 – CHO1 – LIMK1 pathway)** Another recent study reports fundamental role of LATS1/2 in regulation of cytokinesis (Okamoto et al., 2015). LATS1/2 phosphorylates CHO1, a kinesin-like motor protein, at centrosome. The phosphorylated CHO1 associates with LIMK1. The anchored LIMK1 efficiently phosphorylates cofilin, a downstream substrate to initiate appropriate cytokinesis.

Regulation of DNA damage responses. (CHK1 – LATS2 – P-body pathway) In DNA damage response induced by UV irradiation, two LATS2 specific signal cascades were identified; LATS2 works as a molecular switch which causes different outputs to damaged cells. In relatively low dose of UV irradiation, activated ATR, a signal transducer kinase upon DNA damage, phosphorylates CHK1. Then CHK1 phosphorylates LATS2 at S408 to specialize its function. Phosphorylated LATS2 phosphorylates 14-3-3, a scaffold protein to form and mature P-bodies. Since the P-body (mRNA-processing body) coordinates cellular mRNA and miRNA profile to respond to UV damage, This CHK1 – LATS2 – 14-3-3 – P-body axis contributes to rescue damaged cells (Okada et al., 2011). **(CHK1 – LATS2 – p21 pathway)** On the other hand, in high dose of UV irradiation, CHK1 phosphorylates LATS2 at S835 in its kinase domain. Then LATS2 is fully activated by trans-autophosphorylation of S835. Activated LATS2 next phosphorylates p21 protein, a negative regulator of apoptosis during DNA damage response, at S46 to lead proteasomal degradation. This CHK1 – LATS2 – p21 axis entirely functions to induce programed cell death in extremely damaged cells (Suzuki et al., 2013).

1.1.3 Function of LATS2 as a nuclear effector

In the nucleus, LATS2 performs both kinase-dependent and -independent functions in collaboration with a wide range of transcriptional regulators, including TP53, SNAI1, AR, and CTNNB1/BCL9 (Aylon et al., 2010; Li et al., 2013; Powzaniuk et al., 2004; Zhang et al., 2012), thereby regulating various transcription programs of downstream genes. Importantly, in some signals, LATS2 does not always work in a tumor suppressive manner; LATS2 phosphorylates SNAI1 to promote epithelial to mesenchymal transition (EMT), which is an important process in metastasis (Zhang et al., 2012). Furthermore, LATS2 cooperates with TP53 to maintain appropriate un-differentiated state for initiation of normal development. (Aylon et al., 2014; Qin et al., 2012). Together, LATS2 works as a hub of many cellular signals.

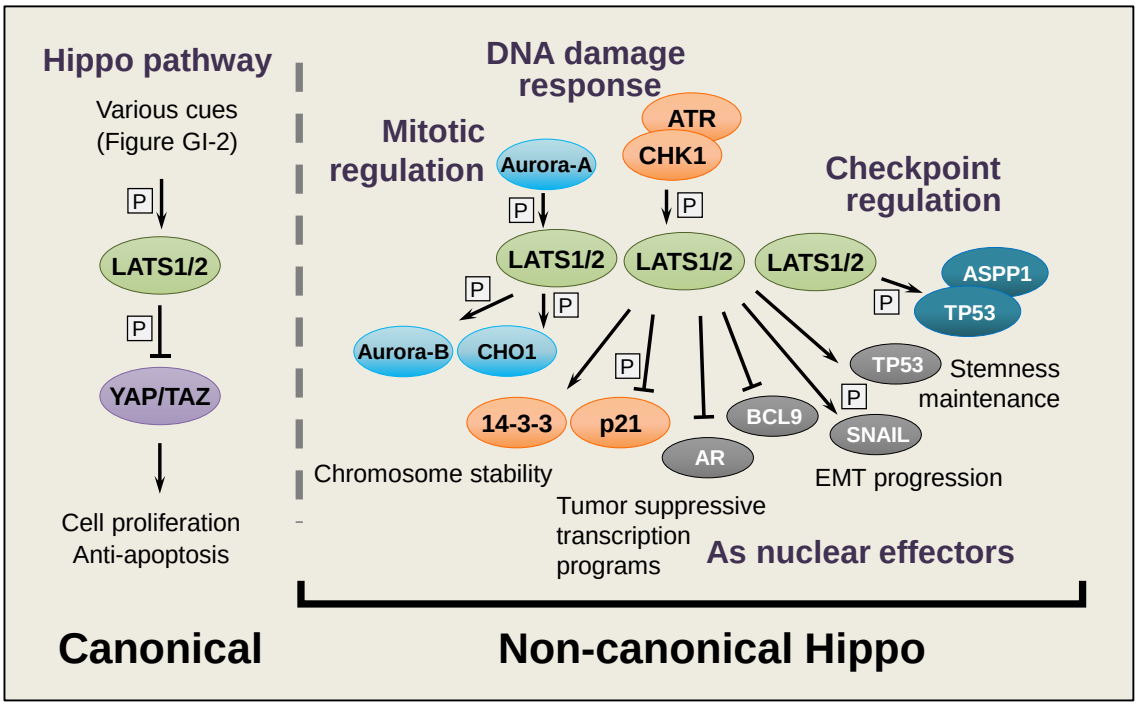

Figure GI-3. Summary of LATS2-ralated cellular signals.

LATS2 (and LATS1) functions as a hub of many cellular signals (mostly in tumor suppressive). The left panel shows the canonical Hippo signal pathway, in which phosphorylation cascades including LATS1/2 end up YAP/YAZ inhibition. The right panel shows LATS1/2 functions which is independent of canonical Hippo pathway, i.e., 'non-canonical Hippo' functions. Arrows, blunt ends indicate activation, inhibition, respectively. 'P' indicates phosphorylation-mediated signal transducing events.

1.1.4 Association of LATS2 with human diseases

Consistent with the LATS2 functions as a tumor suppressor genes not only in the Hippo pathway but also in other signals for maintenance of chromatin stability, LATS2 is often down-regulated in many types of cancers (Yu et al., 2013). In contrast, though LATS2 localizes at 13q11-q12 region, in which a loss of heterozygosity has been frequently observed in many primary cancers, the overall frequencies of genetic mutations or loss of LATS2 is not relatively high (Ishizaki et al., 2002). Down-regulation of LATS2 usually occurs by gene silencing through DNA methylation or over-expression of miRNAs targeting LATS2 mRNA (Jiang et al., 2006; Lee et al., 2009; Mitamura et al., 2014; Yamashita et al., 2012). These facts give us the insight of crucial functions of LATS2 for tumor progression or cell survival through non-tumor suppressive functions. Thus, elucidation of overall LATS2 functions in various cellular contexts is inevitable for understanding of the LATS2-associated tumorigenesis.

Polycomb repressive complexes 2

1.2.1 Epigenetic mechanisms for regulation of gene expression

'Epigenetics' refers to heritable changes in gene expression that does not involve changes to the genomic DNA sequences (Berger et al., 2009). More in the narrow sense, 'epigenetics' refers to changes in gene expression that are caused by biophysical properties of chromatin. Well characterized epigenetic mechanisms through chromatin status are composed of histone modification, DNA methylation and chromatin conformation changes (Figure GI-4). Many types of modification of histone proteins have been identified and characterized their functions for regulation of gene expression (Kouzarides, 2007) (Figure GI-5). DNA methylation occurs at CpG sites (C followed by G) to silence gene expression. Although a novel methylation of nucleotide, 5-hydroxymethylcytosine (5-hmC) was emerged and featured in recent studies, the function of this DNA methylation as an epigenetic signal remains elusive (Plongthongkum et al., 2014). Chromatin conformation is also affects gene expression. Nucleosome positioning or higher order chromatin structure is important for transcription machineries and transcription factors to access and interact with each other on chromatin (Cavalli and Misteli, 2013).

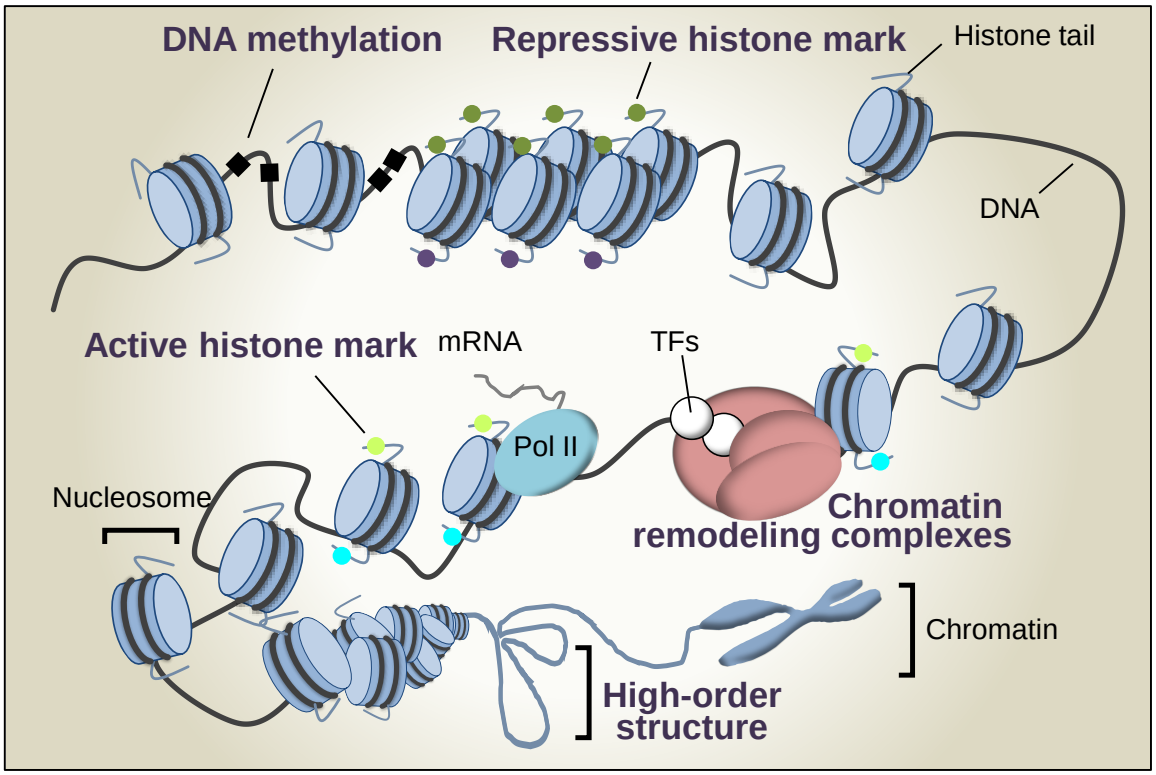

Figure GI-4. Schematic of epigenetic gene regulation.
Epigenetic mechanisms comprise three interrelated layers: DNA methylation, histone posttranslational modifications, and chromatin conformation. (1) DNA methylation (illustrated as black boxes) involves the covalent modification of cytosine in the context of CpG dinucleotides. (2) Posttranslational modifications of the histone tails (illustrated as balls on histone tails) are varied and important for the physical properties and higher-order compaction of chromatin. (3) Chromatin conformation have recently emerged as important regulators of chromatin structure and gene expression. Adopted from Bruneau, 2010.

The dynamic transition and appropriate patterning of epigenetic landscape (epigenome) are crucial for cell homeostasis and normal development; indeed, dysregulation of epigenetic mechanisms and epigenome are often observed in human diseases including cancer (Timp and Feinberg, 2013). Furthermore, recent study reported that epigenetic abnormality initiates tumor formation by itself without any genomic aberrations (Ohnishi et al., 2014).

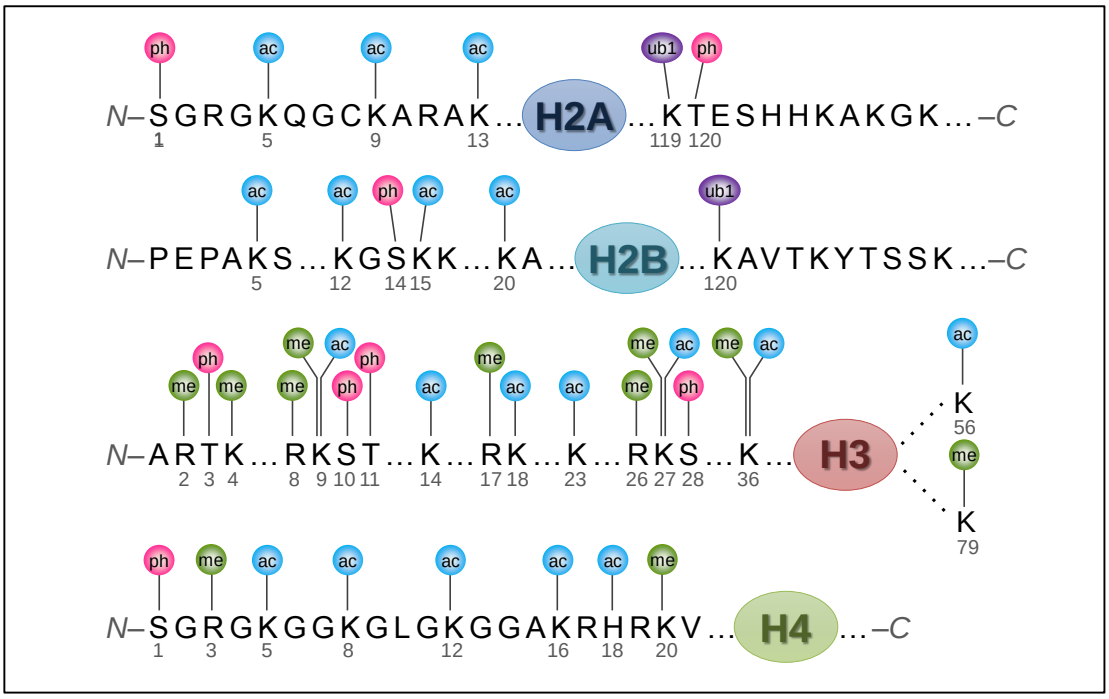

Figure GI-5. Schematic of the most common histone modifications.
Histone modifications usually occur on the N-terminal tails of histones (i.e., 'histone tail') but also on the C-terminal tails and globular domains, e.g., ubiquitination of the C-terminal tails of H2A and H2B and acetylation and methylation of H3 at K56 and K79, respectively. ph; phosphorylation, ac; acetylation, me; methylation, ub1; mono-ubiquitination.

1.2.2 General features of Polycomb repressive complex 2

Polycomb repressive complexes consist of many series of nuclear proteins which mainly regulate gene silencing. PRC2 catalyzes di- and tri-methylation of histone H3 at lysine 27 (H3K27me2/3) and forms Polycomb domains involved in gene silencing (Cao et al., 2002; Czermin et al., 2002; Kuzmichev et al., 2002; Müller et al., 2002). PRC2 is composed of three core components, EZH2, EED, and SUZ12, along with accessory factors including RbAp46/48 and AEBP2 (Figure GI-6). PRC2-mediated gene silencing plays an important role in maintenance of stemness, and its dynamic transition to appropriate patterns is essential for establishment of tissue-specific epigenetic landscapes and their associated transcriptional programs (Margueron and Reinberg, 2011; Schuettengruber and Cavalli, 2009). Because epigenetic alterations affect expression of multiple transcriptional regulators, including transcription factors and non-coding RNAs, epigenetic disorders have been implicated in many human diseases. Indeed, PRC2 is dysregulated in several types of cancers (Bracken and Helin, 2009). Thus, PRC2 and its epigenetic dependent signatures represent

promising therapeutic targets for tumors with specific mutations or alterations (Helin and Dhanak, 2013; Kondo, 2014). Recent studies uncovered precise post-translational regulation of PRC2 components and the molecules with which they collaborate, including non-coding RNAs (Cifuentes-Rojas et al., 2014; Kaneko et al., 2014; Zhao et al., 2010). Moreover, PRC2 interacts with other types of epigenetic modifications such as H3K4me3, H2AK119ub, H3K36me3 and methylated CpG, and forms complicated networks and hierarchy to regulate cellular properties that depends on cellular contexts (Margueron and Reinberg, 2011).

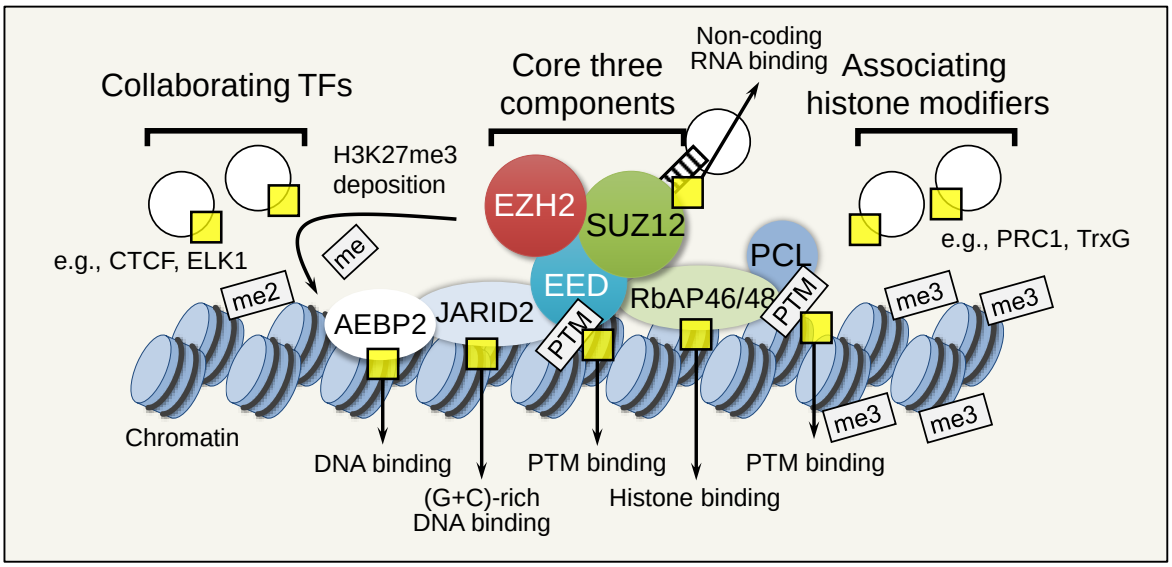

Figure GI-6. Regulation of PRC2 functions by transcription factors, ncRNAs, collaborating elements and protein complexes.

PRC2 is composed of three essential core components, EZH1/2, SUZ12 and EED. Di/tri-methyltransferase activity and its specificity are regulated by complicated mechanisms. PTM; posttranslational modifications of histone proteins, me2/3; di/tri-methylated histone tail, TFs; transcription factors. Yellow boxes represents some molecular interactions which can support PRC2 functions. Adopted from Margueron and Reinberg, 2011.

1.3 Epigenetic integrity and human cancer therapies

Cancer has been known as the disease of genome; dysregulation of oncogenes or tumor suppressors by amplification or mutation and so on, cause disorganized proliferation of cells. These abnormalities of cellular signals for tumor progression should be recovered or reduced by inhibition of responsible signals. Indeed, many traditional anticancer drugs, such as small chemicals and/or bio-molecules have been designed and implemented. In contrast, recent studies reported that epigenomic

landscape and its regulatory enzymes, which can define aberrant gene expression pattern like cancer, alone initiate tumor formations and associate with bad outcomes. From these viewpoints, a lot of small molecules that inhibit the regulatory enzymes of epigenetic machineries including PRC2, have been featured (Kondo, 2014). Meanwhile, because epigenetic integrity is also crucial for the cellular functions of normal tissue, currently available drugs that are indicated for certain types of cancers with tumor-driving mutations in PRC2 cannot be applied to treatment of other types of cancers (Kim et al., 2013; Knutson et al., 2014; Knutson et al., 2012; Konze et al., 2013; McCabe et al., 2012; Qi et al., 2012). In this context, it is essential to elucidate the pertinent upstream signals and their spatiotemporal regulation at the molecular level.

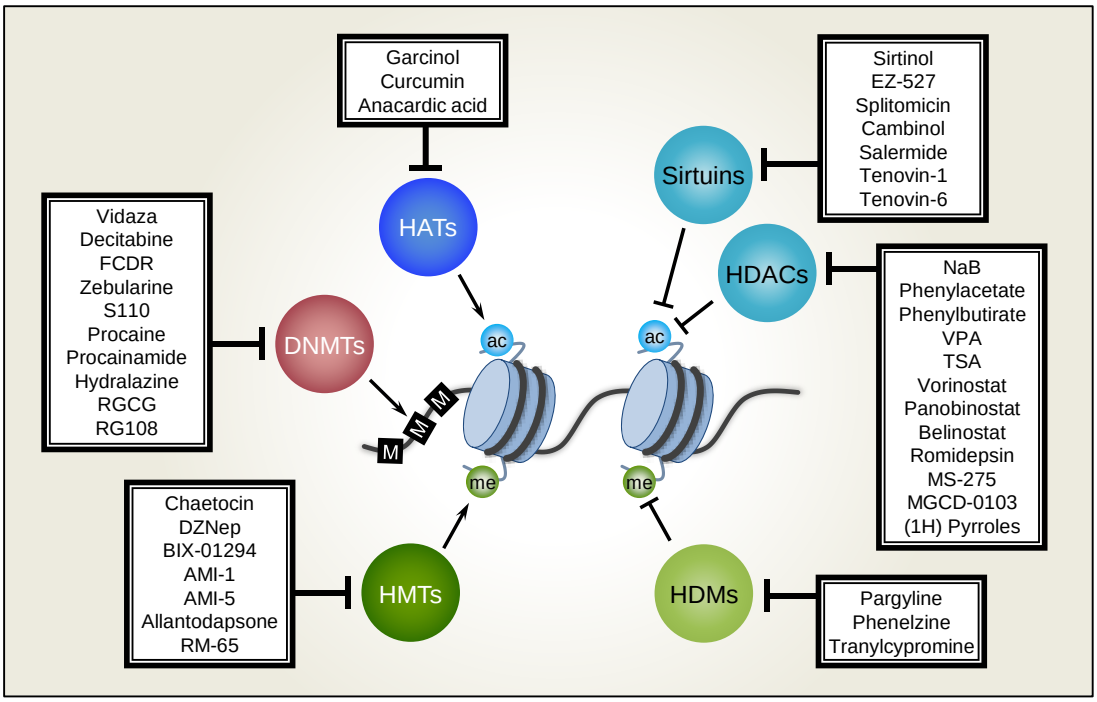

Figure GI-7. Epigenetic drugs for cancer therapy.
Some major epigenetic regulators and chemicals which inhibit their functions are illustrated. ac; histone acetylation, me; histone methylation, M; DNA methylation. Drug discovery for target and regulate epigenetic mechanisms is recent trend in oncology. Adopted from Rodríguez-Paredes and Esteller, 2011

Goal of this study

The overall goal of this thesis is to discover the novel LATS2-dependent cellular signals and reveal their biological significance including human diseases such as cancer. As indicated above, many substrates of phosphorylation by LATS2 (and/or LATS1) kinase have been identified and

characterized in variety of cellular contexts. These fine previous works mainly have been achieved by bottom-up style approaches in which core finding of novel kinase-substrate interactions are extended to physiological functions such as tumor cell death. By contrast, in this thesis, I conducted omics-based approaches which attempt to extract the novel LATS2-dependent cellular signals using transcriptome and epigenome data derived from *LATS2*-defficient human cancer cells.

In the first part of this thesis, I discovered the functional correlations of *LATS2* KO with dysregulation of PRC2, which is responsible for H3K27me3-mark of histone modifications and plays important roles in normal development and stemness maintenance of certain tissues. I tried to characterize functional linkage between LATS2 and PRC2, and biological relevance including human cancer. At the end of this thesis, I will suggest a novel possible strategy which can expand the limitation of today's epigenetic drug discovery.

2. Materials and methods

Cell culture and drug treatment

Lats2-deficient MEFs were described in previous study (Yabuta et al., 2007). MEFs, HeLa-S3, MCF7, and MDA-MB231 cells were cultured in DMEM containing 10% FBS and antibiotics (streptomycin and penicillin) at 37°C in a 5% CO2/95% air atmosphere.

Drug treatment

Cells were treated with 2 μM 5-aza-2'-deoxycytidine (5-aza-dC) (Sigma-Aldrich, St. Louis, MO, USA) for 72 h, trichostatin A (TSA) (Sigma-Aldrich, St. Louis, MO, USA) at 100 nM for 24 h, and 5 μM 3-Deazaneplanocin A (DZNep) (Cayman Chemical Company, Ann Arbor, MI, USA) for 72 h. For 5-aza-dC treatment, the medium was replaced with medium containing freshly added 5-aza-dC every 24 h. For co-treatment of cells with 5-azaC and TSA, 5-aza-dC was added for 48 h, followed by TSA for 24 h.

Generation of TALEN-mediated *LATS2* KO HeLa-S3 cell line

The ORFs of TALEN that target the human *LATS2* locus (Forward: hg19_chr13:21,620,130-21,620,148, and Reverse: hg19_chr13:21,620,095-21,620,113) were synthesized by GeneArt (Thermo Fisher Scientific, Waltham, MA, USA). The Bowtie software was used to confirm that the target sites were unique in the human genome (hg19). The coding region in this entry clone was sub-cloned into an expression vector, pDEST26 (Thermo Fisher Scientific, Waltham, MA, USA), using the Gateway technology. The two resultant expression constructs were transfected into HeLa-S3 cells using Lipofectamine 2000 (Thermo Fisher Scientific, Waltham, MA, USA). Two days after transfection, the transfectant pool was diluted in 96-well plates, and then clones derived from single cells were expanded as candidate KO cell lines. Successful KO of *LATS2* was validated by endonuclease assay, Sanger sequencing of the target locus, and immunoblotting analysis. The KO clone which is the most compatible with LATS2 knockdown was used for downstream analyses. Primers used were listed in Table M1.

Table M1. Primer sequences For genomic sequencing of *LATS2* locus.

Primer name	5' to 3'
HsLATS2-TAL-AscI-Fw	GTCGGCGCGCCAGCATTTTGGGACAGCCGTA
HsLATS2-TAL-NotI-Rv	ATTGCGGCCGCCATGTTGCTCAACCCTCCCA

Generation of add-back rescued cell lines of *LATS2* KO HeLa-S3 cell

The expression constructs, which were coding LATS2 wild-type or kinase-dead (KD, K698M) (Okada et al., 2011) were transfected into LATS2 *KO* HeLa-S3 cells using Lipofectamine 2000 (Thermo Fisher Scientific, Waltham, MA, USA). After two weeks of 800 μg/ml G418 (Nacalai Tesque, Kyoto, Japan) selection, clones derived from single cells were expanded as candidate add-back clones. Stable expression of exogenous LATS2 gene was validated by western blotting analysis.

Plasmids

3xFLAG and 6xMYC-tagged human LATS2 WT and KD were described in previous studies (Okada et al., 2011; Suzuki et al., 2013). pcDNA3.1-human LATS2 WT and KD plasmids for generation of stable expressing cell lines were constructed by sub-cloning each ORF into pcDNA3.1+AscI, a modified version of pcDNA3.1(+). cDNA of human EZH2 was PCR amplified from HEK293T cDNA pool and ligated into the *Asc*I and *Not*I sites of p3Flag+AscI, a modified version of p3xFLAG-CMV-7.1. All PCR amplified sequences were confirmed by Sanger DNA sequencing.

Antibodies

The antibodies used in this study was summarized in Table M2. CST; Cell Signaling Technology, Bethyl; Bethyl Laboratories, Sigma; Sigma-Aldrich. MBL; Medical & Biological Laboratories.

Table M2. Antibodies used in this study.

Manufacturer	Code	Product name
CST	#5246S	Ezh2 (D2C9) XP® Rabbit mAb
Active Motif	39875	EZH2 antibody (mAb)
CST	#3737S	SUZ12 (D39F6) XP® Rabbit mAb
Millipore	17-10034	ChIPAb+ EED - ChIP Validated Antibody
CST	#9733	Tri-Methyl-Histone H3 (Lys27) (C36B11) Rabbit mAb
Millipore	05-623	Anti-RNA polymerase II Antibody, clone CTD4H8
Abcam	ab6002	Anti-Histone H3 (tri methyl K27) antibody - ChIP Grade
Active Motif	39156	Histone H3K27me3 antibody (pAb)
CST	#5327S	Di/Tri-Methyl-Histone H3 (Lys9) (6F12) Mouse mAb
CST	#9751S	Tri-Methyl-Histone H3 (Lys4) (C42D8) Rabbit mAb
CST	#4499	Histone H3 (D1H2) XP® Rabbit mAb
CST	#4353	Acetyl-Histone H3 (Lys27) Antibody
Abcam	ab1791	Anti-Histone H3 antibody - ChIP Grade

Bethyl	A300-479A	Rabbit anti-LATS2 Antibody, Affinity Purified
CST	#3477S	LATS1 (C66B5) Rabbit mAb
Santa Cruz	sc-751	Cyclin A (H-432)
Sigma	T5168	Monoclonal Anti-α-Tubulin, clone B-5-1-2
MBL	M047-3	Anti-Myc-tag mAb
Sigma	F3165	ANTI-FLAG M2 Monoclonal Antibody, Purified IgG
CST	2729S	Normal Rabbit IgG
Millipore	12-371	Normal Mouse IgG

Western blotting analysis

For western blotting, protein samples were prepared by lysing cells in RIPA lysis buffer (50 mM Tris-HCl (pH 8.0), 150 mM NaCl, 0.5% (w/v) sodium deoxycholate, 0.1% (w/v) SDS, and 1.0% (w/v) Nonidet P-40, plus protease and phosphatase inhibitors). Equal amounts of proteins from cell lysates were denatured in sample buffer, subjected to SDS-PAGE, and transferred to PVDF membranes (GE Healthcare, Little Chalfont, UK). The membranes were blocked in 5% nonfat milk or BSA in TBS-T at room temperature for 1 h with gentle shaking. The membranes were then immunoblotted with specific primary antibodies and horseradish peroxidase-conjugated secondary antibodies (Cell Signaling Technology, Danvers, MA, USA), and then visualized with Western Lightning Plus-ECL (PerkinElmer, Waltham, MA, USA). The ratios of the band intensities were determined by ImageJ software using X-ray films with non-saturated signals between the samples.

In vitro kinase assay

Recombinant EZH2/EED/SUZ12/RbAp48/AEBP2 complex (BPS Bioscience, San Diego, CA, USA) (700 ng) was incubated with 100 ng of recombinant LATS2 or LATS1 kinases (Carna Biosciences, Hyogo, Japan) at 30°C for 30 min with kinase reaction buffer (5 mM MOPS-NaOH [pH 7.2], 5 mM MgCl2, 1 mM EGTA, 0.4 mM EDTA, 5 mM glycerol 2-phosphate, 50 μM DTT, and 50 μM ATP). For protein phosphatase (PPase) assay, 200 U of λ-PPase (New England Biolabs, Ipswich, MA, USA) was added to the kinase reaction tube. Each reaction was carried out in a 25 μL volume. The reaction was stopped by addition of 4× Laemmli sample buffer. Proteins were separated by SDS-PAGE in gels containing 50 μM Phos-tag acrylamide (WAKO, Osaka, Japan) and subjected to western blotting.

In vivo kinase assay

To verify the effects of LATS2 kinase activity on the phosphorylation state of EZH2 in living cells, FLAG-tagged human EZH2 was transiently overexpressed in each add-back cell line using

Lipofectamine and PLUS reagents (Thermo Fisher Scientific, Waltham, MA, USA). Whole protein lysates were extracted 48 h after transfection. Proteins were separated by SDS-PAGE in gels containing 50 μM Phos-tag acrylamide (WAKO, Osaka, Japan) and subjected to immunoblotting as described above.

Chromatin fractionation and co-immunoprecipitation

Preparation of the chromatin-associated protein fractionation was performed as described previously (Boulay et al., 2011). Briefly, cells were harvested and lysed for 45 min on a rotator at 4°C in buffer A (50 mM Tris-HCl [pH 7.5], 1 mM DTT, and 0.5% Triton X-100, supplemented with 1× protease inhibitor cocktail containing no EDTA [Roche Life Science, Indianapolis, IN, USA]). After centrifugation at 1,800 g at 4°C for 10 min, pellets were washed twice with buffer A, resuspended in buffer B (50 mM Tris-HCl [pH 8.0] and 1.5 mM CaCl2), and finally treated with 30 units of micrococcal nuclease (Takara Bio, Shiga, Japan) for 35 min at 37°C under mild agitation. Solubilized proteins were clarified by two rounds of centrifugation at 5,000 g at 4°C for 2 min. Before immunoprecipitation, the chromatin fraction was adjusted to a final concentration of 150 mM NaCl and 0.5% Triton X-100. Equal amounts of solubilized chromatin were incubated with each primary antibody at 4°C overnight, followed by addition of 30 μL of Dynabeads M-280 Sheep Anti-Mouse/Rabbit IgG (Thermo Fisher Scientific, Waltham, MA, USA) that had been pre-blocked with 5% BSA in IP buffer. The beads were washed four times with TBS containing 0.1% Triton X-100 and 0.25% Nonidet P-40. Finally, purified proteins were eluted in 1× Laemmli buffer and subjected to western blotting.

In vitro histone methyltransferase assay

Histone methyltransferase activity (HMTase) assay was performed using immunoprecipitated EZH2 and its coprecipitates. Briefly, native chromatin of each sample was extracted as described for ChIP-qPCR below, without fixation procedures. Appropriate amounts of solubilized chromatin were incubated with 2 μg of anti-EZH2 antibody (Active Motif, Carlsbad, CA, USA) and 20 μL of Dynabeads M-280 Sheep Anti-Mouse IgG (Thermo Fisher Scientific, Waltham, MA, USA) at 4°C for 4 h. The beads were washed two times with ChIP buffer (10 mM Tris-HCl [pH 8.0], 200 mM KCl, 1 mM CaCl2, 0.5% Nonidet P-40), two times with Wash buffer (10 mM Tris-HCl [pH 8.0], 500 mM KCl, 1 mM CaCl2, 0.5% Nonidet P-40), once with HMT buffer (20 mM phosphate buffer [pH 7.4], 0.05% Tween-20). The immunoprecipitated protein was incubated with 1 μg of recombinant histone H3.1 protein (New England Biolabs, Ipswich, MA, USA) as substrates and 40 μM S-

adenosylmethionine (SAM; New England Biolabs, Ipswich, MA, USA) as the methyl donor in a mixture of 30 μl of HMT buffer, at 30 °C for 3 h. The reaction was stopped by addition of 4× Laemmli sample buffer. Proteins were separated by SDS-PAGE and subjected to western blotting. Each western blotting signal was quantified by ImageJ software as described above. Then the H3K27me3 level was normalized by the signal of imunoprecipitated EZH2 protein.

Rescue of *LATS2* KO by transient expression of LATS2 and/or EZH2

MYC-tagged LATS2 and/or FLAG-tagged EZH2 were transiently overexpressed in *LATS2* KO HeLa-S3 cells using Lipofectamine and PLUS reagents (Thermo Fisher Scientific, Waltham, MA, USA). To evaluate the synergetic effects and the dose dependency of LATS2, the amount of co-transfected LATS2-plasmid was continuously increased up to the amount used for LATS2 transfection alone. Whole-cell lysates were extracted 48 h after transfection and analyzed by western blotting. Primers used for cloning of human *EZH2* were listed in Table M3.

Table M3. Primer sequences For cloning of human *EZH2*.

Primer name	5' to 3'
HsEZH2-AscI-Fw	TATGGCGCGCCTATGGGCCAGACTGGGAAG
HsEZH2-NotI-Rv	ATACTCGAGCGGCCGCTCAAGGGATTTCCATTTCTCTTTC

Cell-cycle analysis

HeLa-S3 cells were synchronized by the double thymidine-block method and collected at various time points. A portion of the cells was fixed by incubating cells in cold 70% (w/v) ethanol at 4°C for 30 min with brief vortexing. The fixed cells were washed with PBS (-), treated with a propidium iodide solution containing RNase A, and sorted on a FACSCalibur flow cytometer (Becton Dickinson, Franklin Lakes, NJ, USA) using the CellQuest software. Total RNA and whole protein lysates were extracted from the remaining cells using QIAzol and the RNeasy Mini Kit. Each sample was subjected to RT-qPCR analysis and western blotting.

RT-qPCR

To quantitate expression of each gene, total RNAs were extracted from cell cultures by direct lysis of cells on dishes using the QIAzol Lysis Reagent (Qiagen, Hilden, Germany), followed by RNA purification using RNeasy Mini Kits or miRNeasy Mini Kits (Qiagen, Hilden, Germany). cDNAs were synthesized using the High-Capacity cDNA Reverse Transcription Kit (Thermo Fisher

Scientific, Waltham, MA, USA). Quantitative-PCR analysis was performed on a 7900HT Fast Real-Time PCR System (Thermo Fisher Scientific, Waltham, MA, USA), using SYBR Premix Ex Taq II (Tli RNase H Plus) and Premix Ex Taq™ (Perfect Real Time) (Takara Bio, Shiga, Japan) for the SYBR Green method and TaqMan assays (Takara Bio, Shiga, Japan), respectively. Detailed sequences of the primer sets and the Assay IDs of the TaqMan assays used in this study are provided in the Table M4 and M5.

Table M4. Primer sequences For RT-qPCR.

Primer name	5' to 3'
HsGapdh-Fw	TCTCCTCTGACTTCAACAGCGAC
HsGapdh-Rv	CCCTGTTGCTGTAGCCAAATTC
HsACTB-Fw	ATGTGGCCGAGGACTTTGATT
HsACTB-Rv	AGTGGGGTGGCTTTTAGGATG
HsLATS2-Fw	AGATTTCGGCCTCTGCACTG
HsLATS2-Rv	TAGGGTCTTCAGCCTGTCCC
HsCTGF-Fw	AATGCTGCGAGGAGTGGGT
HsCTGF-Rv	CGGCTCTAATCATAGTTGGGTCT
HsSUZ12-Fw	TGGGAGACTATTCTTGATGGGAAG
HsSUZ12-Rv	GGAGCCGTAGATTTATCATTGGTC
HsEZH2-Fw	GGGACAGTAAAAATGTGTCCTGC
HsEZH2-Rv	TGCCAGCAATAGATGCTTTTTG
HsEED-Fw	TCTTACGTGGATGCTGATGC
HsEED-Rv	ATAGCATTTCCATGGCCAAC

Table M5. TaqMan probes used in this study.

Gene name	Assay ID
HsKRT17	Hs01588578_m1
HsHOXA11	Hs00194149_m1
HsFBXO32	Hs01041408_m1
HsIGFBP3	Hs00426289_m1

Microarray analysis

Microarray analyses for coding genes and microRNAs were performed as single-color or two-color hybridizations using Agilent Whole Human/Mouse Genome Oligonucleotide Microarrays (Agilent Technologies, Santa Clara, CA, USA) as described in previous work (Funato et al., 2010). Agilent

Feature Extraction software ver. 10.5.1 (Agilent Technologies, Santa Clara, CA, USA) was used to assess spot quality and extract feature intensity statistics. The Subio Platform ver. 1.18 and Subio Basic Plug-in (Subio, Kagoshima, Japan) were used to calculate fold changes between samples. Briefly, to obtain the list of high-confidence expressing genes upon LATS2 knockown, the spots with wellAboveBG-FLAG = TRUE in each sample group, which mean that these probes are distinguishable from the local background signal across samples were filtered. Additional fold change of 1.4 was applied to generate final list of the differentially expressed genes. For *Lats2* KO MEFs, fold change of 2.0 and $p < 0.05$ (t-test) was applied to determine the differentially expressed genes. The microarray data were deposited in the Gene Expression Omnibus (www.ncbi.nlm.nih.gov/geo) under accession number GSE63538.

Library preparation and RNA-sequencing

Poly(A)+ RNA was isolated with Nucleo-Trap mRNA kit (Macherey-Nagel, Düren, Germany) and double strand cDNA synthesis was carried out using the double-stranded cDNA using SuperScript double-Stranded cDNA synthesis kit (Thermo Fisher Scientific, Waltham, MA, USA) according to manufacturer's instructions. Each double-stranded cDNA (120 ng) was sheared to ~400 bp fragments using an S220 ultrasonicator (Covaris, Woburn, MA, USA) with the following parameter settings: peak incident power, 140 W; duty factor, 10%; cycles per burst, 200; and treatment time, 55 seconds. The resulting DNA fragments were purified using 0.7× volume Agencourt AMPureXP beads (Beckman Coulter, Brea, CA, USA). Illumina libraries were prepared using the KAPA Library Preparation Kit (Kapa Biosystems, Wilmington, MA, USA) and TruSeq adaptors (Illumina, San Diego, CA, USA). Paired-end sequencing (151 bp × 2) of each sample was performed on a HiSeq2500 (Illumina, San Diego, CA, USA).

RNA-seq data analysis

Raw images were processed using Real Time Analysis ver. 1.17.21 (Illumina, San Diego, CA, USA), and conversion to fastq file format was performed using CASAVA ver. 1.8.2 (Illumina, San Diego, CA, USA). Btrim (http://graphics.med.yale.edu/trim/readme) was used to trim low-quality regions of raw reads. The trimmed reads were mapped onto the reference human genome (hg19) using TopHat ver. 2.0.11 in combination with Bowtie ver. 2.2.2 and SAMtools ver. 0.1.19 (Li et al. 2009). Gene expression was quantitated with Cufflinks ver. 2.2.1 (Trapnell et al. 2010). To obtain the list of differentially expressed genes upon *LATS2* KO, hg19 refSeq genes were filtered out by fold change of 2.0 and $p < 0.05$ (t-test).

ChIP-qPCR

Cells were cultured in 10 cm plates to approximately 80% confluence. Formaldehyde (Nacalai Tesque, Kyoto, Japan) was added directly to the culture medium to a final concentration of 0.5%. Crosslinking was allowed to proceed for 5 min at room temperature, and the formaldehyde was neutralized with glycine at a final concentration of 0.125 M for 5 min. After washing twice with ice-cold PBS (-), cells were collected, pelleted, resuspended in swelling buffer (25 mM HEPES [pH 7.8], 1.5 mM MgCl2, 10 mM KCl, 0.1% (w/v) Nonidet P-40, and 1 mM DTT, plus protease and phosphatase inhibitors), and incubated for 10 min on ice. Nuclei were released by subjecting the samples to 30 strokes in a Dounce homogenizer, collected, and resuspended in sonication buffer (50 mM HEPES [pH 7.9], 140 mM NaCl, 1 mM EDTA, 1% [w/v] Triton X-100, 0.1% [w/v] sodium deoxycholate, and 0.1% SDS, plus protease and phosphatase inhibitors). Samples were sonicated in a Tomy UD-201 (TOMY SEIKO, Tokyo, Japan) for five cycles of 1 min each (50% duty, output level 2) separated by intervals of 1 min. Sonicated samples were clarified by spinning at 18,000 g at 4°C for 10 min. Equal amounts of sheared chromatin were incubated with each primary antibody at 4°C overnight, followed by addition of 30 μL of Dynabeads M-280 Sheep Anti-Mouse/Rabbit IgG (Thermo Fisher Scientific, Waltham, MA, USA) that had been pre-blocked with 5% BSA in sonication buffer. The beads were washed twice each with sonication buffer, high-salt wash buffer (sonication buffer containing 500 mM NaCl), LiCl wash buffer (20 mM Tris [pH 8.0], 1 mM EDTA, 250 mM LiCl, 0.5% [w/v] Nonidet P-40, and 0.5% [w/v] sodium deoxycholate), and TE buffer (10 mM Tris [pH 8.0] and 1 mM EDTA). Immunoprecipitates were incubated at 65°C in elution buffer (50mM Tris-HCl [pH 8.0], 10 mM EDTA, and 1% [w/v] SDS) for 30 min, and then treated with 2 μg of Proteinase K (Sigma-Aldrich, St. Louis, MO, USA) overnight for de-crosslinking. Eluate was purified using the ChIP DNA Purification Kit (Active Motif, Carlsbad, CA, USA). For quantitation, ChIP DNA and input genomic DNA were subjected to qPCR on a 7900HT Fast Real-Time PCR System (Thermo Fisher Scientific, Waltham, MA, USA), using SYBR Premix Ex Taq II (Tli RNase H Plus) and Premix Ex Taq™ (Perfect Real Time) (Takara Bio, Shiga, Japan). Primers used were listed in Table M6.

Table M6. Primer sequences For ChIP-qPCR.

Primer name	5' to 3'
HsGAPDH_ChIP_pro-Fw	TACTAGCGGTTTTACGGGCG
HsGAPDH_ChIP_pro-Rv	TCGAACAGGAGGAGCAGAGAGCGA
HsMYT1_ChIP-Fw	ACAAAGGCAGATACCCAACG

HsMYT1_ChIP-Rv	GCAGTTTCAAAAAGCCATCC
HsF2R_ChIP-Fw	TTTAGGGGCAACCCTGTCAC
HsF2R_ChIP-Rv	ACCGGCAAAGTTCAGTTTTCG
HsZBTB16_ChIP-Fw	GATGGGGGACAAGGTTGAGG
HsZBTB16_ChIP-Rv	TGTAGCTCCCTAGCACTGGT
HsWNT10B_ChIP-Fw	GTCTCCCCACGGTTTAAGCA
HsWNT10B_ChIP-Rv	TCCCTGCTTTCCCAGGTCTA
HsKCNH3_ChIP-Fw	CACATTGCTCAGGACACCCT
HsKCNH3_ChIP-Rv	CTGCAGCAGGTGTGAGTACA
HsTPPP3_ChIP-Fw	CAGGGGAGGTCTGAGGTGTA
HsTPPP3_ChIP-Rv	TGGGGGCTGTAGAGTTACGA
HsTMEM59L_ChIP-Fw	CTCCAGTAGTTGACGGGCTG
HsTMEM59L_ChIP-Rv	GTATCGGCCCCTTATCGCAA
HsLHX2_ChIP-Fw	CACCAGAGCCATTTAGGCCA
HsLHX2_ChIP-Rv	TTCCATTTCTGGGCGGTTCA
HsHRK_ChIP-Fw	GGGTCAGGTTTCTAGCCAGG
HsHRK_ChIP-Rv	ACCCAACTTGCCTCGTTTCA

ChIP-sequencing

ChIP DNA and input DNA ends were repaired using T4 DNA polymerase, Klenow enzyme, and T4 polynucleotide kinase (PNK) (New England Biolabs, Ipswich, MA, USA), followed by treatment with Klenow exo- to add an A base to the 3'-end. After ligation of the Genomic Adaptor Oligo Mix (Illumina, San Diego, CA, USA) using TaKaRa Ligation Mix (Takara Bio, Shiga, Japan), the adaptor-ligated DNA fragments were amplified with Paired-End Sample Prep Oligo primers (Illumina, San Diego, CA, USA) for 18 cycles. The amplified library was separated on a 2.0% agarose gel, and the samples were purified using the QIAquick MinElute kit (Qiagen, Hilden, Germany) after each preparation step. The purified library was used for cluster generation and sequencing analysis on a HiSeq 2000 (Illumina, San Diego, CA, USA). The raw Illumina sequencing data are available from the Gene Expression Omnibus database (www.ncbi.nlm.nih.gov/geo) under accession number GSE63538.

ChIP-seq data analysis

Sequence reads for H3K27me3, H3K4me3, and input were aligned to the human genome (hg19) using the Bowtie software (parameter: -v 3 –m 1) (Langmead et al., 2009). The MACS software ver. 1.4.1 was used for peak detection of each histone mark (Feng et al., 2012). The parameters for MACS

were '--nomodel --extsize 146 --broad --to-large --pvalue 1e-3', and the other parameters were the software defaults. Genes were called in association with a given chromatin mark only when peaks were called within ±5 kb of the TSS. To calculate normalized depth around TSSs of all RefSeq genes, and to perform GO analysis of the called genes, the Homer software was used with the default settings (Heinz et al., 2010). P-values were corrected by the FDR (q-value) correction by R for multiple comparisons. To visualize normalized ChIP profiles in genome browser, BigWig files were generated using custom scripts and visualized using the IGV software from the Broad Institute (Thorvaldsdóttir et al., 2013).

Immunofluorescence imaging

Exponentially growing HeLa-S3 cells were plated on coverslips and fixed for 15 min at room temperature in 4% formaldehyde in PBS, 0.1% Triton X-100 in PBS (-), and 0.05% Tween-20 in PBS. Fixed cells were rinsed three times in 1× PBS for 5 min each. To visualize H3K27me3 and RNAPII, cells were blocked in blocking buffer (1× PBS, 5% FBS and 0.3% Triton X-100) for 60 min, then incubated with anti-H3K27me3 (Cell Signaling Technology, Danvers, MA, USA) and anti-RNA polymerase II clone STD4H8 (Millipore, Billerica, MA, USA) antibodies, followed by incubation with Alexa Fluor 488 and 594 (Thermo Fisher Scientific, Waltham, MA, USA)-conjugated anti-rabbit/mouse IgG in 1× PBS containing 1% BSA and 0.3% Triton X-100. DNA was stained using Hoechst 33258 (Sigma-Aldrich, St. Louis, MO, USA), and cells were observed on a FluoView FV10i microscope (Olympus, Tokyo, Japan).

Statistical analysis by NextBio

For meta-analysis and exploration of massive preprocessed omics data (reported in previous studies) that showed significant correlation with my own data, each processed omics dataset was uploaded into the NextBio enterprise software (Illumina, San Diego, CA, USA), and the statistical significance of the relationships was evaluated as reported previously (Kupershmidt et al., 2010). For Canonical pathway enrichment analysis, p-values were corrected by the FDR (q-value) correction by R.

GSEA

To determine whether gene sets of interest were statistically enriched in sets of up- and down-regulated genes, I analyzed my non-redundant list of genes using the GSEA 2.0 program for pre-ranked lists (Subramanian et al., 2005). The gene sets used were obtained from Broad Molecular Signatures Database (MSigDB), as well as my custom .gmx files from previous studies.

Promoter classification

To classify human coding genes by the CG status of their promoters, human coding gene IDs were obtained from Ensembl database. Genes >3 kb in length, with no other genes within 500 bp of their TSSs, were used for the promoter analysis. A BED format file of the filtered genes' promoters (from -1200 bp to +300 bp relative to the TSS) was generated, and each promoter region was divided into 500 bp sliding windows (5 bp offset), and the CpG ratio and CG% were calculated using Bedtools (Quinlan and Hall, 2010). Next, each promoter was classified into one of three types according to the criteria described in previous studies (Mikkelsen et al., 2007). The resultant lists of genes were uploaded into the NextBio platform and subjected to successive statistical analyses. For statistical analysis of RNA-seq data, fold changes were calculated for each actively transcribed gene, and then the Wilcoxon rank-sum test was performed to evaluate statistical significance.

Analysis of TCGA data

To visualize expression patterns of LATS1 and LATS2 genes in many types of human cancers, PANCAN normalized RNA-seq data from the TCGA project were downloaded from the Cancer Browser website. Cancer datasets with at least one normal solid tissue sample were visualized as box-and-whisker plots. For analysis of glioblastoma multiforme (GBM) samples, level 3 preprocessed expression data from Agilent 244K custom gene-expression G4502A_07_2 microarrays of 483 clinical samples, along with the corresponding clinical data, were downloaded from the TCGA Data Portal. Data were visualized as box-and-whisker plots for each sample groups and then the Wilcoxon rank-sum test was performed to evaluate statistical significance; Kaplan–Meier survival analysis followed by a log-rank test was performed using the 'survival' package in R. For GSEA analysis of the aggregated expression profile based on LATS2 expression level, a non-redundant list of genes was generated based on the mean fold change, and then GSEA for pre-ranked lists was performed as described above.

Data access

The gene and miRNA expression raw data and sequencing raw data have been submitted to the NCBI Gene Expression Omnibus database under accession number GSE63538.

3. Results

1. TAL-effector nuclease (TALEN) mediated knockout of *LATS2* gene in HeLa-S3 cells

First, to explore the cellular functions and/or signals that potentially fluctuate in LATS2 dependent fashions, I established *LATS2* KO HeLa-S3 strains by inducing TALEN-mediated double-strand breaks, followed by successive generation of frameshift mutations by non-homologous end joining (Christian et al., 2010). In this section, I described construction of *LATS2* KO HeLa-S3 and validation of this cell line.

1.1 TALEN-mediated *LATS2* KO in HeLa-S3 cells

I designed TALENs which target human *LATS2* locus. TALEN is a nickase which is able to target and nick specific target sequence in the genome. The concept of gene knockout using TALENs is very simple. Briefly, two TALENs positioned at appropriate distance in both directions, causes double-strand breaks at targeted genomic locus. Then non-homologous end joining (NHEJ) event occurs frame-shift and successive non-sense mutation on target gene (Christian et al., 2010). Transient expression of TALENs targeting the *LATS2* gene locus (Forward: hg19_chr13:21,620,130-21,620,148; Reverse: hg19_chr13:21,620,095-21,620,113) resulted in successful knockout of *LATS2* (genomic: Figure 1.1A, protein level: Figure 1.1B). Expression analysis of *CTGF* (1.6-fold increase in *LATS2* KO cells), a downstream target gene of the Hippo pathway that should negatively correlate with LATS2 kinase activity, revealed downregulation of intrinsic LATS2 kinase function in *LATS2* KO cells (Figure 2.1C).

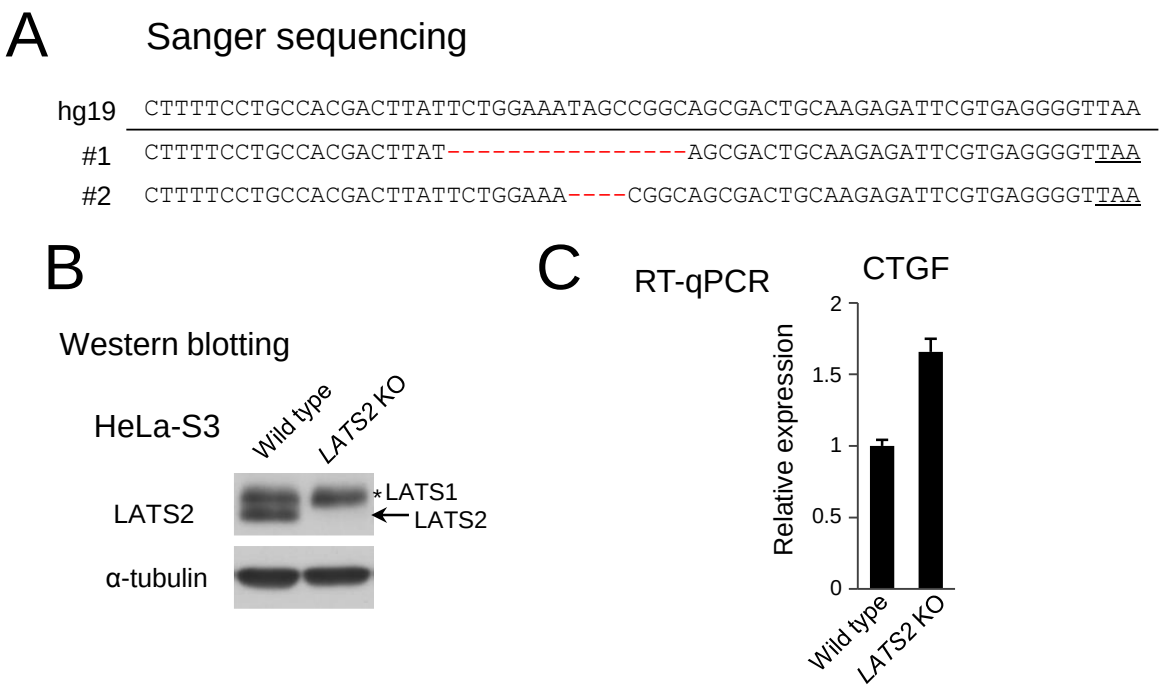

Figure 1.1 Construction of *LATS2* KO HeLa-S3 cells.

(**A**) Genomic sequences of the wild type *LATS2* locus (hg19) and the obtained *LATS2* KO HeLa-S3 cells. The TALEN-targeted region of the genome ware amplified by genomic PCR, and then PCR products were sub-cloned then each clone was subjected to Sanger sequencing. 'TAA' represents stop codon that was generated by TALEN-mediated NHEJ events (**B**) Confirmation of *LATS2* KO by western blotting. The anti-LATS2 polyclonal antibody used recognizes the N-termini of both LATS2 and LATS1. The arrow represents LATS2 signals. '*LATS1' represents LATS1 signals. (**C**) Gene expression analysis of *CTGF*, which is under the control of YAP/TAZ, showing perturbation of the intrinsic Hippo signal. RT-qPCR was performed in two independent experiments, and mRNA levels were normalized to *ACTB*; Error bars show standard deviation (SD).

1.2 Validation of *LATS2* KO using transcriptome data

To confirm the dependency of the overall expression profile on LATS2 and exclude the possibility of obvious off-target effects of the TALEN system, I calculated the correlation between differentially expressed genes (DEGs) in *LATS2* KO HeLa-S3 cells and siRNA-mediated LATS2-knockeddown cells. Although I used different analytical platforms (RNA-sequencing (RNA-seq) for *LATS2* KO cells, microarray for the knockdown study) (summarized in Fig. 1.2A and B), a significant portion of DEGs (15%; 118 of 769 genes) overlapped and positively correlated ($p = 6.1E-25$, Fisher's exact test) between the two types of cells (Fig. 1.2C). Some DEGs detected in both cell types were

also validated by RT-qPCR analysis (Fig. 1.2D). Following these validation, I subjected this *LATS2* KO HeLa-S3 cell line to further analysis (section 2 and 3).

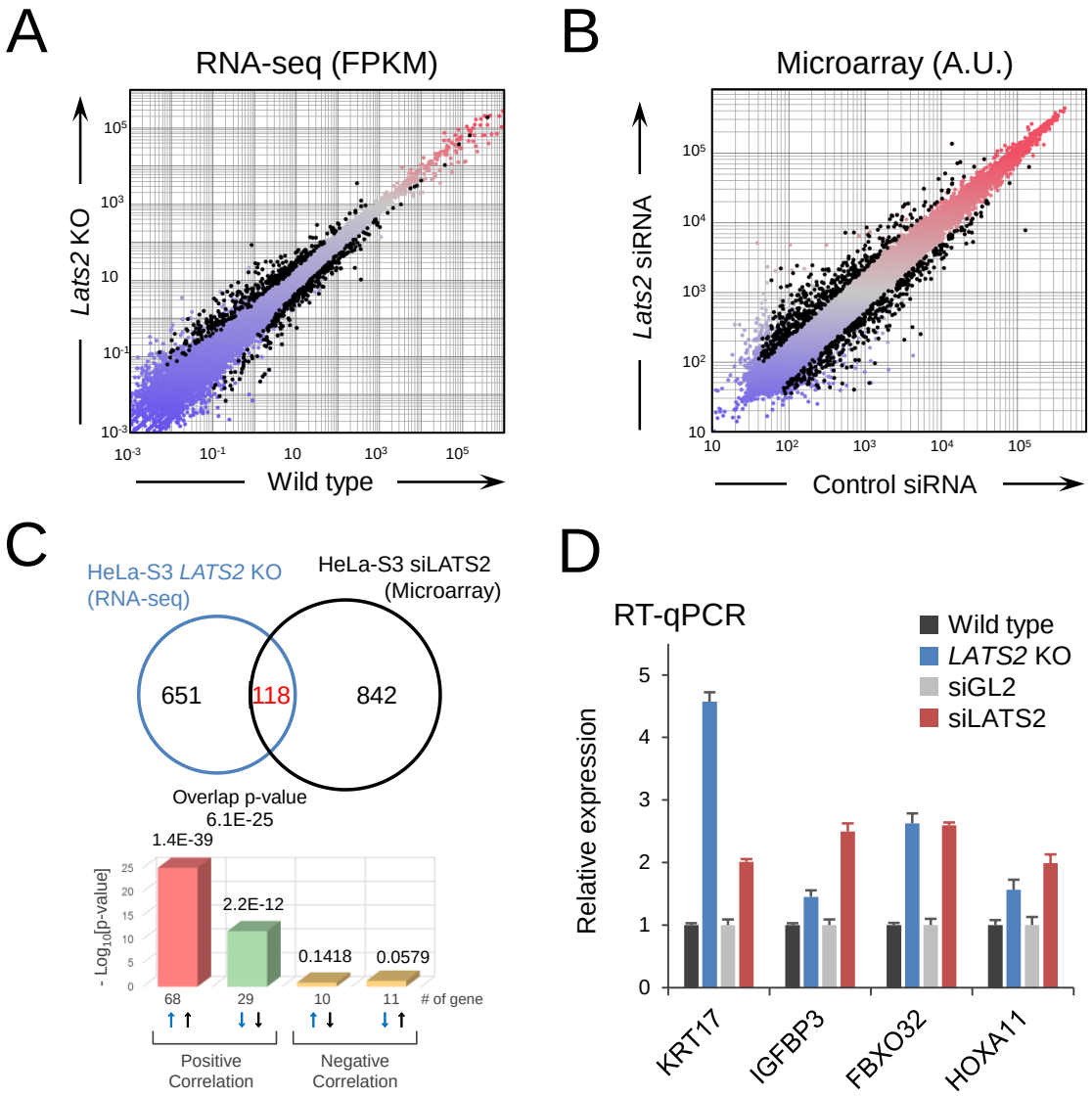

Figure 1.2 Validation of *LATS2* KO using transcriptome data.

(**A**) Scatter plot of RNA-seq data comparing *LATS2* KO and wild type HeLa-S3 cells. DEGs (≥2-fold, p-value <0.05) are highlighted in black dots. (**B**) Scatter plot of microarray data comparing LATS2 knockdown and control siRNA HeLa-S3 cells. DEGs (≥1.4-fold, probes expressing in both samples (i.e. 'wellAboveBG-FLAG' is TRUE) are highlighted in black dots. (**C**) Significant overlap of DEGs in *LATS2* KO HeLa-S3 cells with those in HeLa-S3 cells treated with siRNA targeting LATS2. DEGs in *LATS2* KO and siLATS2 HeLa-S3 cells were subjected to NextBio analysis. Venn diagrams show the number of common and unique genes in both sets. Bar plots show the significance of overlap in

each direction. (**D**) Gene expression analysis for a series of DEGs in *LATS2* KO HeLa-S3 cells and LATS2-knockdown HeLa-S3 cells. RT-qPCR was performed in two independent experiments, and levels of each transcript were normalized to *ACTB*. Error bars show SD. Ratios to control samples (wild type for *LATS2* KO, treated by control siRNA for LATS2 knockdown, respectively) were calculated.

1.3 Summary of section 1

1. *LATS2* KO HeLa-S3 cell line was successfully constructed by using TALEN-mediated genome editing technology.

2. Multiple omics analysis of *LATS2* KO HeLa-S3 cells

Next, I sought to identify the gene signatures associated with LATS2, using RNA-seq data of *LATS2* KO HeLa-S3 cells. In this section, I described the initial transcriptome analysis of *LATS2* KO HeLa-S3 cells to extract H3K27me3-related signals, then characterized epigenetic state using high-throughput sequencing of ChIP-enriched DNA (ChIP-seq) for H3K27me3 marks.

2.1 *LATS2* KO causes downregulation of H3K27me3

To extract cellular functions and/or signals associated with LATS2 without bias, I performed gene set enrichment analysis (GSEA) (Subramanian et al., 2005) using 'C2_CGP gene sets' in the Molecular Signature Database (MSigDB; http://software.broadinstitute.org/gsea/msigdb/) gene sets collections of Broad Institute. This collection includes gene sets representing expression signatures of genetic and chemical perturbations in many previous omics-based studies. *LATS2* KO cells were positively correlated with high expression of epigenetically silenced genes, especially H3K27me3-marked genes (p-value < 0.001) (Figure 2.1A). To confirm the impact of *LATS2* KO on the level of H3K27me3, I performed immunofluorescence imaging. Consistent with the positive correlation of LATS2 with H3K27me3 in GSEA, *LATS2* KO decreased the H3K27me3 level (Fig. 2.1B). This result suggests that LATS2 exerts a positive effect on PRC2 function, and that deletion of LATS2 therefore causes genome-wide downregulation of H3K27me3 in human cells.

To more precisely determine the impact of LATS2 on epigenetic landscapes, I performed ChIP-seq for H3K27me3 marks. Consistent with the results shown in Figure 2.1A and B, H3K27me3 levels were reduced at target loci (*HOXA* locus as a representative; Fig. 2.1C), as well as at promoter regions, on a genome-wide scale (aggregated for all transcription start sites [TSSs]; Fig. 2.1D). To ensure the phenotype, I examined H3K27me3 levels at known PRC2 target loci, i.e., genes that have the H3K27me3 mark and are bound by SUZ12 and EED on their promoters in human embryonic stem cells (Ben-Porath et al., 2008). Although the magnitude of fluctuations determined by ChIP-qPCR varied, I observed an overall trend toward downregulation of H3K27me3 levels at these loci (Fig. 2.1E).

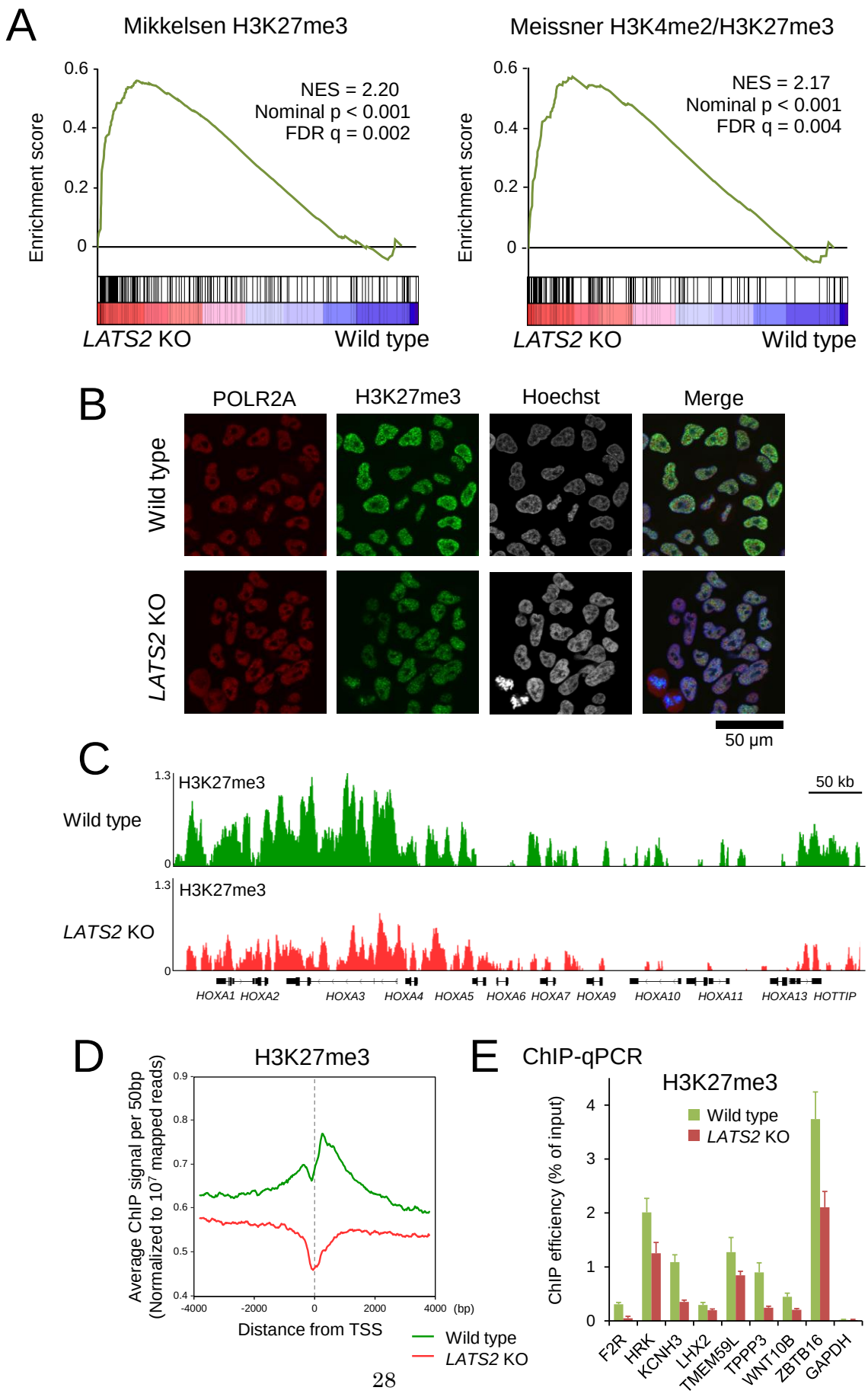
A
Mikkelsen H3K27me3
Meissner H3K4me2/H3K27me3
Enrichment score
NES = 2.20
Nominal p < 0.001
FDR q = 0.002
NES = 2.17
Nominal p < 0.001
FDR q = 0.004
LATS2 KO
Wild type
B
POLR2A
H3K27me3
Hoechst
Merge
Wild type
LATS2 KO
50 μm
C
H3K27me3
50 kb
Wild type
LATS2 KO
HOXA1 HOXA2 HOXA3 HOXA4 HOXA5 HOXA6 HOXA7 HOXA9 HOXA10 HOXA11 HOXA13 HOTTIP
D
H3K27me3
Average ChIP signal per 50bp (Normalized to 10^7 mapped reads)
Distance from TSS
(bp)
Wild type
LATS2 KO
E
ChIP-qPCR
H3K27me3
ChIP efficiency (% of input)
Wild type
LATS2 KO
F2R
HRK
KCNH3
LHX2
TMEM59L
TPPP3
WNT10B
ZBTB16
GAPDH

Figure 2.1 Dysregulation of epigenetic regulation upon *LATS2* KO.
(**A**) GSEA of *LATS2* KO HeLa-S3 cells for gene sets related to H3K27me targets. Genes are ranked by fold change in a RNA-seq experiment (KO vs. wild type). A positive enrichment score indicates higher expression after *LATS2* KO. (**B**) Immunofluorescence showing reduction of global H3K27me3 in *LATS2* KO HeLa-S3 cells relative to wild type. RNAPII and nuclei were counter-stained. Bar indicates 50 μm. (**C**) Snapshots of ChIP-seq traces for H3K27me3 in the wild type HeLa-S3 (green) and *LATS2* KO cells (red). The *HOXA* gene cluster is depicted as a representative locus showing a reduction of H3K27me3 following *LATS2* KO. (**D**) Aggregate plots of H3K27me3 ChIP-seq signals centered at TSSs of all RefSeq genes in wild type HeLa-S3 (green) and *LATS2* KO cells (red). (**E**) ChIP-qPCR analysis for H3K27me3 on a series of known PRC2 target loci. All ChIP experiments were performed at least twice independently; error bars show SD.

2.2 Identification of genes marked by 'LATS2–responsive H3K27me3'

The aggregate plots in Figure 2.1D suggested an existence of unidentified genes fluctuated strongly upon *LATS2* KO. To investigate the chromatin state in more detail, I divided the genes into three groups depending on their H3K27me3 status: 1) H3K27me3-overlap, genes possessing peaks that were called by the MACS software (Feng et al., 2012) within +/- 5 kb of each TSS in both wild-type and *LATS2* KO cells (1546 genes); 2) H3K27me3-loss, genes possessing peaks only in wild-type cells (2380 genes), and 3) H3K27me3-gain, genes possessing peaks only in *LATS2* KO cells (1035 genes) (Figure 2.2A, upper panel). The aggregate analysis for each module revealed that the H3K27me3-gain module maintained the same level of H3K27me3 between wild type and *LATS2* KO cells (Figure 2.2A, lower panels). This observation suggests that *LATS2* KO has mostly inhibitory effects on H3K27me3 maintenance, and that sensitivity to this effect varies across the genome. The significant reduction in H3K27me3 at specific genes raised the possibility that this event was accompanied by transcriptome changes, i.e., de-repression of genes in 'H3K27me3-loss' module. The association of epigenetic changes with transcriptome changes was further examined by GSEA using 'H3K27me3-loss' module and RNA-seq data of *LATS2* KO cells ($p < 0.001$) (Figure 2.2B). To examine the functional relevance, I next calculated the enrichment of gene ontology (GO) terms using 'Canonical pathways' in the NextBio statistical platform (Kupershmidt et al., 2010) for genes in the H3K27me3-loss module, the module most sensitive to *LATS2* KO. Indeed, the H3K27me3-loss module exhibited significant enrichment in GO terms related to neural functions (Figure 2.2C). This intriguing enrichment might reflect the specific function of this module in the nervous system.

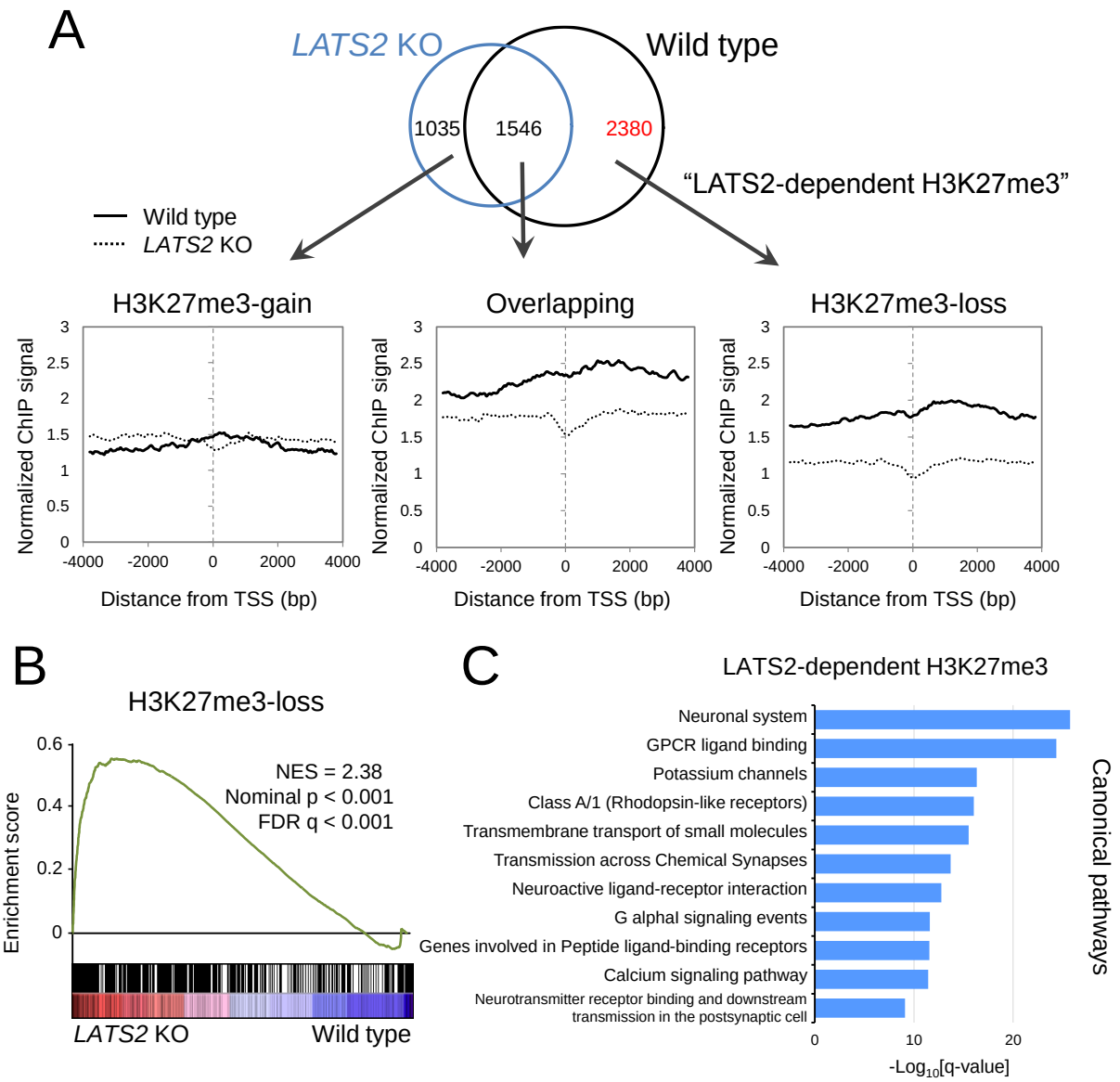

Figure 2.2 ChIP-seq analysis of H3K27me3 in *LATS2* KO HeLa-S3.

(**A**) Top: Venn diagram showing the overlap of genes with H3K27me3 peaks within ±5 kb of the TSS in parental WT HeLa-S3 (blue) and *LATS2* KO cells (black). Bottom: Aggregate plots of H3K27me3 ChIP-seq signals centered at TSSs of RefSeq genes for each module of parental WT (solid line) and *LATS2* KO (dashed line). (**B**) GSEA of *LATS2* KO HeLa-S3 cells, for genes with *LATS2* KO–responsive H3K27me3 marks in their promoters. Genes are ranked by fold change, derived from the RNA-seq experiment (KO vs. wild type). A positive enrichment score indicates increased expression after *LATS2* KO. (**C**) GO enrichment analysis of canonical pathways for LATS2-dependent H3K27me3 targets. The x-axis represents statistical significance. The y-axis represents gene sets belonging to 'canonical pathways' from MSigDB (Broad Institute).

2.3 *LATS2* affects H3K27me3 regulation in a kinase-dependent fashion

I next performed an add-back rescue experiment by constructing cell lines in which LATS2 was stably expressed (Figure 2.3A). Overall expression profile of HeLa-S3 cells upon *LATS2* KO was restored by stable expression of exogenous *LATS2* gene (Figure 2.3B). Next, I performed GSEA to examine the impact of LATS2 kinase activity to expression pattern of H3K27me3-marked genes. GSEA of RNA-seq data of the rescued *LATS2* KO cells revealed that cells expressing wild type LATS2 (*LATS2* WT), but not a kinase-dead form of LATS2 (*LATS2* KD), re-repressed the genes in the H3K27me3-loss module (WT: enrichment score = -0.583, KD: enrichment score = 0.344, p-value < 0.001) (Figure 2.3C and D). This observation supports the idea that LATS2 depletion causes downregulation of PRC2 and H3K27me3 signatures, and that this phenotype depends on LATS2 kinase activity.

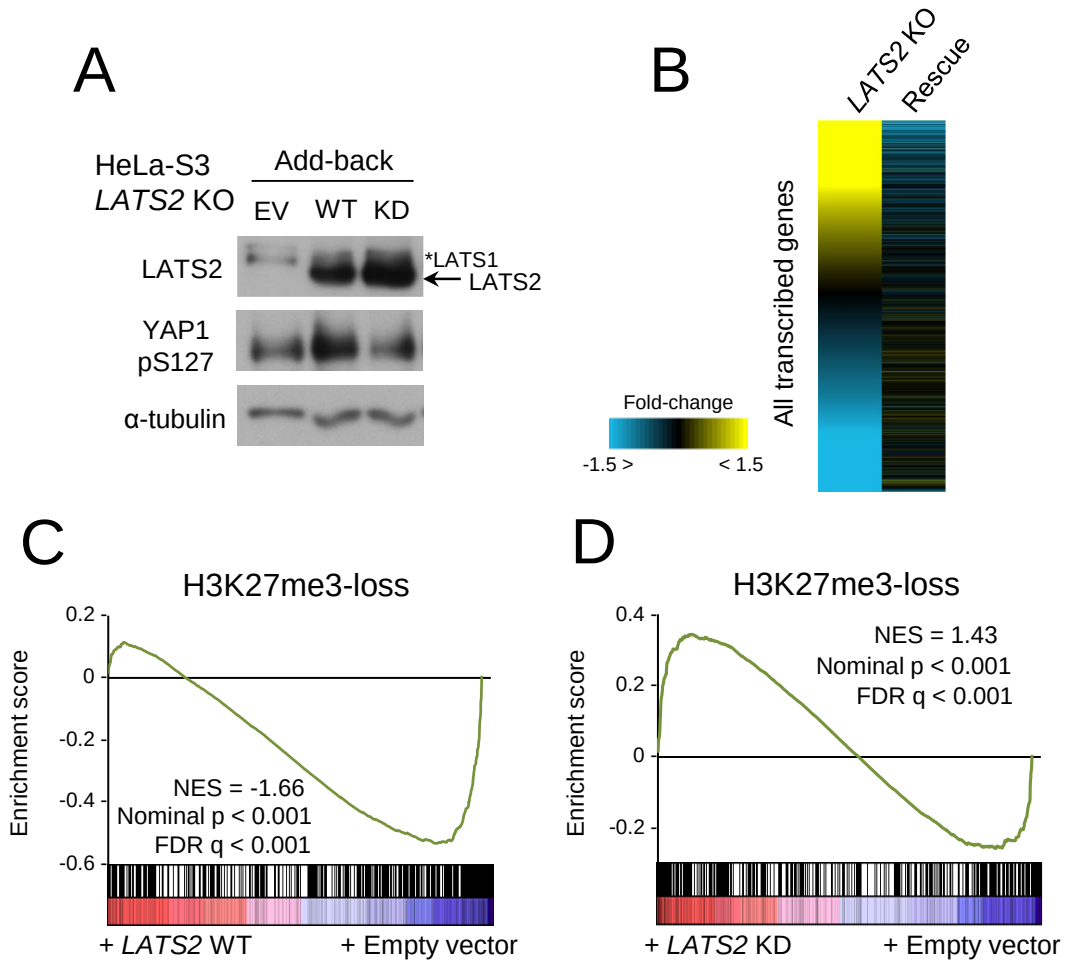

Figure 2.3 Add-back of *LATS2* restored the expression of 'H3K27me3-loss' genes in kinase dependent fashion.

(**A**) Western blotting of whole cell lysate of rescued *LATS2* KO HeLa-S3 cells. Phosphorylated YAP was blotted as an indicator of LATS2 kinase activity. EV, empty vector. WT, kinase active. KD, kinase-inactive mutant. (**B**) A heatmap illustrating successful rescue of overall expression profile of *LATS2* KO by add-back of wild-type *LATS2* gene (Rescue) to KO cells. (**C**–**D**) GSEA of rescued *LATS2* KO HeLa-S3 cells, for genes with LATS2–responsive H3K27me3 marks in their promoters, i.e., 'H3K27me3-loss' in the text. Genes are ranked by fold change, derived from the RNA-seq experiment (LATS2 add-back vs. empty vector). A positive enrichment score indicates increased expression upon LATS2 add-back. WT, kinase active. KD, kinase-inactive mutant.

Summary of section 2

1. *LATS2* KO HeLa-S3 exhibits reduction of H3K27me3-mark and successive transcriptome changes.
2. ChIP-seq analysis determined genes marked by high-sensitive H3K27me3 upon *LATS2* KO.
3. LATS2 kinase activity was able to restore the expression of H3K27me3-marked genes.

3. Characterization of PRC2 status in *LATS2* KO HeLa-S3 cells

To determine how *LATS2* KO causes genome-wide downregulation of H3K27me3, I characterized the status of PRC2 in *LATS2* KO HeLa-S3 cells. LATS2 is one of central mitotic kinases which can affect cell cycle progression and chromatin state upon its dysregulation. Thus, in this section, I also confirmed and discussed cell cycle dependency of the status of each component of PRC2 at both protein and transcription levels.

3.1 *LATS2* KO causes downregulation of PRC2 at both the protein and mRNA levels

Western blotting of the solubilized chromatin fraction revealed that the levels of three core components of PRC2 (EZH2, SUZ12, and EED) were reduced in *LATS2* KO cells (Figure 3.1A). Consistent with the ChIP-seq analysis, immunoblotting of whole chromatin revealed a significant reduction in H3K27me3 (13% of wild type level) (Figure 3.1A). RT-qPCR revealed that PRC2 was also downregulated at a transcriptional level; specifically, expression of EZH2 (42% of the wild-type level) and EED (57%), but not SUZ12, was reduced upon *LATS2* KO (Figure 3.1B). Moreover, to confirm the effects of LATS2 and EZH2 on genome-wide H3K27me3 level and the transcription level of PRC2, I performed another add-back rescue experiment. Transient add-back of LATS2 and/or EZH2 revealed that co-overexpression of LATS2 and EZH2 restored the reduction of H3K27me3 in *LATS2* KO cells in a LATS2 dose–dependent fashion, although transient overexpression of LATS2 or EZH2 alone exerted no effect on global H3K27me3 level (Figure 3.1C). It should also be noted that overexpression of LATS2 or EZH2 increased endogenous transcription of EZH2 and EED (Figure 3.1D). These results suggest that LATS2 downregulates PRC2 not only protein at protein level but also transcription level, and a threshold amount of EZH2 is required to restore the global H3K27me3 level.

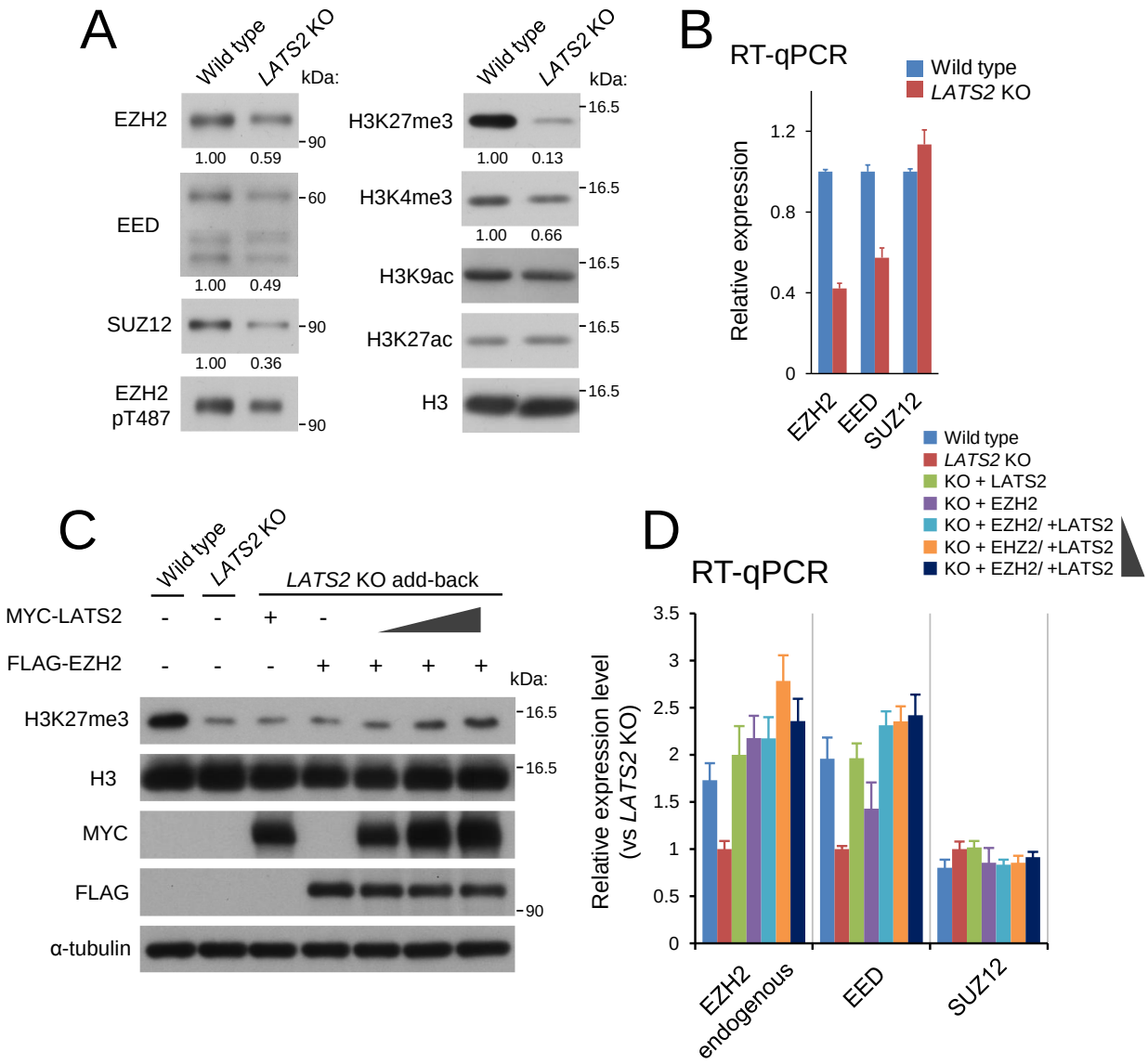

Figure 3.1 *LATS2* KO downregulates PRC2 at both the protein and mRNA levels. (**A**) Polycomb components and major histone marks following *LATS2* KO. The chromatin-bound fraction was subjected to western blotting. (**B**) Gene expression analysis for the core components of PRC2: EZH2, EED, and SUZ12. RT-qPCR was performed in two independent experiments, and transcript levels were normalized against *ACTB*; Error bars show SD. (**C**) Western blotting of rescued *LATS2* KO cells by transient overexpression of MYC-tagged LATS2 and/or FLAG-tagged EZH2. The synergetic effects and the dose dependency of LATS2 were evaluated by increasing amounts of LATS2. (**D**) Gene expression analysis for the core components of PRC2 in the same setup in (C). The expression level of endogenous EZH2 was quantified by using primers targeted 3'UTR region of mRNA. RT-qPCR was performed in two independent experiments, and transcript levels were normalized against *ACTB*; Error bars show SD.

3.2 Downregulation of PRC2 in *LATS2* KO cells is not due to cell cycle aberrations

Although LATS2 is a mitotic kinase involved in the G1/S and tetraploidy checkpoints (Aylon et al., 2006; Li et al., 2003), downregulation of PRC2 was not a result of cell-cycle retention due to *LATS2* KO, as flow cytometry analysis revealed no significant difference in cell-cycle progression between asynchronous wild type and *LATS2* KO HeLa-S3 cells (Figure 3.2A and B). Furthermore, in wild type HeLa-S3 cells, PRC2 expression was not reduced at either the protein or mRNA level during time-course monitoring, though the level of H3K27me3 oscillates during the cell cycle, possibly reflecting an increase in the chromatin content per cell followed by DNA replication. (Figure 3.2C and D). These observations suggest that down-regulation of PRC2 and H3K27me3 upon *LATS2* KO is not due to cell-cycle aberrations caused by LATS2 depletion.

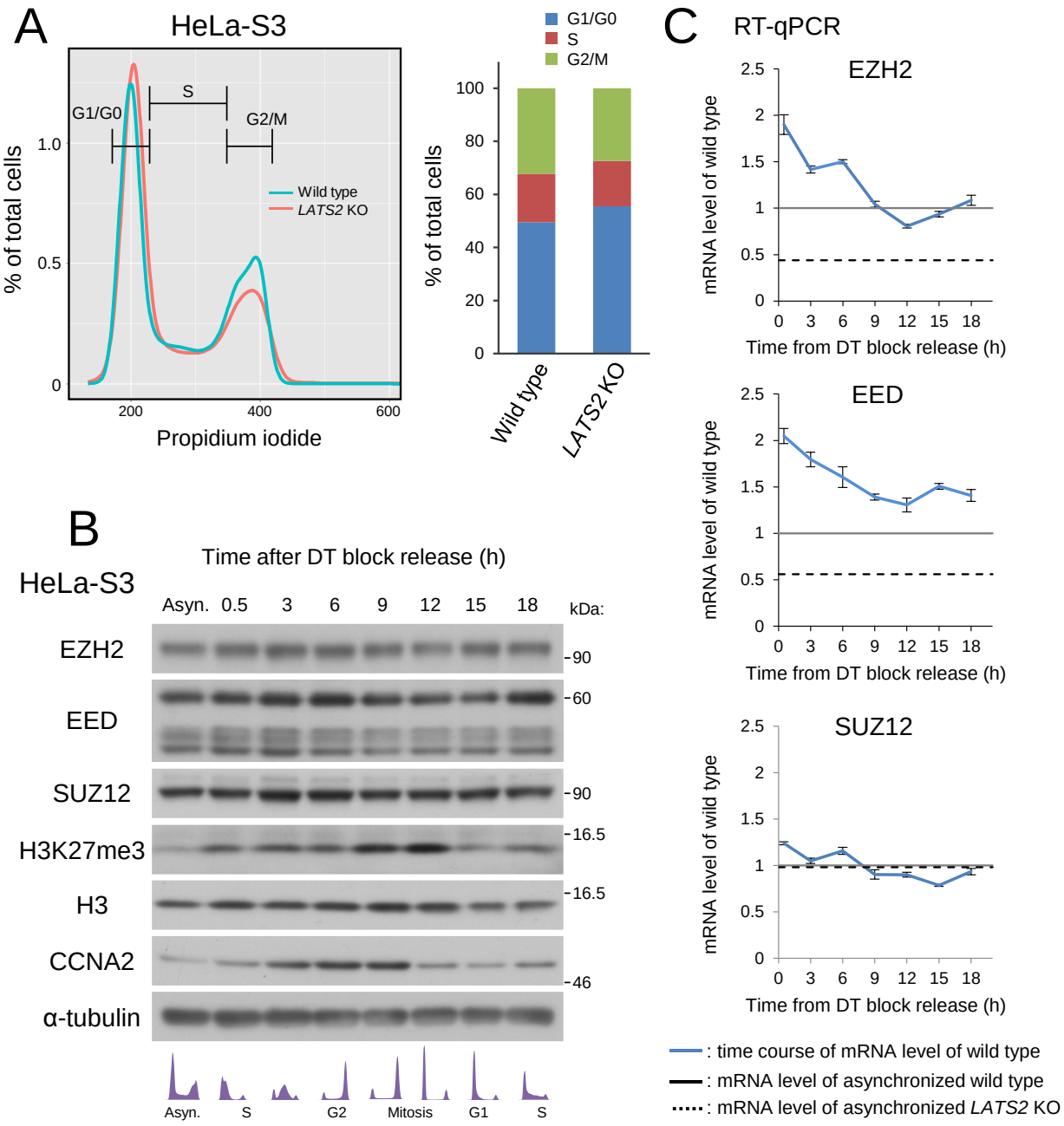

Figure 3.2 Downregulation of PRC2 upon *LATS2* KO is not due to cell cycle aberrations.

(**A–B**) No differences in the cell cycle were observed in HeLa-S3 cells upon KO. Cell-cycle analysis by FACS showing that growing, asynchronous *LATS2* KO HeLa-S3 cells do not exhibit retention at any stage of the cell cycle. (**C**) Western blotting of PRC2 components and the H3K27me3 mark in wild type HeLa-S3 cells throughout the cell cycle. α-tubulin and H3 were used as loading controls, and CCNA2 was used as a cell-cycle indicator. A portion of the cells was analyzed by FACS, and is depicted in the bottom panel. (**D**) RT-qPCR analysis of PRC2 components in wild type HeLa-S3 cells. Black line and dotted line

indicate the expression level of each gene in asynchronous wild type and *LATS2* KO HeLa-S3 cells, respectively. The expression levels of EZH2 and EED oscillate during the cell cycle but do not reach the level attained in *LATS2* KO cells. Each transcript level was normalized against *ACTB*; Error bars show SD.

3.3 LATS2 supports histone methyltransferase activity of PRC2 in a kinase dependent manner

Inhibition of histone methyltransferase activity (HMTase) of EZH2 by small molecules such as 3-deazaneplanocin A not only reduces the catalytic ability of this protein, but also downregulates its transcription via negative-feedback mechanisms (Tan et al., 2007), suggesting downregulation of HMTase activity upon *LATS2* KO. Indeed, the significant reduction in H3K27me3 level could not be explained by reduction of PRC2 expression alone. ChIP-qPCR analysis of EZH2 revealed that the magnitude of reduction in the occupancy of EZH2 at PRC2 target loci (analyzed in Figure 2.1E) was relatively moderate (Figure 3.3A). To determine whether HMT activity was also affected in *LATS2* KO cells, I performed *in vitro* HMTase assays using recombinant H3.1 and endogenous immunoprecipitated EZH2 from each sample. The results revealed a decrease in methyltransferase activity in *LATS2* KO cells (60% of wild type activity; normalized to the amount of EZH2 protein in each tube) (Figure 3.3B). Further *in vitro* HMTase assays using the add-back cell lines revealed that HMTase was affected by LATS2 kinase activity (2.3-fold higher in the WT than in the KD mutant) (Figure 3.3C). These results suggest that HMTase of EZH2 is positively regulated by LATS2 kinase.

A

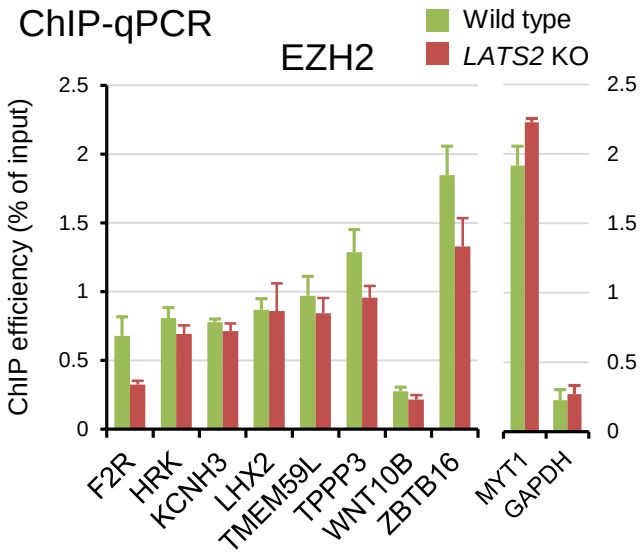
ChIP-qPCR
EZH2
Wild type
LATS2 KO
ChIP efficiency (% of input)
2.5
2
1.5
1
0.5
0
F2R
HRK
KCNH3
LHX2
TMEM59L
TPPP3
WNT10B
ZBTB16
MYT1
GAPDH

B

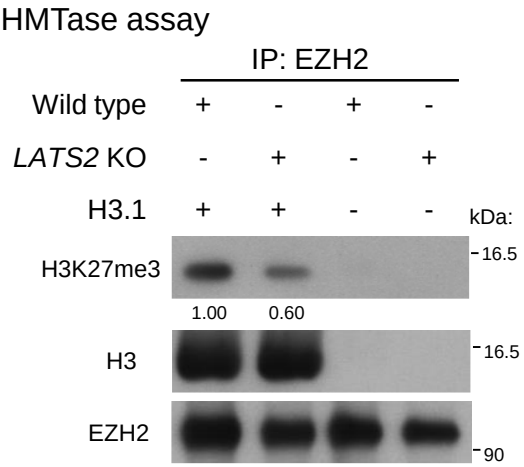
HMTase assay
IP: EZH2
Wild type + - + -
LATS2 KO - + - +
H3.1 + + - -
kDa:
H3K27me3
16.5
1.00 0.60
H3
16.5
EZH2
90

C

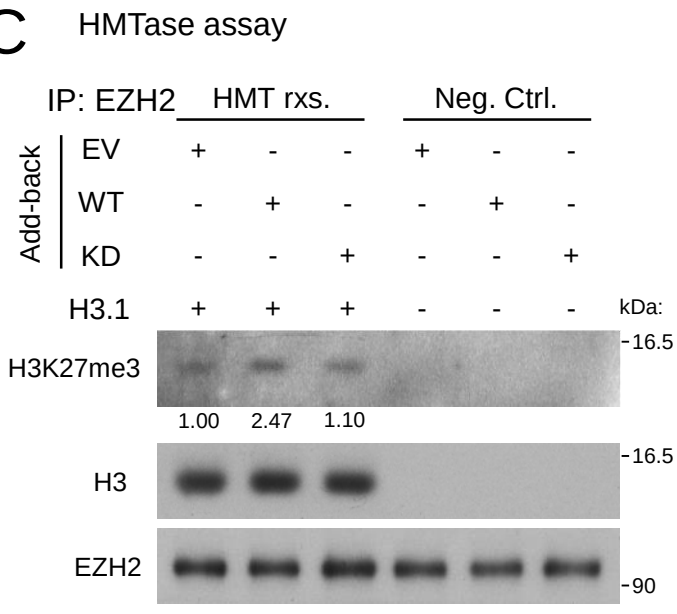
HMTase assay
IP: EZH2
HMT rxs.
Neg. Ctrl.
Add-back
EV + - - + - -
WT - + - - + -
KD - - + - - +
H3.1 + + + - - -
kDa:
H3K27me3
16.5
1.00 2.47 1.10
H3
16.5
EZH2
90

Figure 3.3. LATS2 affects HMTase activity of PRC2 in kinase dependent fashion. (**A**) ChIP-qPCR analysis for EZH2 in a series of known PRC2 targets assessed in Figure 2.1E. The MYT1 locus and GAPDH locus are positive and negative control regions for EZH2, respectively. All ChIP experiments were performed at least twice independently; error bars show SD. (**B**) *In vitro* HMTase assay with immunoprecipiated EZH2 of *LATS2* KO cells. Endogenous PRC2 was purified by immunoprecipitation of active chromatin fraction of each cell line. The background H3K27me3-level was validated in no-substrate setup. The amount of EZH2 protein in IP-input was titrated beforehand, the equivalent EZH2 between samples was used for HMTase reaction. Each H3K27me3 level was normalized by the signal of immunoprecipitated EZH2. (**C**) *In vitro* HMTase assay with immunoprecipiated EZH2 of each add-back cell line. Endogenous PRC2 was purified by immunoprecipitation of active chromatin fraction of each add-back cell line. The background H3K27me3-level was validated in no-substrate setup (Negative control; Neg. Ctrl.), and HMTase activity of each add-back cell line was evaluated by western blotting (HMTase reaction; HMT rxs.). EV, empty vector. WT, kinase active. KD, kinase-inactive mutant. Each H3K27me3 level was normalized by the signal of immunoprecipitated EZH2.

3.4 *LATS2* KO also exhibits downregulation of H3K4me3-maks at genome wide

I observed downregulation of transcription of *EZH2* and *EED* in Figure 3.1B. As I mentioned above, it has been reported that inhibition of EZH2 histone methyltransferase activity by small molecules also causes downregulation of its transcription via unknown feedback mechanisms (Tan et al., 2007). One possible explanation of the molecular mechanisms underlying transcriptional regulation of EZH2 and EED is that other epigenetic mechanisms are perturbed by PRC2 dysfunction upon *LATS2* KO. Hence, to explore the possible mechanism of downregulation of *EZH2* and *EED* in transcription level upon *LATS2* KO, I investigated the genome-wide signature of H3K4me3, which functions in transcriptional activation. Indeed, I detected moderate genome-wide reduction of H3K4me3 (Figure 3.4A). Consistent with the RT-qPCR results in Figure 3.1B, further analysis revealed a trend toward downregulation of H3K4me3 at *EZH2* and *EED*, but not the *SUZ12* locus, in *LATS2* KO cells (Figure 3.4B and C). These results suggest that LATS2 positively affects PRC2 function, thus depletion of LATS2 causes dysregulation of the H3K27me3 signature. In addition, this phenomenon may be reinforced by positive-feedback mechanisms involving down-regulation of H3K4me3 to reduce PRC2 expression.

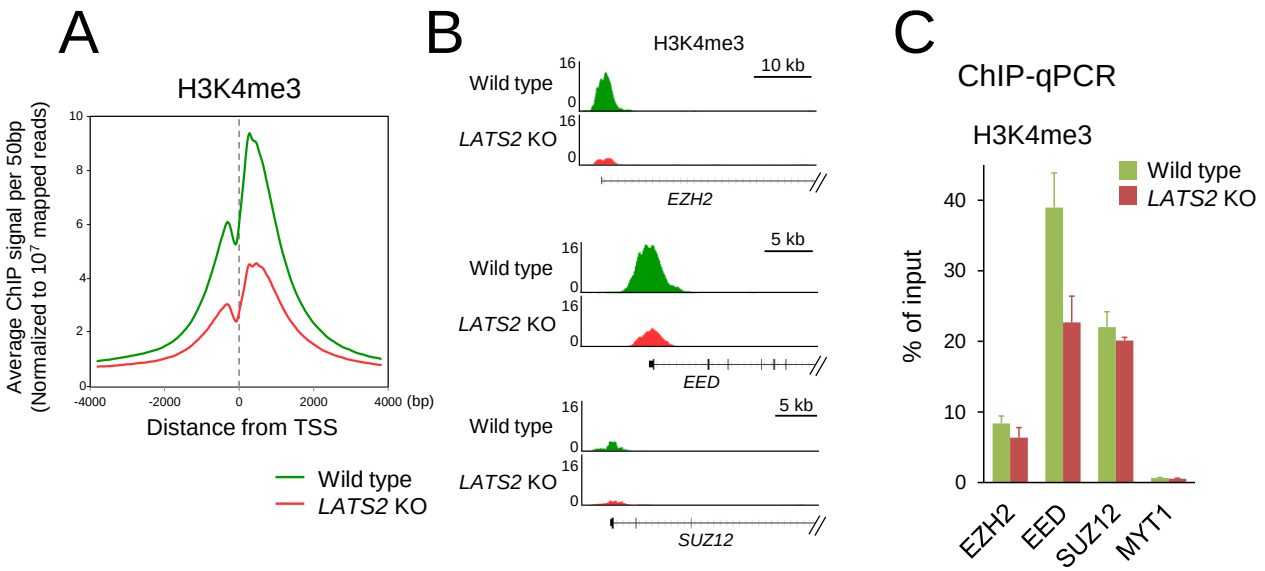

Figure 3.4 Characterization of H3K4me3 for PRC2 expression in *LATS2* KO HeLa-S3 cells.

(**A**) Aggregate plots of H3K4me3 ChIP-seq signals centered at TSSs of all RefSeq genes in wild type HeLa-S3 (green) and *LATS2* KO cells (red). (**B**) Snapshots of ChIP-seq traces for H3K4me3 in parental WT HeLa-S3 (green) and *LATS2* KO cells (red) at loci encoding the PRC2 core components. (**C**) ChIP-qPCR analysis for H3K4me3 at TSSs of genes encoding the core components of PRC2. The analysis reveals the loss of the H3K4me3 mark at the TSSs of EZH2 and EED, which are down-regulated by *LATS2* KO. The MYT1 locus is a negative control region for H3K4me3, an active histone mark. All ChIP experiments were performed at least twice independently; error bars show SD.

3.5 Summary of section 3

1. *LATS2* KO causes down-regulation of PRC2 at both protein and transcription levels.
2. Certain threshold level of EZH2 is necessary to maintain genome-wide H3K27me3 integrity.
2. LATS2 kinase also positively support HMTase activity of EZH2.
4. Dysregulation of PRC2 upon *LATS2* KO is not due to cell cycle aberration.
5. Active H3K4me3-mark is also reduced upon *LATS2* KO to reinforce downregulation of PRC2 at transcription level.

4. Characterization of molecular association between PRC2 and LATS2 on chromatin

The data presented above suggest that LATS2 somehow affects PRC2 function. One simple explanatory model is that LATS2 phosphorylates PRC2 on chromatin, thereby supporting or specializing its function. Indeed, previous studies suggested that EZH2 undergoes several post-translational modifications including phosphorylation. In this section, to understand how LATS2 kinase regulates PRC2 function, I performed further molecular biological analyses.

4.1 LATS2, but not LATS1 localizes on chromatin

To investigate my hypothesis, I first examined whether LATS2 localizes on chromatin. Western blotting analysis of the chromatin-bound fraction revealed that LATS2 was present in the chromatin fraction of HeLa-S3 and MDA-MB231 cells (Figure 4.1 A and B). Furthermore, western blotting using an antibody that recognizes the N-termini of both LATS2 and LATS1 revealed that LATS2, but not LATS1, was primarily localized on chromatin (Figure 4.1A and B). This result is consistent with a previous study showing that LATS2, but not LATS1, binds to chromatin along with effectors of Wnt signaling (Li et al., 2013). This result also suggests that LATS2 exerts some functions on chromatin that are distinct from those of canonical Hippo signaling, in which LATS2 works in concert with LATS1 in response to the same upstream signals.

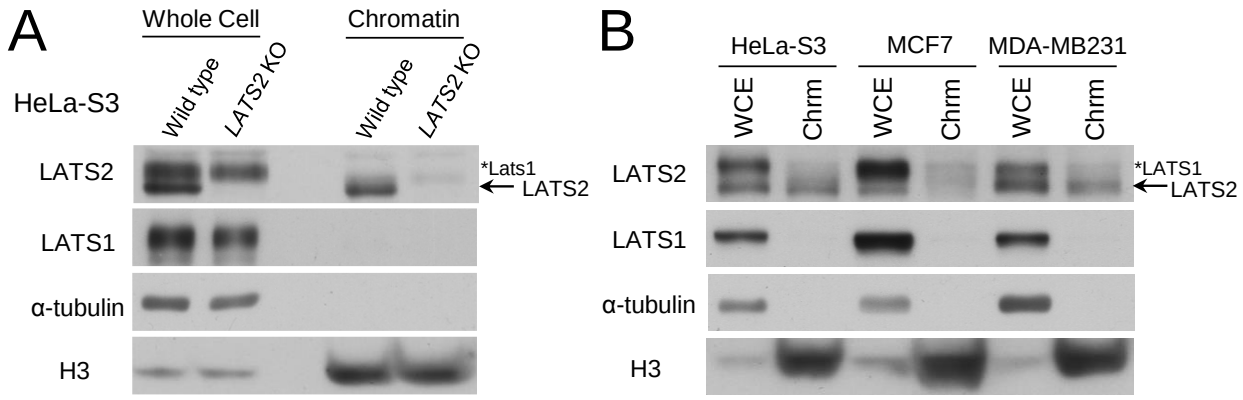

Figure 4.1 LATS2 but not LATS1 localizes on chromatin in some cancer cell lines.
(**A**) Western blotting of LATS2 in *LATS2* KO HeLa-S3 cells. Immunoblotting analysis to demonstrate that LATS2 binds to chromatin more stably than LATS1. The arrow represents LATS2 signals. '*LATS1' represents LATS1 signals. (**B**) Western blot analysis of LATS2 in some human cancer cell lines. α-tubulin and H3 were used to confirm successful fractionation. Arrow represents Lats2 signals. '*Lats1' represents Lats1 signals. WCE, whole cell extract. Chrm, solubilized chromatin fraction.

4.2 LATS2 associates with EZH2 on chromatin

I next performed binding assay using co-immunoprecipitation of LATS2 and PRC2 core components to confirm association of these proteins in living cells. Because the absolute level of endogenous LATS2 on chromatin is relatively very low compared to PRC2, I performed the immunoprecipitation experiment in HeLa-S3 cells overexpressing FLAG-tagged LATS2. I detected an association between FLAG-tagged LATS2 (Figure 4.2A) and endogenous EZH2 in reciprocal immunoprecipitation experiments (Figure 4.2B).

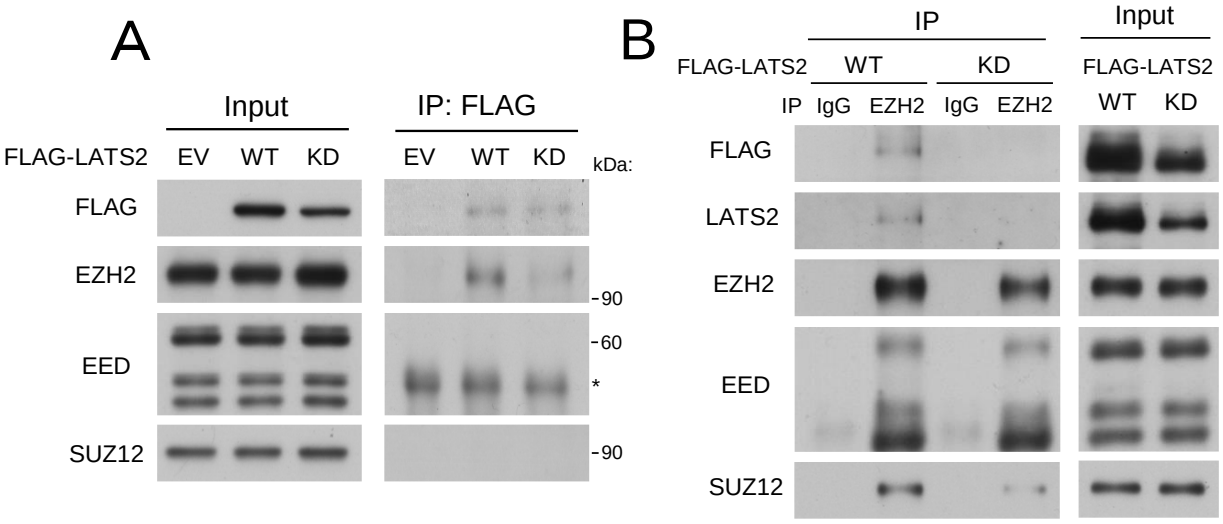

Figure 4.2 LATS2 physically associates to EZH2 on chromatin.

(**A**) Co-immunoprecipitation of endogenous PRC2 with FLAG-tagged LATS2 from transiently transfected HeLa-S3 cells. Input represents 10% of the total solubilized chromatin fraction used for each immunoprecipitation. Right, anti-FLAG precipitates immunoblotted to detect FLAG-tagged proteins and endogenous PRC2. EV, empty vector. WT, kinase active. KD, kinase-inactive mutant. The asterisk represents non-specific signals. (**B**) Co-immunoprecipitation of transiently expressed FLAG-tagged LATS2 with endogenous EZH2 from transiently transfected HeLa-S3 cells. Input represents 10% of the total solubilized chromatin fraction used for each immunoprecipitation. Anti-EZH2 precipitates were immunoblotted for the FLAG-tagged LATS2 and endogenous PRC2 proteins. Anti-IgG precipitates were analyzed as negative controls. EV, empty vector. WT, kinase active. KD, kinase-inactive mutant. Asterisk represents non-specific signals.

4.3 LATS2, but not LATS1 phosphorylates PRC2 components

The results described above suggest that LATS2 associates with PRC2 on chromatin and affects

its functions. Indeed, some kinases belonging to the Hippo signaling cascade, including LATS2, localize on chromatin along with transcriptional regulators and function as nuclear effectors that regulate expression of downstream genes (Aylon et al., 2010; Cinar et al., 2011; Hergovich and Hemmings, 2009; Li et al., 2013; Zhang et al., 2012). To determine whether LATS2 can phosphorylate PRC2, I performed *in vitro* kinase assays using a Phos-tag–based technique. A phosphorylation-dependent motility shift was detected in EZH2 and SUZ12 in the presence of LATS2, but not in the presence of LATS1 (Figure 4.3A and B). Based on the result of immunoprecipitation assay, in which LATS2 shows association with EZH2, I focused on EZH2 and performed further experiments. Consistent with the result of *in vitro* analysis in figure 4.3A and B, Phos-tag analysis using transiently expressed FLAG-tagged EZH2 protein in add-back cell lines, showed different motility only in LATS2 WT cells but not in LATS2 KD cells (fig. 4.3C). Further Phos-tag analysis of *LATS2* KO HeLa-S3 cells using equal amount of EZH2 showed a reduction in motility pattern of EZH2 in *LATS2* KO HeLa-S3 cells (Fig. 4.3.1D). It also noteworthy that in the cellular Phos-tag analysis, the shifted band was broad and smeared (Fig. 4.3C and D), suggesting that LATS2 may phosphorylate EZH2 on multiple sites *in vivo*. Based on these findings, I concluded that LATS2 can associate with PRC2, especially EZH2 on chromatin and phosphorylate it.

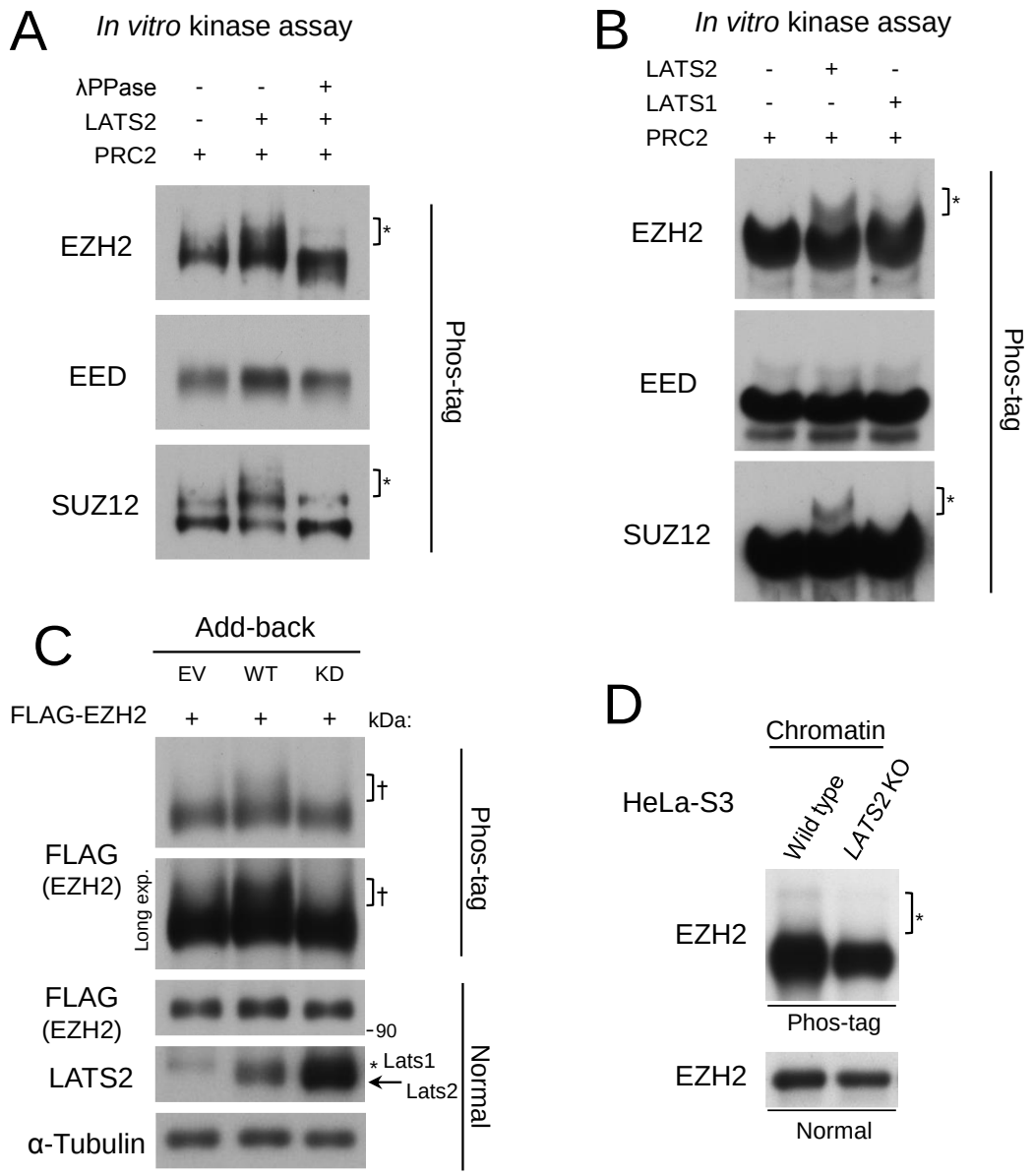

Figure 4.3 LATS2 but not LATS1 phosphorylates PRC2 components.

(**A**) Phos-tag–based *in vitro* kinase assay demonstrating that LATS2 can phosphorylate PRC2. Recombinant PRC2 complex was incubated with recombinant LATS2 in the presence of ATP. Phosphorylation of PRC2 components was assessed by immunoblotting in the presence of Phos-tag. The asterisks indicate phosphorylation-dependent motility shifts. Phosphatase treatment demonstrated that the motility shift was dependent upon phosphorylation. (**B**) *In vitro* kinase assay including recombinant LATS1 kinase. (**C**) Phos-tag–based western blot analysis of add-back cells overexpressing FLAG-tagged EZH2. The dagger (†) indicates the phosphorylation-dependent motility shift. The arrow indicates LATS2 signals. '*LATS1' indicates LATS1 signals. EV, empty vector. WT, kinase active. KD, kinase-dead mutant. (**D**) Phos-tag–

based western blot analysis showing the difference in motility of endogenous EZH2, dependent on the phosphorylation level, between WT and *LATS2* KO HeLa-S3 cells. The solubilized chromatin fraction from each cell type was separated, and EZH2 phosphorylation was assessed by immunoblotting in the presence of Phos-tag. The asterisks indicate phosphorylation-dependent motility shifts.

4.4 Summary of section 4

1. LATS2 localizes on chromatin more stably than LATS1.
2. LATS2 associates with PRC2, especially EZH2 on chromatin.
3. Not LATS1 but LATS2 phosphorylates EZH2 *in vitro* and *in vivo*.

5. Biological relevance of LATS2 – PRC2 axis in differentiation

Above results suggest that there are two aspects of LATS2-dependent PRC2 coordination; LATS2 maintains genome-wide H3K27me3 integrity and loss of LATS2 causes up-regulation of universal PRC2 target genes. In contrast, some genes have high sensitivity to LATS2 fluctuation as shown in Figure 2.2A. In this section, I performed functional analysis of this 'LATS2-dependent H3K27me3' (I referred this genes as 'H3K27me3-loss' in ChIP-seq section) to obtain insight of biological relevance in detail.

5.1 'LATS2-dependent H3K27me3 targets' correlates with the signature of un-differentiated cells

I attempted to explore the potential physiological relevance of the LATS2-responsive PRC2 signal. To more precisely evaluate the LATS2-dependent epigenetic signature, I analyzed ChIP-seq and RNA-seq data based on properties of their promoters. To this end, I categorized promoters of protein-coding genes into three classes based on their CpG content (Mikkelsen et al., 2007): 1) High-CpG promoter (HCP), associated with both housekeeping genes and other genes with complicated expression patterns during development. This class often includes genes with bivalent states, i.e., those that possess both H3K27me3 and H3K4me3 marks in their promoters; 2) Low-CpG promoter (LCP), associated with genes that are under control of tissue-specific transcription factors and are often repressed by DNA methylation. This class exhibits tissue-specific expression pattern during differentiation; and 3) Intermediate-CpG promoter (ICP), i.e., genes which are neither HCPs nor LCPs. (HCP, LCP and ICP) (Figure 5.1A). Promoter analysis of potential LATS2-dependent epigenetic signatures, i.e., 'H3K27me3-loss' module from HeLa-S3 study, revealed that this module significantly correlated with the LCP class ($p = 5.2E-117$, Fisher's exact test) (Figure 5.1B). Consistent with this, fluctuations in gene expression were larger in the LCP class than in HCP or ICP (Figure 5.1C). LCP genes are associated with tissue-specific transcription programs during differentiation. Indeed, the LATS2-responsive PRC2 target genes in HeLa-S3 cells correlated with genes harboring the H3K27me3 mark specifically in human ES cells rather than differentiated cells (vs. human fibroblasts, used as a reference sample) ($p = 2.0E-173$, Fisher's exact test) (Figure 5.1D).

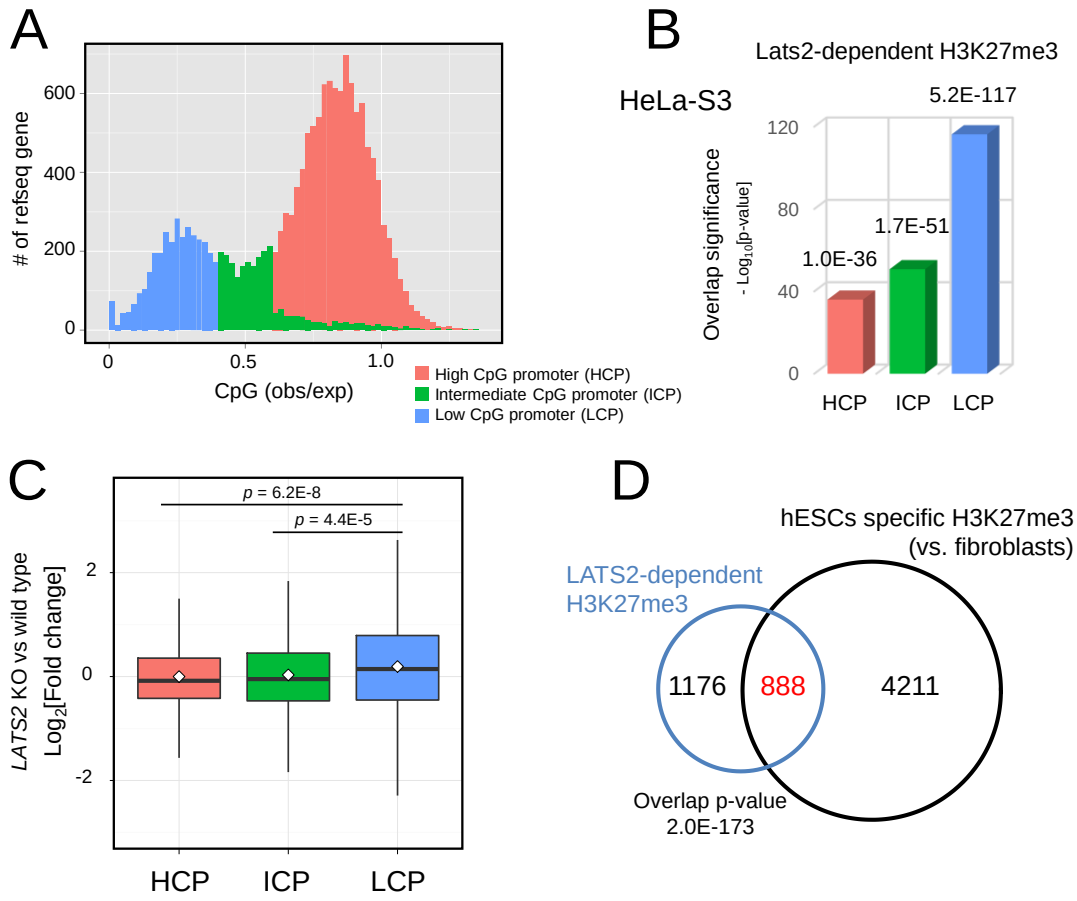

Figure 5.1 *LATS2* KO HeLa-S3 cells exhibit significant activation of LCPs.
(**A**) Histogram showing the distribution of observed versus expected CpG frequencies for all promoters of protein-coding genes. The histogram shows a bimodal distribution of CpG-rich and CpG-poor promoters. All promoters were classified into three non-redundant three groups based on their CpG content as described previously (Mikkelsen *et al.* 2007). (**B**) Bar plot showing the significance of overlap of genes with each class of promoters with genes containing LATS2-dependent H3K27me3 marks. (**C**) Box-and-whisker plots showing the expression level of transcriptionally active genes with different promoter classes, based on RNA-seq experiments. p-value was calculated by the Wilcoxon rank-sum test for comparison of two unpaired groups. In *LATS2* KO HeLa-S3 cells, significant genomic perturbations were observed in LCP promoters. (**D**) Venn diagram showing the overlap of genes in which H3K27me3 peaks within ±5 kb of the TSS decreased after *LATS2* KO in HeLa-S3 cells (blue) with genes harboring H3K27me3 marks specifically in human ESCs (i.e., genes in which the H3K27me3 level was significantly higher in hESCs than in human fibroblasts) (black). The 'H3K27me3-loss' genes from ChIP-seq experiment were subjected to NextBio analysis as LATS2-dependent H3K27me3 targets.

5.2 Nervous system specific alternation of expression of LATS2 – H3K27me3 targets

LCP genes are often associated with tissue-specific transcription programs during differentiation. Next, to reveal the tissue or context specificity of LATS2-dependent H3K27me3, I explored expression pattern of this module by Body Atlas tool of NextBio statistical platform. This tool enables us to review expression pattern of queried genes in various tissues by using uniformly processed thousands of microarray studies. Interestingly, LATS2-dependent H3K27me3 targets were expressed relatively low levels in embryonic cells, but were over-expressed in the nervous system (Figure 5.2A and B). These observations indicate that the expression pattern of the LATS2–PRC2 signal is converted to an active state during neurogenesis. This is consistent with the observation that Lats2-deficient mice showing fundamental functions of Lats2 in this tissue, i.e., *Lats2* KO mice exhibit embryonic lethality due to a defect in development of the central nervous system (Yabuta et al., 2007). Furthermore, the correlation of LATS2-depedent H3K27me3 targets with expression of nervous functions have been already described in GO analysis in Figure 2.2D.

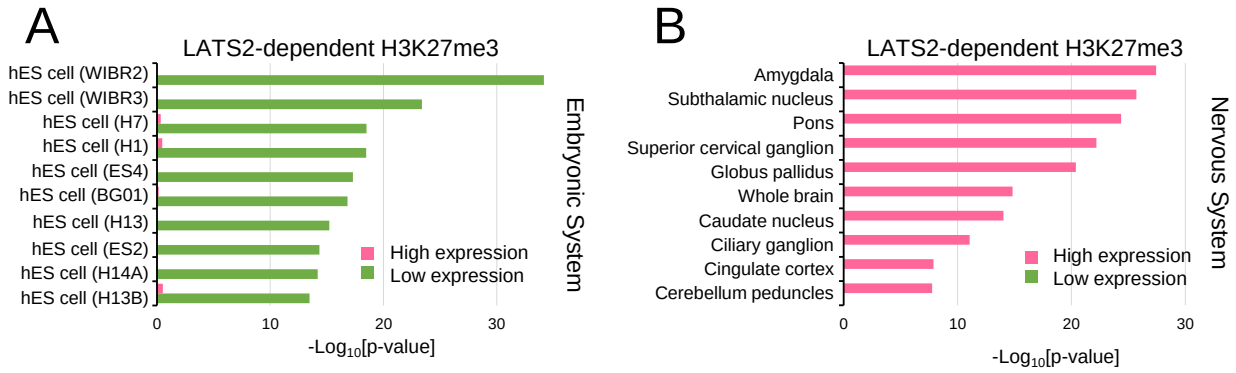

Figure 5.2 'LATS2-dependent H3K27me3 targets' show unique expression pattern in nervous system.

(**A–B**) The 'H3K27me3-loss' module exhibits an inverse expression pattern between embryonic cells and the nervous system. The 'H3K27me3-loss' genes were subjected to NextBio analysis as LATS2-dependent H3K27me3 targets, and then the tissue-specific expression pattern was extracted from the Body Atlas tool.

5.3 Induction of 'LATS2-dependent H3K27me3 targets' during neurogenesis

The association of Lats2 with PRC2 during neurogenesis is further supported by a previous study in *Drosophila*: a mutant of *Wts*, the *Drosophila* homolog of Lats1/2, phenocopies the effect of

Polycomb group (PcG) mutants on dendrite maintenance (Parrish et al., 2007). Indeed, the expression profile of *LATS2* KO HeLa-S3 cells (relative to wild type HeLa-S3 cells) positively correlated with that of differentiated neurons relative to neural stem cells (Figure 5.3A) (i.e., the expression profile of cells with LATS2 correlated with that of neural stem cells). Further analysis revealed that the expression of genes with Lats2-dependent H3K27me3 marks in HeLa-S3 was highly induced during the differentiation of ES cells into mature neuron cells (Figure 5.3B). These results suggest that potential LATS2-responsive H3K27me3 targets are repressed in dedifferentiated cells, and then gradually induced in the proneural stage.

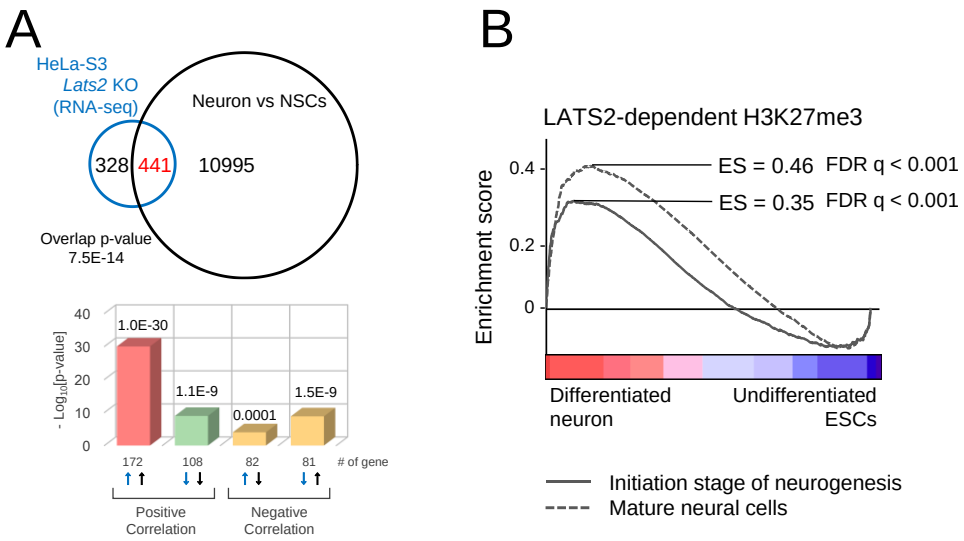

Figure 5.3 'LATS2-dependent H3K27me3 targets' are induced during neurogenesis.

(**A**) Significant overlap of genes differentially expressed in *LATS2* KO HeLa-S3 cells with genes involved in neurogenesis. Genes differentially expressed in *LATS2* KO HeLa-S3 cells (≥2-fold, p-value <0.05) were subjected to NextBio analysis. Venn diagrams show the number of common and unique genes in both sets. Bar plots show the significance of overlap in each direction. (**B**) GSEA for the 'H3K27me3-loss' genes in human ES cells after induction of neural differentiation. Genes are ranked according to the fold change, derived from microarray experiments (differentiating cells vs. ES cells) (GSE28633). A positive enrichment score indicates increased expression after the induction of neural differentiation.

5.4 LATS2 – PRC2 axis in other differentiation models

To evaluate the neural specificity of the expression pattern of LATS2-dependent H3K27me3

targets in development processes, I explored other transcriptome datasets in previous studies. GSEA of LATS2-dependent H3K27me3 targets for some differentiation models such as cardiac, pancreatic, erythroid, hematopoietic, neural and hepatocyte differentiation models from human embryonic stem cells, neural progenitors or erythroblasts, clearly showed that only for neural differentiation model, LATS2-dependent H3K27me3-marked genes ware strongly induced during differentiation. It should be noted that time-course study for neural differentiation (GSE28046) in Figure 5.4 is a different study with that I analyzed in Figure 5.3 (GSE28633). This results strongly indicates fundamental roles of this gene module for neural differentiation processes.

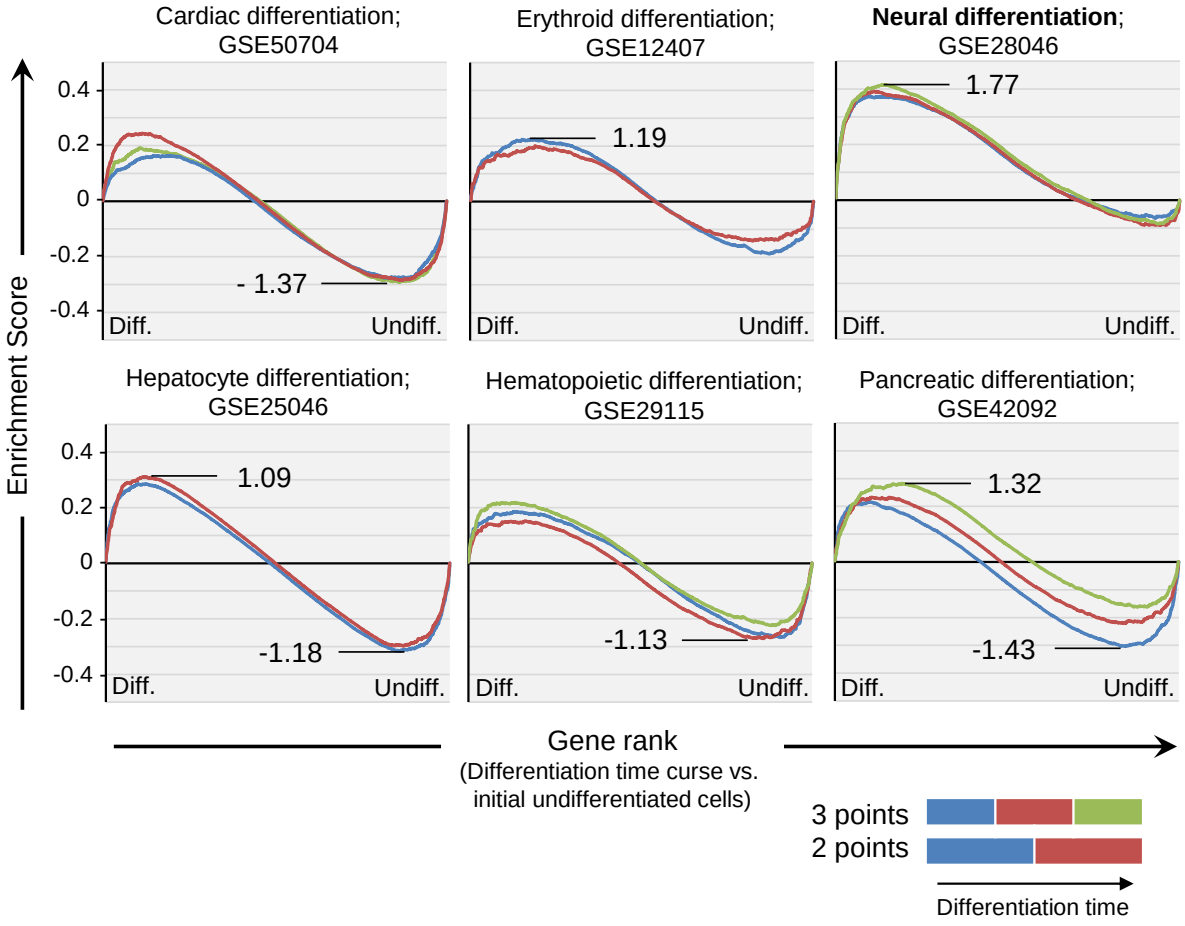

Figure 5.4 GSEA showing neural specific induction of 'LATS2-dependent H3K27me3 targets'.

GSEA for 'H3K27me3-loss' genes in various differentiation systems. Previous time-course studies of differentiation induction from un-differentiated cells were re-analyzed. Genes are ranked according to the fold change, derived from each microarray experiments (i.e., [each time point]/[un-differentiated samples]). A positive enrichment score indicates increased expression of LATS2-PRC2 targets after

the induction of differentiation. Normalized enrichment scores were represented in each panel.

5.5 Summary of section 5

1. LATS2-dependent H3K27me3 target genes which were defined in ChIP-seq analysis of *LAS2* KO HeLa-S3 cells, were significantly correlate to neural functions.
2. LATS2-dependent H3K27me3 targets were specifically induced during neural differentiation.

6. Association between LATS2 and PRC2 in brain tumorigenesis

Because LATS2 may contribute (via PRC2) to maintenance of the dedifferentiated state in the nervous system, I hypothesized that LATS2 can contribute to tumorigenesis in neural cells. In this section, I tried to obtain an association between LATS2 expression and clinical prognosis, using the datasets from The Cancer Genome Atlas (TCGA) (Cancer Genome Atlas Research Network, 2008).

6.1 LATS2 exhibits a unique expression pattern in glioblastoma multiforme (GBM)

First, to characterize the expression of LATS2 in various types of cancer, I visualized the relative expression level of the LATS2 gene using 8,415 RNA-seq datasets from TCGA. In many types of cancer, LATS2 tended to be expressed at low levels in tumor samples relative to normal solid tissue, consistent with the known tumor-suppressive properties of LATS2. By contrast, in GBM, the most common and most aggressive malignant primary brain tumor, LATS2 was expressed at higher levels in tumor samples than in normal tissue (Figure 6.1A, upper panel). To characterize the expression of LATS2 in detail, I examined array-based transcriptome data from 583 samples, including ten normal brain samples, from the TCGA portal site. In this dataset, I again observed significantly high LATS2 expression in primary tumor samples (Figure 6.1B, left panel). Common GBM patients can be divided into four expression subtypes (Verhaak et al., 2010); LATS2 expression was elevated in all but the proneural subtype (Figure 6.1C), which has a transcription signature related to neurogenesis and exhibits a more differentiated expression pattern than the other subtypes. Intriguingly, LATS1 did not exhibit a similar expression pattern in GBM (Figure 6.1A, lower panel and 6.1B, right panel), suggesting that up-regulation of LATS2 is not simply a result of activation of the canonical Hippo signal cascade, in which LATS2 and LATS1 are functionally complementary to each other. These results are consistent with my model in which LATS2 expression contributes to dedifferentiation of neural cells.

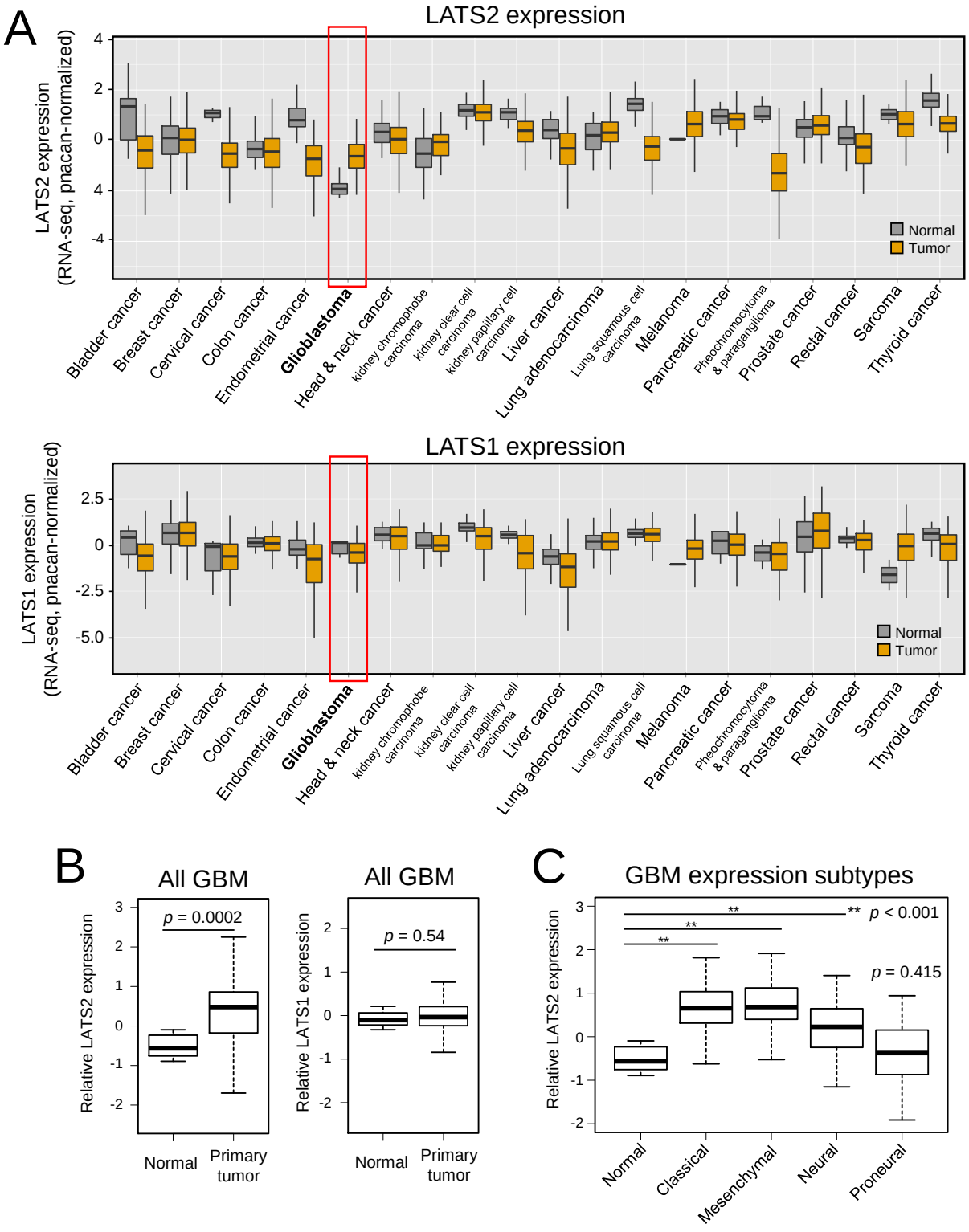

Figure 6.1 LATS2 is upregulated in some type of GBM except for proneural subtype.

(**A**) Box-and-whisker plots of mRNA expression of LATS2 in normal tissues and human cancers. mRNA expression data of LATS2 for various cancers and normal tissue samples

were obtained from TCGA pan-cancer cohorts. Cancers with at least one normal sample were analyzed and visualized. (**B**) Box-and-whisker plots of *LATS2* mRNA expression in normal brain and primary glioblastoma multiforme (GBM). *LATS2* mRNA expression data for GBM and normal tissue samples were obtained from level 3 preprocessed expression data from Agilent 244K custom gene-expression G4502A_07_2 microarrays. Statistical significance of differences between normal brain and primary tumor was evaluated by Wilcoxon rank-sum test. (**C**) Box-and-whisker plots of *LATS2* mRNA expression in normal brain and predefined gene-expression subtypes of GBM. Statistical significance between normal brain and each subtype was evaluated by paired Wilcoxon rank-sum test.

6.2 Enhancement of LATS2 expression correlates with epigenetic dysregulation and poor prognosis in GBM

I next performed GSEA to determine whether genes potentially targeted by H3K27me3 or genes related to neurogenesis are differentially expressed in LATS2-low GBM (i.e., whether positive effects of LATS2 on PRC2-mediated repression of genes for neural differentiation were disturbed). To obtain gene expression profiles that depend on LATS2, I first divided GBM cases into two groups: those with higher expression of LATS2 than the median for normal brain (n = 411, 'LATS2-high') and those with lower-than-median expression (n = 54, 'LATS2-low'). I performed GSEA using this profile. Consistent with my hypothesis, known H3K27me3 targets were highly expressed in LATS2-low GBM samples (Figure 6.2A). Moreover, some neuron-specific transcripts were positively associated with LATS2-low GBM samples (Figure 6.2B), whereas the stem-cell signature was enriched in LATS2-high GBM samples (Figure 6.2C). Furthermore, I discovered a correlation between LATS2 expression and clinical prognosis. Kaplan–Meier curves and estimates of survival data revealed that patients with higher-than-median LATS2 expression exhibit poorer clinical prognoses than patients with lower-than-median LATS2 expression (n = 466; p = 0.00512) (Figure 6.2D). Importantly, the difference in the survival probability simply reflects the difference between the proneural subtype and the other subtypes. I observed a similar tendency in survival probability in an analysis using only proneural samples (n = 115) (Figure 6.2E). These results support the impact of the LATS2 signal via PRC2 in both development and dedifferentiation of the nervous system.

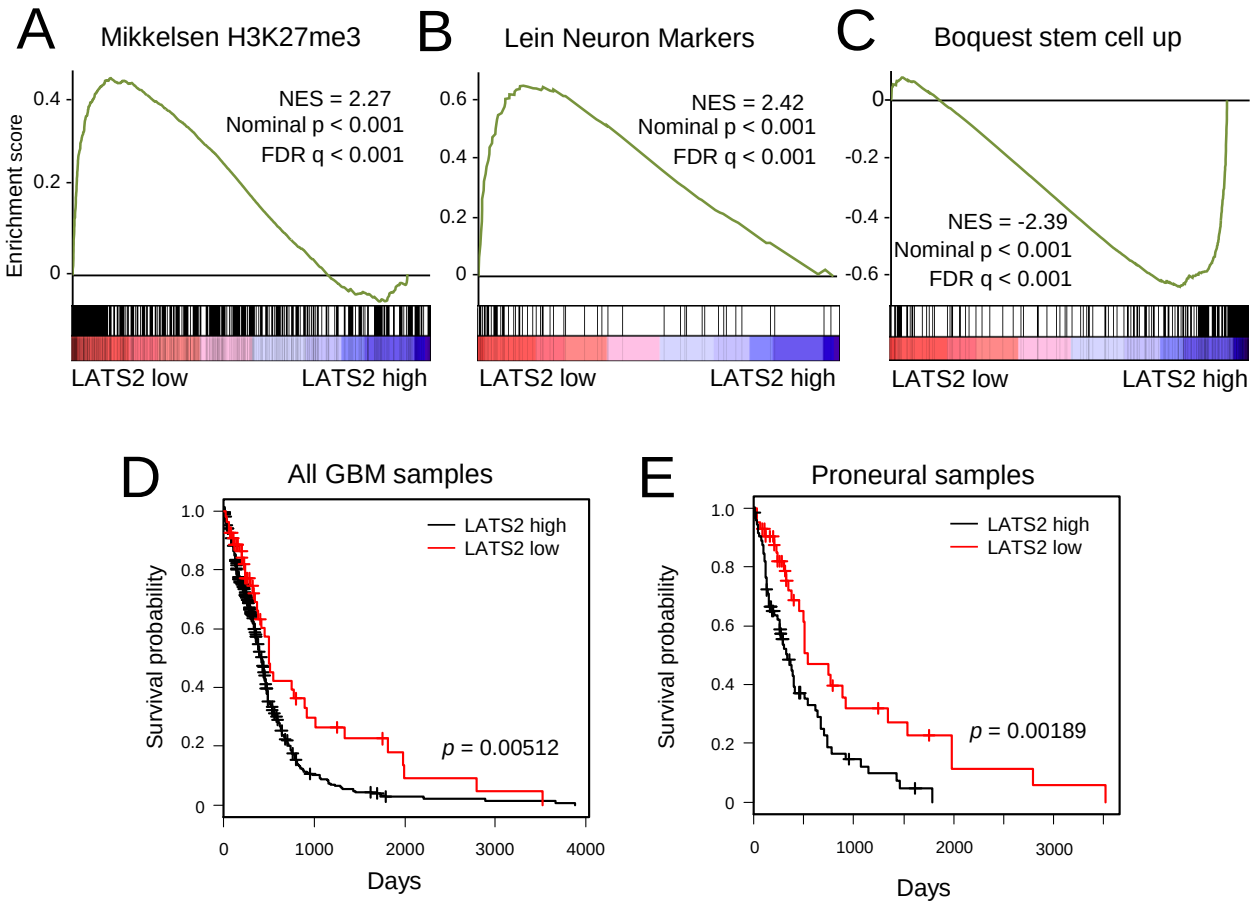

Figure 6.2 Expression level of LATS2 correlates with epigenetic dysregulation and poor prognosis of GBM

(**A–C**) GSEA of GBM samples divided into two groups based on LATS2 level, for H3K27me3 targets (A), neuron marker genes (B), and stemness marker genes (C), respectively. Genes are ranked according to the average fold change derived from level 3 preprocessed expression data from Agilent 244K custom gene-expression G4502A_07_2 microarrays (samples with low LATS2 expression vs. samples with high LATS2 expression). A positive enrichment score indicates increased expression in LATS2-low GBM samples, and negative enrichment score indicates increased expression in LATS2-high GBM samples. (**D**) Kaplan–Meier survival curves for survival (days) of all GBM patients, stratified by LATS2 mRNA expression level. GBM patients were divided into two groups based on the median of normal samples. Statistical significance was assessed by log-rank test. (**E**) Kaplan–Meier survival curves for survival (days) of proneural-subtype patients, stratified by LATS2 mRNA expression level. Proneural-subtype samples were divided into two groups based on the median of normal samples. Statistical significance was assessed by a log-rank test.

6.3 Summary of section 6

1. LATS2, not but LATS1 shows enhanced expression specifically in GBM.
2. This observation suggests that up-regulation of LATS2 does not simply reflect up-regulation of canonical Hippo signaling in GBM.
3. LATS2-high GBM shows low-expression of H3K27me target genes and correlates with more dedifferentiated expression signature and poor prognoses.

7. Transcriptome analysis of *Lats2* KO mouse embryonic fibroblasts (MEFs)

Based on the correlation of LATS2 with PRC2 related signals in nervous system, I next examined if Lats2 also plays fundamental roles through PRC2 in mice. As I mentioned above, *Lats2* KO mice exhibit embryonic lethality due to a defect in development of the central nervous system (Yabuta et al., 2007). In this section, I performed transcriptome analysis of *Lats2* KO MEFs and reviewed correlation with PRC2 and differentiation related signals in mouse

7.1 *Lats2* KO MEFs also exhibits dysregulation of PRC2 functions

I performed a microarray-based transcriptome analysis using *Lats2* KO MEFs (generated in previously; (Yabuta et al., 2007) (Figure 7.1A). Microarray experiment detected dozens hundreds of DEGs upon *Lats2* KO (Figure 7.1B). To examine whether potential H3K27me3 target genes fluctuated upon *Lats2* KO, I performed GSEA using two typical gene sets from previous studies. GSEA revealed significant enrichment of genes marked with H3K27me3 at their promoters, as well as target genes of PRC2 in *LATS2* KO MEFs ($p < 0.001$, Figure 7.1C, D). These correlations were further supported by a similar analysis using other MEF cell lines (Figure7.2A–C).

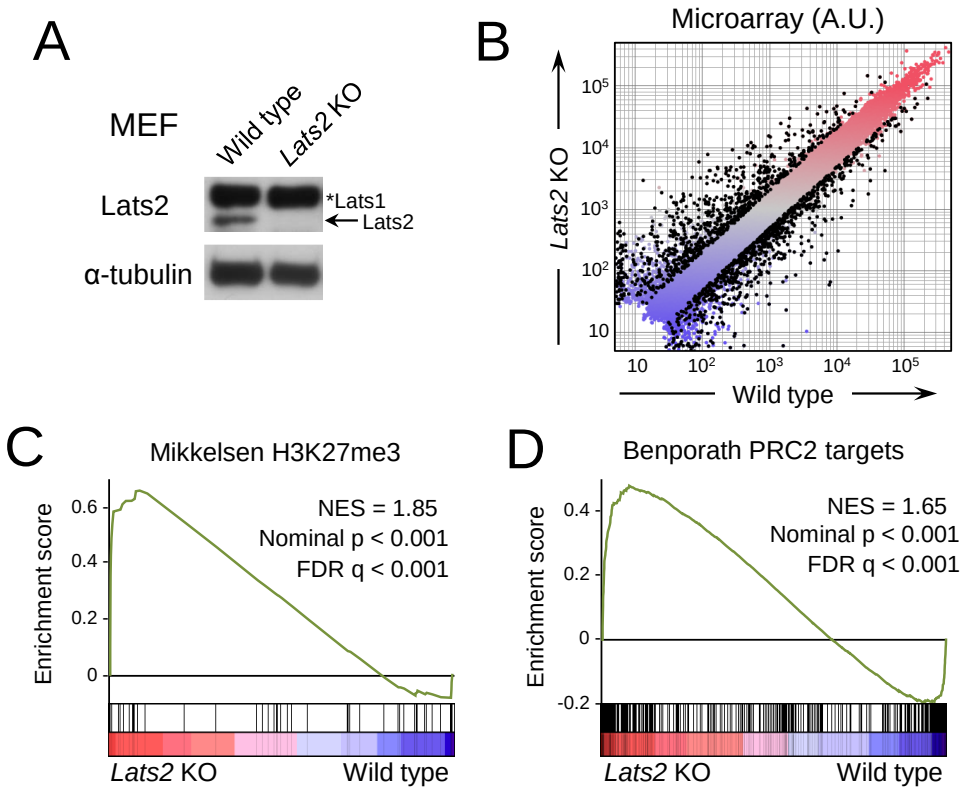

Figure 7.1 *Lats2* KO MEFs exhibit dysregulation of repressive epigenetic integrity
(**A**) Confirmation of *Lats2* KO by western blotting. The anti-Lats2 polyclonal antibody

used here recognizes the N-termini of both Lats2 and Lats1. The arrow represents Lats2 signals. '*Lats1' represents Lats1 signals. (**B**) Scatter plot of microarray data comparing *Lats2* KO and wild type MEFs. DEGs (≥2-fold, p-value <0.05) are highlighted in black dots. (**C**–**D**) GSEA of *Lats2* KO MEFs for potential H3K27me3-marked genes in iPS cells (C) and PRC2 targets in ES cells (D). Genes are ranked according to fold change (KO vs. wild type littermate control). A positive enrichment score indicates elevated expression after *Lats2* KO.

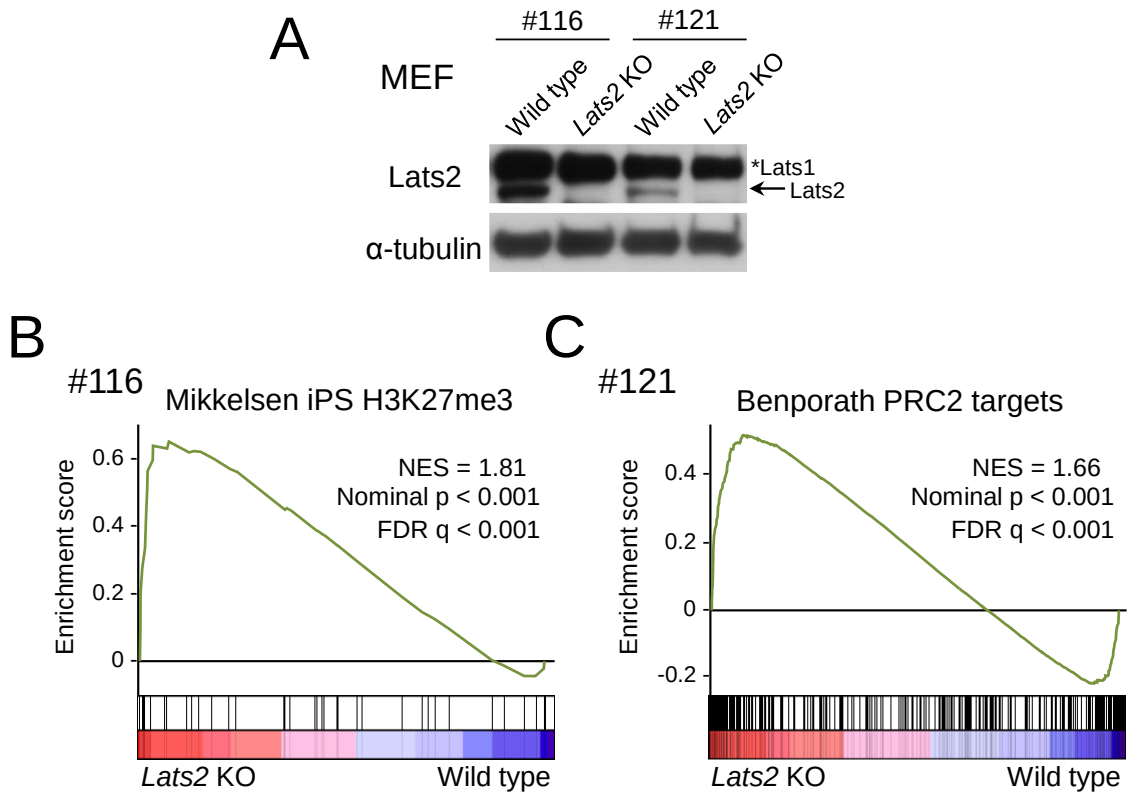

Figure 7.2 Other *Lats2* KO MEF lines also exhibit de-repression of PRC2 targets. (**A**) Representative western blot analysis of Lats2 in the other two lines of *Lats2* KO MEFs (#116 and #121), alongside cells from their wild type littermate. The arrow represents Lats2 signals. '*Lats1' represents Lats1 signals. (**B**) GSEA of genes with H3K27me3 marks in ES cells in *Lats2* KO MEF clone #116. Genes are ranked by fold change (KO vs. wild type littermate control). A positive enrichment score indicates enrichment in the set of genes that exhibit increased expression after *Lats2* KO. (**C**) GSEA of genes reported as PRC2 targets in *Lats2* KO MEF clone #121. Genes are ranked by fold change (KO vs. wild type littermate control). A positive enrichment score indicates enrichment in the set of genes that exhibit increased expression after *Lats2* KO.

7.2 *Lats2* KO causes up-regulation of genes for differentiation

These results suggest that Lats2 exerts repressive effects on epigenetically silenced genes in mice. Interestingly, Lats2 maintains pluripotency and regulates initiation of appropriate differentiation of ES cells (Aylon et al., 2014). I next investigated whether the dysregulation of repressive epigenetic mechanisms caused by *Lats2* KO (as shown in Figure 7.1 and 7.2) is related to differentiation processes or maintenance of stemness. I performed GSEA on the expression profile of *Lats2* KO MEFs, using signatures of differentiation or stemness defined in a previous meta-analysis of human ES cells and differentiating stem cells (Assou et al., 2007). In agreement with previous study, *Lats2* KO was associated with a significant enrichment of genes that are expressed during developmental processes (Differentiation signature; NES = 1.69, $p < 0.001$, Stem cell signature; NES = -1.27, $p = 0.022$) (Figure 7.3A and B). These correlations were also validated by knowledge-based meta-analysis by Ingenuity Pathway Analysis software: genes related in cellular and tissue development were fluctuated to facilitate each processes (Figure 7.3C).

Consistent with the observations above, some well-known epigenetically regulated transcripts associated with differentiation, such as homeotic genes, were up-regulated in *Lats2* KO MEFs (p = -5.6E-8, Fisher's exact test) (Figure 7.4A–E). The unidirectional expression change that I observed at the *Hoxb* locus indicates that the cells were undergoing locus-wide epigenetic changes such as changes in chromatin accessibility. Further exploration revealed another locus-wide de-repressed region at the *Dlk1–Dio3* locus, a well-characterized imprinted locus on chromosome 12qF1 (da Rocha et al., 2008) (Figure 7.5A and B). This locus contains non-coding RNA clusters whose expression levels affect the differentiation capacity of mouse ES cells (Stadtfeld et al., 2010) (Figure 7.5A and C). Array-based microRNA profiling (Figure 7.5D) revealed that non-coding RNAs in this locus were also highly up-regulated in *Lats2* KO MEFs, and were also responsive to some epigenetic inhibitors (Figure 7.5E, orange dots). These results suggest that PRC2 target genes which respond to differentiation processes, are specifically de-repressed upon *LATS2* KO.

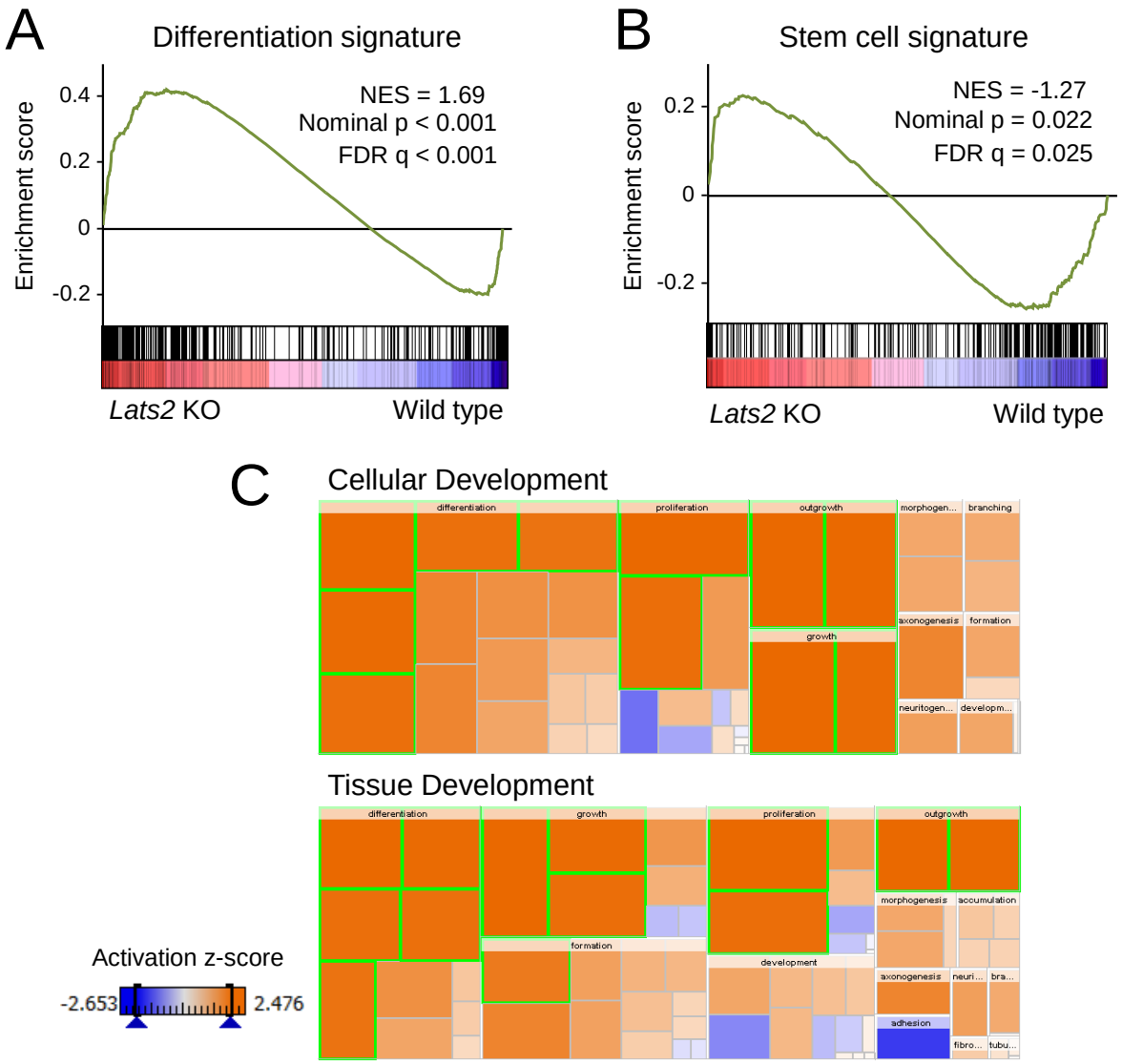

Figure 7.3 *Lats2* KO MEFs exhibit up-regulation of genes involved in differentiation processes.

(**A–B**) GSEA of *Lats2* KO MEFs for hES-specific and differentiation-related genes. Expression changes (all expressing probes in three independent cell lines were combined into a single rank ordered gene list) upon *Lats2* KO were subjected to GSEA as signature dependent on loss of Lats2. hESC-specific genes were those over-expressed in human ES cells in 5 or more of 20 profiling studies, and differentiation genes were those over-expressed in differentiated cells in 4 or more studies (Assou et al., 2007). (**C**) Heatmaps showing facilitation of differentiation processes upon *Lats2* KO. DEGs in *Lats2* KO MEFs (≥2-fold, gene ranking in (A)) were applied to IPA software. Heat-color represents correlation of genes with differentiation-progressive signatures.

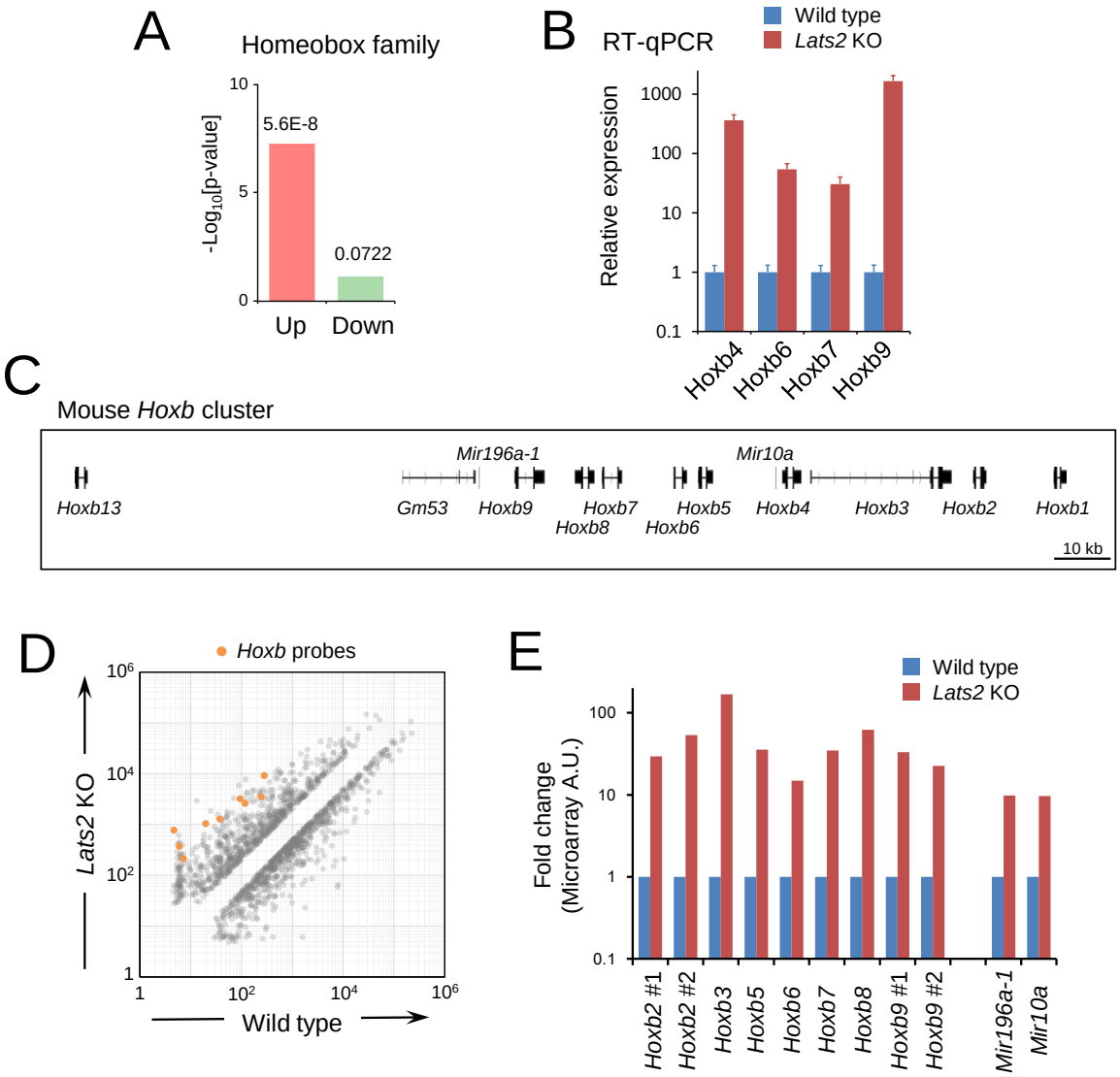

Figure 7.4 *Lats2* KO MEFs exhibit up-regulation of homeotic genes.

(**A**) Enrichment analysis for protein families showing significant overlap of up-regulated genes in *Lats2* KO MEFs with Homeobox protein family. Genes differentially expressed in *Lats2* KO MEFs (≥2-fold, p-value <0.05) were subjected to NextBio analysis. (**B**) Gene expression analysis of Hoxb genes detected by microarray analysis in (A). The *Hoxb* cluster is highly de-repressed in *Lats2* KO MEFs. RT-qPCR was performed in two independent experiments, and levels of each transcript were normalized to *Gapdh*. Error bars show SD. (**C**) Schematic representation of the murine *Hoxb* cluster, showing the genomic position of each gene. (**D**) Scatter plot of microarray data comparing *Lats2* KO and wild type MEFs with DEGs (2-fold, p-value <0.05). Probes for *Hoxb* genes are highlighted in orange. (**E**) Bar plots showing de-repression of *Hoxb* loci. Fold change for each *Hoxb* gene, as determined by microarray experiments. miR-196a and miR-10a are intergenic microRNAs in the *Hoxb* locus.

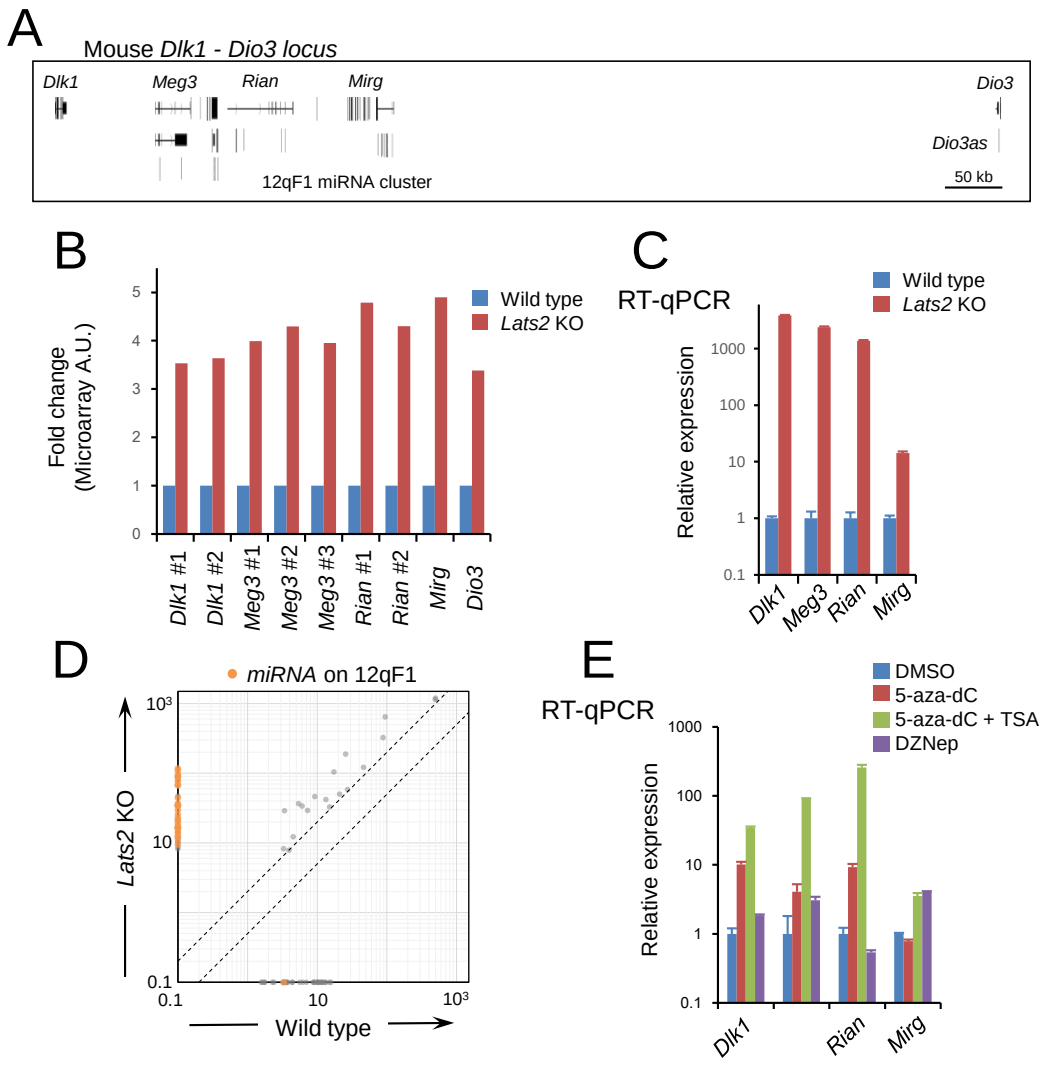

Figure 7.5 *Lats2* KO MEFs exhibit up-regulation of imprinted genes silenced by epigenetic mechanisms.

(**A**) Schematic representation of the murine *Dlk1–Dio3* locus, showing the genomic position of each gene. (**B**) Bar plots showing de-repression of transcripts in the *Dlk1–Dio3* locus. Fold change of probes in microarray experiments are represented. (**C**) Gene-expression analysis for coding/non-coding genes detected by microarray analysis. (**D**) Scatter plot of microarray data comparing *Lats2* KO and wild type MEFs with differentially expressed microRNAs (≥2-fold, p-value <0.05). Probes for microRNAs in the 12qF1 locus are highlighted in orange. (**E**) RT-qPCR analysis showing the epigenetic inhibitor-induced expression of genes in 12qF1 in wild-type MEFs. Wild-type MEFs were treated with 5-aza-2'-deoxycytidine (5-aza-dC), trichostatin A (TSA), or 3-deazaneplanocin A (DZNep), and then subjected to RT-qPCR. Gapdh was used as an internal control.

7.3 Elevation of differentiation-related genes upon *Lats2* KO is independent of output of canonical Hippo pathway

Lats2 kinase inhibits the oncogenic transcription co-activators Yap and Taz, components of the Hippo signaling pathway (Pan, 2010). This 'canonical' Hippo pathway contributes to various processes related to both normal development and tumorigenesis. The significant overlap of up-regulated genes in *Lats2* KO MEFs with genes for differentiation that I observed here may be simply a result of canonical Hippo–YAP/TAZ signaling, which is caused by activation of Yap/Taz due to *Lats2* depletion (Figure 7.6A).

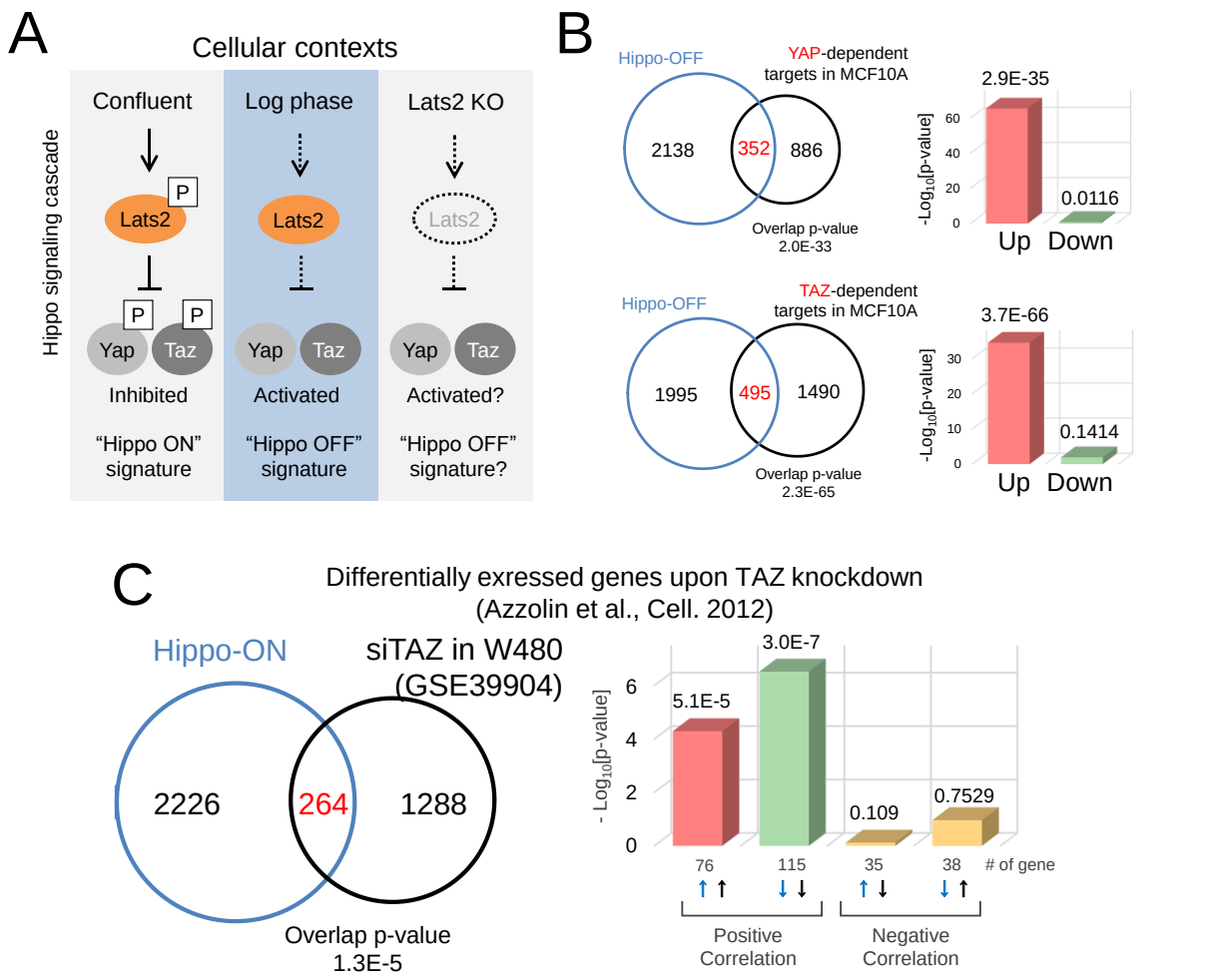

Figure 7.6 Characterization of Hippo-OFF/ON signature for comparison with *Lats2* KO profile.

(**A**) Schematic representation of the canonical Hippo signaling cascade and the putative state caused by *Lats2* KO. (**B**) Significant overlap of differentially expressed

genes in growing MEFs (i.e., Hippo-OFF; Lats2 is not activated) with genes up-regulated upon over-expression of YAP (top) or TAZ (bottom) in MCF10A cells in previous study. Genes differentially expressed upon contact inhibition (growing vs. confluent) (≥2-fold, p-value <0.05) were subjected to NextBio analysis. Venn diagrams show the number of common and unique genes in both sets. Bar plots show the significance of overlap in each direction. (**C**) Similar analysis to (B), excepts for using Hippo-OFF signature (i.e., confulent vs. growing) and differentially expressed genes upon TAZ knockdown in glioma cell line W480.

To determine whether my *Lats2* KO expression signature was Yap/Taz-dependent, I compared gene expression in *Lats2* KO MEFs and rapidly growing wild type MEFs in log-phase, which have active Yap/Taz (i.e., 'Hippo OFF' signature). Before precise functional analyses, I reviewed the validity of this "Hippo OFF" signature as a Yap/Taz dependent signature in MEFs. Comparison analyses between 'Hippo OFF (or ON)' signature and some previously defined potential YAP/TAZ targets or gene signature, revealed that my 'Hippo OFF' signature based on MEFs includes known YAP/TAZ dependent profile (e.g. NextBio platform; $p < 2.3E-65$, Fisher's exact test for TAZ target genes) (Figure 7.6B and C). Then I performed GO analysis of ontological terms related to differentiation processes by using both '*Lats2* KO' and 'Hippo OFF' signature. This comparison analysis revealed that growing cells, in which the intrinsic Hippo pathway is turned off and Yap/Taz is active, show associations with differentiation processes less significantly than *Lats2* KO profile. (Figure 7.7). This result indicates that the association of up-regulated genes in *Lats2* KO MEFs with differentiation processes does not simply reflect the output of the canonical Hippo pathway. Thus, Lats2 may have the ability to maintain a dedifferentiated state by repressing genes involved in development, and this regulatory function is partially independent of canonical Hippo activity.

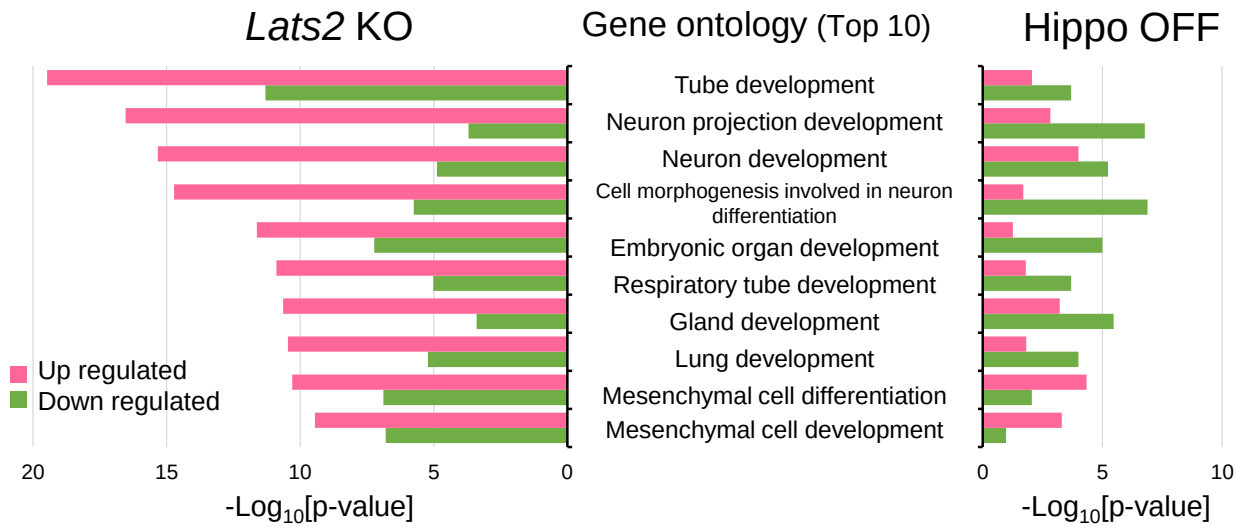

Figure 7.7 *Lats2* KO causes up-regulation of genes for differentiation processes without depending on the canonical Hippo signals.

GO enrichment analysis for canonical pathways related to differentiation processes. Genes differentially expressed (≥2-fold, p-value <0.05) in *Lats2* KO MEFs and in a Hippo-inactive state (growing in log-phase/high-density culture of wild type MEFs) were subjected to NextBio analysis. *Lats2* KO profile shows associations with differentiation processes more significantly than Yap/Taz-dependent profile. Statistical significance was calculated by Fisher's exact test.

7.4 Summary of section 7

1. *Lats2* KO MEFs exhibit transcriptome signature indicating dysregulation of PRC2.
2. *Lats2* positively contributes to repression of genes for differentiation processes.
3. These correlations are independent of canonical Hippo signaling.

4. Discussion

Many studies showed that PRC2 and other epigenetic coordinators play fundamental roles in stemness maintenance, development, and tumorigenesis (Margueron and Reinberg, 2011; Schuettengruber and Cavalli, 2009). These advances were made possible in large part by advances in high-throughput sequencing technologies. Accordingly, massive epigenome datasets from many type of cells were generated by global projects such as the ENCODE consortium (ENCODE Project Consortium, 2012). Despite the increased availability of public datasets, these data primarily consist of 'snapshot' images of specific targets and cell lines. On the other hand, due to the challenges of characterizing the multiple responsible elements of each complex and searching for novel accessory components, their upstream signals and downstream specificity remain poorly understood at a molecular level. Although some studies revealed the impacts of post-translational modification of PRC2 components on the function of the complex (Chu et al., 2014; Kaneko et al., 2010; Wei et al., 2011; Zeng et al., 2011), the diversity of modifications and alternative components imply the existence of complicated cross-talk and complementation of many cellular signals, making it difficult to understand the spatiotemporal regulation of epigenetic integrity. Based on many studies of epigenomic profiles, including analyses of DNA methylation patterns, histone modification states, and higher-order chromatin conformation, it is clear that changes in the epigenetic landscape are associated with many human diseases, including cancers (Feinberg, 2007; Margueron and Reinberg, 2011). Indeed, novel drugs were developed to inhibit the enzymes that regulate the epigenetic machinery (Helin and Dhanak, 2013). In contrast to traditional drugs that target a single cellular signal, these drugs can influence many cellular signals and signatures of disease development simultaneously, making them promising candidates for treating complex diseases such as cancer. However, the epigenetic signatures targeted by these drugs differ across cell types and tissues. To overcome this problem, current drugs target known somatic mutations of epigenetic regulators to ensure their specificity (Kondo, 2014). Based on this situation, it is clear that understanding of the upstream signals of epigenetic regulators will be necessary to achieve more effective and accurate clinical applications.

In this study, I showed that LATS2, a pivotal Ser/Thr kinase of the Hippo signaling pathway, is a novel upstream regulator of PRC2. The LATS2–PRC2 axis seems to be independent of the canonical Hippo signal cascade. Although LATS2 is a core tumor suppressor, involved not only in the Hippo signaling pathway but also in regulation of the cell cycle and the DNA-damage response (Visser and Yang, 2010), recent studies suggested that LATS2 also cooperates with TP53 and is crucial for maintenance of stemness in ES cells (Aylon et al., 2014). LATS2 may also serve an essential function

in dedifferentiated states, as evidenced by observations of knockout mice: *Lats2* KO mice exhibit embryonic lethality (Yabuta et al., 2007), whereas *Lats1* KO mice do not (McPherson et al., 2004; Mukai et al., 2015; St John et al., 1999), suggesting that Lats2 plays essential roles in developmental processes other than Hippo signaling. It has been reported that *Lats2* KO mice exhibit developmental defects in the central nervous system (Yabuta et al., 2007). Consistent with this observation, omics-based analysis revealed that the genes differentially regulated in *LATS2* KO HeLa-S3 cells and *Lats2* KO MEFs relative to the corresponding wild type parental cells are significantly associated with differentiation processes, especially neurogenesis. In both HeLa-S3 cells and MEFs, these Lats2-dependent signatures also correlate with dysregulation of PRC2 and the H3K27me3 mark for which it is responsible. The association of Lats2 with Polycomb genes was first identified in *Drosophila* dendrite neuron maintenance (Parrish et al., 2007), but no further precise characterization was performed. Thus, my findings in this study expand the importance of Lats2 in neurogenesis from *Drosophila* to higher organisms.

The down-regulation of PRC2 and the resultant reduction in H3K27me3 following *LATS2* KO in HeLa-S3 was observed at both the protein and mRNA levels of PRC2. ChIP-seq analysis of *LATS2* KO HeLa-S3 cells revealed that not only H3K27me3, but also H3K4me3-mark was reduced throughout the genome. This reduction in H3K4me3 may cause transcriptional down-regulation of EZH2 and EED. The H3K27me3 mark antagonizes the effect of the H3K4me3 mark at many promoters (Schmitges et al., 2011). Therefore, bivalent domains, in which both repressive H3K27me3 and active H3K4me3 marks co-exist at the same locus, should arise in specific cellular contexts such as embryogenesis. By contrast, my observation of global reduction of both H3K27me3 and H3K4me3 suggests interdependence of these two histone marks. Indeed, previous study revealed that PRC2 components cooperate with TrxG proteins, which are responsible for H3K4me3 marks (Kim et al., 2007). The LATS2 signal in HeLa-S3 cells forms a feedback loop that maintains H3K27me3 and H3K4me3 integrity. In addition, other statistical analyses showed that DEGs in *LATS2* KO HeLa-S3 cells significantly overlapped with genes regulated by other epigenetic machineries such as HDACs, DNMTs, and KDM1A (unpublished data). Based on these observations, the next challenge is to elucidate the crosstalk of these epigenetic mechanisms dependent on LATS2 kinase.

Another novel insight of this study is that through PRC2, LATS2 is associated with both development and dedifferentiation of the nervous system. The correlation between the *LATS2* KO signature and neural function, revealed in a series of statistical analyses of both HeLa-S33 cells and MEFs, strongly suggests that LATS2 plays fundamental roles in neural stemness. Indeed, LATS2 exhibited a unique expression pattern in GBM. Recent studies revealed that dysregulation of

H3K27me3 landscape is closely associated with glioma formation (Kondo et al., 2014). Moreover EZH2 plays important roles to maintain glioblastoma cancer stem cells (Natsume et al., 2013; Orzan et al., 2011). The low expression of LATS2 in normal brain, relative to other normal organs, may reflect the low level of cell proliferation in this tissue. By contrast, high expression of LATS2 in GBM indicates that LATS2 is required for robust growth of tumor cells. Consistent with this insight, although LATS2 has been characterized as a tumor suppressor for a decade, deletion or mutation of LATS2 in cancer patients is much less common than mutations in its known tumor-suppressive collaborators such as TP53 or pRb (Ishizaki et al., 2002). On the other hand, the determinant collaborators of LATS2 or signals which are responsible for tissue specific epigenetic coordination (e.g. nervous systems) remain elusive.

Taken together, results suggest that known tumor-suppressor genes may function as coordinators of oncogenic landscapes in specific tissues through regulation of the epigenome and/or transcriptome. Thus, even traditional tumor suppressors may become feasible target molecules for effective cancer therapies. Based on the above described results, I would propose a novel strategy that targets the cancer-associating epigenetic signatures. Namely, instead of directly inhibiting histone modifying enzymes such as PRC2, we might inhibit upstream regulators of PRC2 to guarantee the tissue- and/or tumor-specificity in cancer treatment (i.e., LATS2 inhibition may cause re-differentiation or reduce malignancy of GBM cells).

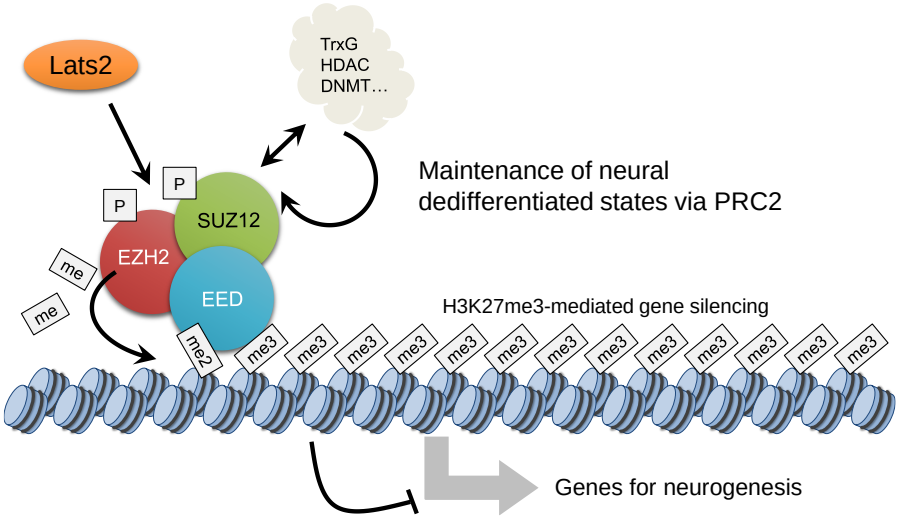

Figure D1. Schematic of the model which was revealed in this thesis.
LATS2 associates with PRC2 and phosphorylates them to support their ability to construct appropriate H3K27me3 landscapes. This signal may affects other epigenetic integrity (such as H3K4me3). LATS2 – PRC2 axis is important for both genome-wide H3K27me3 pattern and some tissue specific H3K27me3 patterns. In contrast, the determinant factors which collaborates with LATS2 and are responsible for tissue specificity, remain elusive.

References

Assou, S., Le Carrour, T., Tondeur, S., Ström, S., Gabelle, A., Marty, S., Nadal, L., Pantesco, V., Réme, T., Hugnot, J. P., *et al.* (2007). A meta-analysis of human embryonic stem cells transcriptome integrated into a web-based expression atlas. Stem Cells *25*, 961-973.

Aylon, Y., Michael, D., Shmueli, A., Yabuta, N., Nojima, H., and Oren, M. (2006). A positive feedback loop between the p53 and Lats2 tumor suppressors prevents tetraploidization. Genes Dev *20*, 2687-2700.

Aylon, Y., Ofir-Rosenfeld, Y., Yabuta, N., Lapi, E., Nojima, H., Lu, X., and Oren, M. (2010). The Lats2 tumor suppressor augments p53-mediated apoptosis by promoting the nuclear proapoptotic function of ASPP1. Genes Dev *24*, 2420-2429.

Aylon, Y., Sarver, A., Tovy, A., Ainbinder, E., and Oren, M. (2014). Lats2 is critical for the pluripotency and proper differentiation of stem cells. Cell Death Differ *21*, 624-633.

Ben-Porath, I., Thomson, M. W., Carey, V. J., Ge, R., Bell, G. W., Regev, A., and Weinberg, R. A. (2008). An embryonic stem cell-like gene expression signature in poorly differentiated aggressive human tumors. Nat Genet *40*, 499-507.

Berger, S. L., Kouzarides, T., Shiekhattar, R., and Shilatifard, A. (2009). An operational definition of epigenetics. Genes Dev *23*, 781-783.

Boulay, G., Rosnoblet, C., Guérardel, C., Angrand, P. O., and Leprince, D. (2011). Functional characterization of human Polycomb-like 3 isoforms identifies them as components of distinct EZH2 protein complexes. Biochem J *434*, 333-342.

Bracken, A. P., and Helin, K. (2009). Polycomb group proteins: navigators of lineage pathways led astray in cancer. Nat Rev Cancer *9*, 773-784.

Bruneau, B. G. (2010). Epigenetic regulation of the cardiovascular system: introduction to a review series. Circ Res *107*, 324-326.

Cancer Genome Atlas Research Network. (2008). Comprehensive genomic characterization defines human glioblastoma genes and core pathways. Nature *455*, 1061-1068.

Cao, R., Wang, L., Wang, H., Xia, L., Erdjument-Bromage, H., Tempst, P., Jones, R. S., and Zhang,

Y. (2002). Role of histone H3 lysine 27 methylation in Polycomb-group silencing. Science *298*, 1039-1043.

Cavalli, G., and Misteli, T. (2013). Functional implications of genome topology. Nat Struct Mol Biol *20*, 290-299.

Chan, S. W., Lim, C. J., Guo, K., Ng, C. P., Lee, I., Hunziker, W., Zeng, Q., and Hong, W. (2008). A role for TAZ in migration, invasion, and tumorigenesis of breast cancer cells. Cancer Res *68*, 2592-2598.

Christian, M., Cermak, T., Doyle, E. L., Schmidt, C., Zhang, F., Hummel, A., Bogdanove, A. J., and Voytas, D. F. (2010). Targeting DNA double-strand breaks with TAL effector nucleases. Genetics *186*, 757-761.

Chu, C. S., Lo, P. W., Yeh, Y. H., Hsu, P. H., Peng, S. H., Teng, Y. C., Kang, M. L., Wong, C. H., and Juan, L. J. (2014). O-GlcNAcylation regulates EZH2 protein stability and function. Proc Natl Acad Sci U S A *111*, 1355-1360.

Cifuentes-Rojas, C., Hernandez, A. J., Sarma, K., and Lee, J. T. (2014). Regulatory interactions between RNA and polycomb repressive complex 2. Mol Cell *55*, 171-185.

Cinar, B., Collak, F. K., Lopez, D., Akgul, S., Mukhopadhyay, N. K., Kilicarslan, M., Gioeli, D. G., and Freeman, M. R. (2011). MST1 is a multifunctional caspase-independent inhibitor of androgenic signaling. Cancer Res *71*, 4303-4313.

Czermin, B., Melfi, R., McCabe, D., Seitz, V., Imhof, A., and Pirrotta, V. (2002). Drosophila enhancer of Zeste/ESC complexes have a histone H3 methyltransferase activity that marks chromosomal Polycomb sites. Cell *111*, 185-196.

da Rocha, S. T., Edwards, C. A., Ito, M., Ogata, T., and Ferguson-Smith, A. C. (2008). Genomic imprinting at the mammalian Dlk1-Dio3 domain. Trends Genet *24*, 306-316.

ENCODE Project Consortium. (2012). An integrated encyclopedia of DNA elements in the human genome. Nature *489*, 57-74.

Feinberg, A. P. (2007). Phenotypic plasticity and the epigenetics of human disease. Nature *447*, 433-440.

Feng, J., Liu, T., Qin, B., Zhang, Y., and Liu, X. S. (2012). Identifying ChIP-seq enrichment using MACS. Nat Protoc *7*, 1728-1740.

Funato, Y., Terabayashi, T., Sakamoto, R., Okuzaki, D., Ichise, H., Nojima, H., Yoshida, N., and Miki, H. (2010). Nucleoredoxin sustains Wnt/β-catenin signaling by retaining a pool of inactive dishevelled protein. Curr Biol *20*, 1945-1952.

Heinz, S., Benner, C., Spann, N., Bertolino, E., Lin, Y. C., Laslo, P., Cheng, J. X., Murre, C., Singh, H., and Glass, C. K. (2010). Simple combinations of lineage-determining transcription factors prime cis-regulatory elements required for macrophage and B cell identities. Mol Cell *38*, 576-589.

Helin, K., and Dhanak, D. (2013). Chromatin proteins and modifications as drug targets. Nature *502*, 480-488.

Hergovich, A., and Hemmings, B. A. (2009). Mammalian NDR/LATS protein kinases in hippo tumor suppressor signaling. Biofactors *35*, 338-345.

Hirota, T., Morisaki, T., Nishiyama, Y., Marumoto, T., Tada, K., Hara, T., Masuko, N., Inagaki, M., Hatakeyama, K., and Saya, H. (2000). Zyxin, a regulator of actin filament assembly, targets the mitotic apparatus by interacting with h-warts/LATS1 tumor suppressor. J Cell Biol *149*, 1073-1086.

Ishizaki, K., Fujimoto, J., Kumimoto, H., Nishimoto, Y., Shimada, Y., Shinoda, M., and Yamamoto, T. (2002). Frequent polymorphic changes but rare tumor specific mutations of the LATS2 gene on 13q11-12 in esophageal squamous cell carcinoma. Int J Oncol *21*, 1053-1057.

Jiang, Z., Li, X., Hu, J., Zhou, W., Jiang, Y., Li, G., and Lu, D. (2006). Promoter hypermethylation-mediated down-regulation of LATS1 and LATS2 in human astrocytoma. Neurosci Res *56*, 450-458.

Justice, R. W., Zilian, O., Woods, D. F., Noll, M., and Bryant, P. J. (1995). The Drosophila tumor suppressor gene warts encodes a homolog of human myotonic dystrophy kinase and is required for the control of cell shape and proliferation. Genes Dev *9*, 534-546.

Kaneko, S., Bonasio, R., Saldaña-Meyer, R., Yoshida, T., Son, J., Nishino, K., Umezawa, A., and Reinberg, D. (2014). Interactions between JARID2 and noncoding RNAs regulate PRC2 recruitment to chromatin. Mol Cell *53*, 290-300.

Kaneko, S., Li, G., Son, J., Xu, C. F., Margueron, R., Neubert, T. A., and Reinberg, D. (2010). Phosphorylation of the PRC2 component Ezh2 is cell cycle-regulated and up-regulates its binding to

ncRNA. Genes Dev *24*, 2615-2620.

Kim, S. Y., Levenson, J. M., Korsmeyer, S., Sweatt, J. D., and Schumacher, A. (2007). Developmental regulation of Eed complex composition governs a switch in global histone modification in brain. J Biol Chem *282*, 9962-9972.

Kim, W., Bird, G. H., Neff, T., Guo, G., Kerenyi, M. A., Walensky, L. D., and Orkin, S. H. (2013). Targeted disruption of the EZH2-EED complex inhibits EZH2-dependent cancer. Nat Chem Biol *9*, 643-650.

Knutson, S. K., Kawano, S., Minoshima, Y., Warholic, N. M., Huang, K. C., Xiao, Y., Kadowaki, T., Uesugi, M., Kuznetsov, G., Kumar, N., *et al.* (2014). Selective inhibition of EZH2 by EPZ-6438 leads to potent antitumor activity in EZH2-mutant non-Hodgkin lymphoma. Mol Cancer Ther *13*, 842-854.

Knutson, S. K., Wigle, T. J., Warholic, N. M., Sneeringer, C. J., Allain, C. J., Klaus, C. R., Sacks, J. D., Raimondi, A., Majer, C. R., Song, J., *et al.* (2012). A selective inhibitor of EZH2 blocks H3K27 methylation and kills mutant lymphoma cells. Nat Chem Biol *8*, 890-896.

Kondo, Y. (2014). Targeting histone methyltransferase EZH2 as cancer treatment. J Biochem.

Kondo, Y., Katsushima, K., Ohka, F., Natsume, A., and Shinjo, K. (2014). Epigenetic dysregulation in glioma. Cancer Sci *105*, 363-369.

Konze, K. D., Ma, A., Li, F., Barsyte-Lovejoy, D., Parton, T., Macnevin, C. J., Liu, F., Gao, C., Huang, X. P., Kuznetsova, E., *et al.* (2013). An orally bioavailable chemical probe of the Lysine Methyltransferases EZH2 and EZH1. ACS Chem Biol *8*, 1324-1334.

Kouzarides, T. (2007). Chromatin modifications and their function. Cell *128*, 693-705.

Kupershmidt, I., Su, Q. J., Grewal, A., Sundaresh, S., Halperin, I., Flynn, J., Shekar, M., Wang, H., Park, J., Cui, W., *et al.* (2010). Ontology-based meta-analysis of global collections of high-throughput public data. PLoS One *5*.

Kuzmichev, A., Nishioka, K., Erdjument-Bromage, H., Tempst, P., and Reinberg, D. (2002). Histone methyltransferase activity associated with a human multiprotein complex containing the Enhancer of Zeste protein. Genes Dev *16*, 2893-2905.

Langmead, B., Trapnell, C., Pop, M., and Salzberg, S. L. (2009). Ultrafast and memory-efficient

alignment of short DNA sequences to the human genome. Genome Biol *10*, R25.

Lee, K. H., Goan, Y. G., Hsiao, M., Lee, C. H., Jian, S. H., Lin, J. T., Chen, Y. L., and Lu, P. J. (2009). MicroRNA-373 (miR-373) post-transcriptionally regulates large tumor suppressor, homolog 2 (LATS2) and stimulates proliferation in human esophageal cancer. Exp Cell Res *315*, 2529-2538.

Li, J., Chen, X., Ding, X., Cheng, Y., Zhao, B., Lai, Z. C., Al Hezaimi, K., Hakem, R., Guan, K. L., and Wang, C. Y. (2013). LATS2 suppresses oncogenic Wnt signaling by disrupting β-catenin/BCL9 interaction. Cell Rep *5*, 1650-1663.

Li, Y., Pei, J., Xia, H., Ke, H., Wang, H., and Tao, W. (2003). Lats2, a putative tumor suppressor, inhibits G1/S transition. Oncogene *22*, 4398-4405.

Margueron, R., and Reinberg, D. (2011). The Polycomb complex PRC2 and its mark in life. Nature *469*, 343-349.

McCabe, M. T., Ott, H. M., Ganji, G., Korenchuk, S., Thompson, C., Van Aller, G. S., Liu, Y., Graves, A. P., Della Pietra, A., Diaz, E., *et al.* (2012). EZH2 inhibition as a therapeutic strategy for lymphoma with EZH2-activating mutations. Nature *492*, 108-112.

McPherson, J. P., Tamblyn, L., Elia, A., Migon, E., Shehabeldin, A., Matysiak-Zablocki, E., Lemmers, B., Salmena, L., Hakem, A., Fish, J., *et al.* (2004). Lats2/Kpm is required for embryonic development, proliferation control and genomic integrity. EMBO J *23*, 3677-3688.

Mikkelsen, T. S., Ku, M., Jaffe, D. B., Issac, B., Lieberman, E., Giannoukos, G., Alvarez, P., Brockman, W., Kim, T. K., Koche, R. P., *et al.* (2007). Genome-wide maps of chromatin state in pluripotent and lineage-committed cells. Nature *448*, 553-560.

Mitamura, T., Watari, H., Wang, L., Kanno, H., Kitagawa, M., Hassan, M. K., Kimura, T., Tanino, M., Nishihara, H., Tanaka, S., and Sakuragi, N. (2014). microRNA 31 functions as an endometrial cancer oncogene by suppressing Hippo tumor suppressor pathway. Mol Cancer *13*, 97.

Moroishi, T., Hansen, C. G., and Guan, K. L. (2015). The emerging roles of YAP and TAZ in cancer. Nat Rev Cancer *15*, 73-79.

Mukai, S., Yabuta, N., Yoshida, K., Okamoto, A., Miura, D., Furuta, Y., Abe, T., and Nojima, H. (2015). Lats1 suppresses centrosome overduplication by modulating the stability of Cdc25B. Sci Rep *5*, 16173.

Müller, J., Hart, C. M., Francis, N. J., Vargas, M. L., Sengupta, A., Wild, B., Miller, E. L., O'Connor, M. B., Kingston, R. E., and Simon, J. A. (2002). Histone methyltransferase activity of a Drosophila Polycomb group repressor complex. Cell *111*, 197-208.

Natsume, A., Ito, M., Katsushima, K., Ohka, F., Hatanaka, A., Shinjo, K., Sato, S., Takahashi, S., Ishikawa, Y., Takeuchi, I., *et al.* (2013). Chromatin regulator PRC2 is a key regulator of epigenetic plasticity in glioblastoma. Cancer Res *73*, 4559-4570.

Ohnishi, K., Semi, K., Yamamoto, T., Shimizu, M., Tanaka, A., Mitsunaga, K., Okita, K., Osafune, K., Arioka, Y., Maeda, T., *et al.* (2014). Premature termination of reprogramming in vivo leads to cancer development through altered epigenetic regulation. Cell *156*, 663-677.

Okada, N., Yabuta, N., Suzuki, H., Aylon, Y., Oren, M., and Nojima, H. (2011). A novel Chk1/2-Lats2-14-3-3 signaling pathway regulates P-body formation in response to UV damage. J Cell Sci *124*, 57-67.

Okamoto, A., Yabuta, N., Mukai, S., Torigata, K., and Nojima, H. (2015). Phosphorylation of CHO1 by Lats1/2 regulates the centrosomal activation of LIMK1 during cytokinesis. Cell Cycle *14*, 1568-1582.

Orzan, F., Pellegatta, S., Poliani, P. L., Pisati, F., Caldera, V., Menghi, F., Kapetis, D., Marras, C., Schiffer, D., and Finocchiaro, G. (2011). Enhancer of Zeste 2 (EZH2) is up-regulated in malignant gliomas and in glioma stem-like cells. Neuropathol Appl Neurobiol *37*, 381-394.

Pan, D. (2010). The hippo signaling pathway in development and cancer. Dev Cell *19*, 491-505.

Parrish, J. Z., Emoto, K., Jan, L. Y., and Jan, Y. N. (2007). Polycomb genes interact with the tumor suppressor genes hippo and warts in the maintenance of Drosophila sensory neuron dendrites. Genes Dev *21*, 956-972.

Plongthongkum, N., Diep, D. H., and Zhang, K. (2014). Advances in the profiling of DNA modifications: cytosine methylation and beyond. Nat Rev Genet *15*, 647-661.

Powzaniuk, M., McElwee-Witmer, S., Vogel, R. L., Hayami, T., Rutledge, S. J., Chen, F., Harada, S., Schmidt, A., Rodan, G. A., Freedman, L. P., and Bai, C. (2004). The LATS2/KPM tumor suppressor is a negative regulator of the androgen receptor. Mol Endocrinol *18*, 2011-2023.

Qi, W., Chan, H., Teng, L., Li, L., Chuai, S., Zhang, R., Zeng, J., Li, M., Fan, H., Lin, Y., *et al.* (2012).

Selective inhibition of Ezh2 by a small molecule inhibitor blocks tumor cells proliferation. Proc Natl Acad Sci U S A *109*, 21360-21365.

Qin, H., Blaschke, K., Wei, G., Ohi, Y., Blouin, L., Qi, Z., Yu, J., Yeh, R. F., Hebrok, M., and Ramalho-Santos, M. (2012). Transcriptional analysis of pluripotency reveals the Hippo pathway as a barrier to reprogramming. Hum Mol Genet *21*, 2054-2067.

Quinlan, A. R., and Hall, I. M. (2010). BEDTools: a flexible suite of utilities for comparing genomic features. Bioinformatics *26*, 841-842.

Rodríguez-Paredes, M., and Esteller, M. (2011). Cancer epigenetics reaches mainstream oncology. Nat Med *17*, 330-339.

Schmitges, F. W., Prusty, A. B., Faty, M., Stützer, A., Lingaraju, G. M., Aiwazian, J., Sack, R., Hess, D., Li, L., Zhou, S., *et al.* (2011). Histone methylation by PRC2 is inhibited by active chromatin marks. Mol Cell *42*, 330-341.

Schuettengruber, B., and Cavalli, G. (2009). Recruitment of polycomb group complexes and their role in the dynamic regulation of cell fate choice. Development *136*, 3531-3542.

St John, M. A., Tao, W., Fei, X., Fukumoto, R., Carcangiu, M. L., Brownstein, D. G., Parlow, A. F., McGrath, J., and Xu, T. (1999). Mice deficient of Lats1 develop soft-tissue sarcomas, ovarian tumours and pituitary dysfunction. Nat Genet *21*, 182-186.

Stadtfeld, M., Apostolou, E., Akutsu, H., Fukuda, A., Follett, P., Natesan, S., Kono, T., Shioda, T., and Hochedlinger, K. (2010). Aberrant silencing of imprinted genes on chromosome 12qF1 in mouse induced pluripotent stem cells. Nature *465*, 175-181.

Steinhardt, A. A., Gayyed, M. F., Klein, A. P., Dong, J., Maitra, A., Pan, D., Montgomery, E. A., and Anders, R. A. (2008). Expression of Yes-associated protein in common solid tumors. Hum Pathol *39*, 1582-1589.

Subramanian, A., Tamayo, P., Mootha, V. K., Mukherjee, S., Ebert, B. L., Gillette, M. A., Paulovich, A., Pomeroy, S. L., Golub, T. R., Lander, E. S., and Mesirov, J. P. (2005). Gene set enrichment analysis: a knowledge-based approach for interpreting genome-wide expression profiles. Proc Natl Acad Sci U S A *102*, 15545-15550.

Suzuki, H., Yabuta, N., Okada, N., Torigata, K., Aylon, Y., Oren, M., and Nojima, H. (2013). Lats2

phosphorylates p21/CDKN1A after UV irradiation and regulates apoptosis. J Cell Sci *126*, 4358-4368.

Tan, J., Yang, X., Zhuang, L., Jiang, X., Chen, W., Lee, P. L., Karuturi, R. K., Tan, P. B., Liu, E. T., and Yu, Q. (2007). Pharmacologic disruption of Polycomb-repressive complex 2-mediated gene repression selectively induces apoptosis in cancer cells. Genes Dev *21*, 1050-1063.

Thorvaldsdóttir, H., Robinson, J. T., and Mesirov, J. P. (2013). Integrative Genomics Viewer (IGV): high-performance genomics data visualization and exploration. Brief Bioinform *14*, 178-192.

Timp, W., and Feinberg, A. P. (2013). Cancer as a dysregulated epigenome allowing cellular growth advantage at the expense of the host. Nat Rev Cancer *13*, 497-510.

Toji, S., Yabuta, N., Hosomi, T., Nishihara, S., Kobayashi, T., Suzuki, S., Tamai, K., and Nojima, H. (2004). The centrosomal protein Lats2 is a phosphorylation target of Aurora-A kinase. Genes Cells *9*, 383-397.

Verhaak, R. G., Hoadley, K. A., Purdom, E., Wang, V., Qi, Y., Wilkerson, M. D., Miller, C. R., Ding, L., Golub, T., Mesirov, J. P., *et al.* (2010). Integrated genomic analysis identifies clinically relevant subtypes of glioblastoma characterized by abnormalities in PDGFRA, IDH1, EGFR, and NF1. Cancer Cell *17*, 98-110.

Visser, S., and Yang, X. (2010). Identification of LATS transcriptional targets in HeLa cells using whole human genome oligonucleotide microarray. Gene *449*, 22-29.

Wei, Y., Chen, Y. H., Li, L. Y., Lang, J., Yeh, S. P., Shi, B., Yang, C. C., Yang, J. Y., Lin, C. Y., Lai, C. C., and Hung, M. C. (2011). CDK1-dependent phosphorylation of EZH2 suppresses methylation of H3K27 and promotes osteogenic differentiation of human mesenchymal stem cells. Nat Cell Biol *13*, 87-94.

Yabuta, N., Fujii, T., Copeland, N. G., Gilbert, D. J., Jenkins, N. A., Nishiguchi, H., Endo, Y., Toji, S., Tanaka, H., Nishimune, Y., and Nojima, H. (2000). Structure, expression, and chromosome mapping of LATS2, a mammalian homologue of the Drosophila tumor suppressor gene lats/warts. Genomics *63*, 263-270.

Yabuta, N., Mukai, S., Okada, N., Aylon, Y., and Nojima, H. (2011). The tumor suppressor Lats2 is pivotal in Aurora A and Aurora B signaling during mitosis. Cell Cycle *10*, 2724-2736.

Yabuta, N., Okada, N., Ito, A., Hosomi, T., Nishihara, S., Sasayama, Y., Fujimori, A., Okuzaki, D.,

Zhao, H., Ikawa, M., *et al.* (2007). Lats2 is an essential mitotic regulator required for the coordination of cell division. J Biol Chem *282*, 19259-19271.

Yamashita, S., Yamamoto, H., Mimori, K., Nishida, N., Takahashi, H., Haraguchi, N., Tanaka, F., Shibata, K., Sekimoto, M., Ishii, H., *et al.* (2012). MicroRNA-372 is associated with poor prognosis in colorectal cancer. Oncology *82*, 205-212.

Yu, F. X., Zhao, B., and Guan, K. L. (2015). Hippo Pathway in Organ Size Control, Tissue Homeostasis, and Cancer. Cell *163*, 811-828.

Yu, T., Bachman, J., and Lai, Z. C. (2013). Evidence for a tumor suppressor role for the large tumor suppressor genes LATS1 and LATS2 in human cancer. Genetics *195*, 1193-1196.

Zeng, X., Chen, S., and Huang, H. (2011). Phosphorylation of EZH2 by CDK1 and CDK2: a possible regulatory mechanism of transmission of the H3K27me3 epigenetic mark through cell divisions. Cell Cycle *10*, 579-583.

Zhang, K., Rodriguez-Aznar, E., Yabuta, N., Owen, R. J., Mingot, J. M., Nojima, H., Nieto, M. A., and Longmore, G. D. (2012). Lats2 kinase potentiates Snail1 activity by promoting nuclear retention upon phosphorylation. EMBO J *31*, 29-43.

Zhao, J., Ohsumi, T. K., Kung, J. T., Ogawa, Y., Grau, D. J., Sarma, K., Song, J. J., Kingston, R. E., Borowsky, M., and Lee, J. T. (2010). Genome-wide identification of polycomb-associated RNAs by RIP-seq. Mol Cell *40*, 939-953.